Separation of P and Mn from Steelmaking Slag and Manganese Ore by Selective Reduction

Ph.D Dissertation

Separation of P and Mn from Steelmaking Slag and Manganese Ore by Selective Reduction

選択還元による製鋼スラグ及びマンガン鉱石からのPとMnの分離

Dong Jun Shin

Department of Metallurgy
Graduate School of Engineering
Tohoku University

2019

Advising Professor at Tohoku Univ.	Prof. Shinya Kitamura
Research Advisor at Tohoku Univ.	Prof. Shinya Kitamura
Dissertation Committee Members Name marked with "○" is the Chief Examiner	○ Prof. Shinya Kitamura 1 Prof. Hiroshi Nogami　2 Prof. Hiroyuki Shibata 3 ＿＿＿＿＿＿＿＿　4 ＿＿＿＿＿＿＿＿ 5 ＿＿＿＿＿＿＿＿　6 ＿＿＿＿＿＿＿＿

Contents

Lists of Tables & Figures

Chapter 1

Introduction

Chapter 2

Optimum condition of selective reduction of steelmaking slag

Chapter 3

Measurement of Activity Coefficient of P and Mn in Fe-P-Mn-C(sat.) alloy

Chapter 5

Application of the selective reduction to the production of low P ferromanganese alloy

Chapter 1 Introduction

1.1 Utilization of steelmaking slag & Consideration for circulation use

The steel-industry consumes a large amount of raw materials and energy to produce steel, and it generates various kinds of by-products. These byproducts contain a large amount of valuable resources that can be recycled, such as iron, carbon, limestone, etc.; thus landfilling them is a waste of resources and energy, and is costly to handle. Moreover, the global environment is becoming a big issue nowadays, the amount of by-products should be reduced as much as possible, and the generated by-products should be retreated by recycling to reduce the cost of process and prevent environmental pollution.

The major by-products from the steel-industry are ironmaking slag and steelmaking slag and typical chemical compositions of them are shown in **Table 1.1.** Chemical and physical properties of those slags are widely different, thus their application areas and method are also different. In case of ironmaking slag, most of slag is valuably reused as the material for cement production, due to its similar chemical composition to the Portland cement. However, steelmaking slag is used as relatively low value materials for road base or civil engineering work due to its chemical properties [1, 2, 3]. It is because that steelmaking slag contains a few percent of unreacted CaO (free-CaO) which collapse the product made by slag by the volume expansion caused by the reaction with water. Despite the generation of steelmaking slag is smaller than ironmaking slag, the main issue for steel industry that should be solved about its by-product is steelmaking slag due to difficulty in recycling.

Nevertheless, considering depletion of high-grade iron ore in near future, the use of low grade iron ore containing impurity, especially phosphorus, is inevitable; thus it is expected that the generation amount of steelmaking slag will increase gradually. For these reasons, various researches have been

conducting to develop another valorization method for steelmaking slag, and “Ferroform" for port and harbor civil work, “Marine Block" to restore coastal algae grounds and "Restoration materials" for sodium removal and nutrient supply have been proposed [4, 5, 6].

Table 1.1 Typical slags composition (mass %)

Type / Component	Ironmaking slag	Steelmaking slag		
		Converter slag (De-P slag)	Oxidizing slag	Reducing slag
CaO	41.7	45.8	22.8	55.1
SiO_2	33.8	11.0	12.1	18.8
T-Fe	0.4	17.4	29.5	0.3
MgO	7.4	6.5	4.8	7.3
Al_2O_3	13.4	1.9	6.8	16.5
S	0.8	< 0.1	0.2	0.4
P_2O_5	< 0.1	1.7	0.3	0.1
MnO	0.3	5.3	7.9	1.0

Considering the high content of CaO and T.Fe in steelmaking slag, it is a good raw material for the sintering process. Therefore a circulation process can be considered by reusing steelmaking slag as raw material of sintering process. In this case, not only a great effect in decreasing the generation of steelmaking slag, but also a benefit to recover useful resources that are discarded are obtained. Furthermore, if all steelmaking slag can be used to the sintering process, the ironmaking slag becomes the only generated slag from the integrated steelmaking mill which is easy to reuse as cement.

However, the existence of P and Mn in steelmaking slag is a conflict point with this circulation use. Considering the reduction of P and Mn in sinter by ironmaking process, most of the Mn and P are

reduced and accumulated into hot metal. The P and Mn in hot metal are oxidized in steelmaking process and discharged as steelmaking slag again. This indicates the accumulation of P and Mn in ironmaking and steelmaking process. Therefore, it is necessary to eliminate Mn and P from steelmaking slag for this circulation use.

1.2 Value of P and Mn in steelmaking slag as secondary recourse

As the industry becomes more sophisticated, demand for high-performance steel products is increasing, and high Mn-steel having good physical and chemical properties is considered as a suitable solution to meet this requirements [7, 8, 9]. Also as increasing global population, the demand of P is increasing which is an essential nutrient in agricultural production. In last 5 years, the global consumption of Mn and P was not decreased; moreover many experts predict that the global demand of them will continue to grow up [10, 11]. Nevertheless, the deposits of those elements are substantially biased in the world, and top 5 countries occupy more than 70% of total deposits in earth [10, 11]. Since Japan is one of country which is highly dependent on natural resource imported from oversea, the stable supply of those resources is an important national issue. In particular, as Japan is the second largest steel producer in the world, the consumption of Mn is very high, and the Mn has been designated as a stockpile metal to deal with the resource crisis.

Fig. 1.1 shows material flow of P and Mn in Japan [12, 13]. Approximately 537 kilotons of Mn as ferro-alloys and Mn-ores, and 110 kilotons of P as phosphate rock are imported from overseas. However the amount of P and Mn in steelmaking slag originated from iron ore are close to that of imported amount. It indicates that if the P and Mn are effectively separate from the steelmaking slag, the steelmaking slag can be regarded as alternative resources for P and Mn. For these reasons, many researchers, who considered the steelmaking slag as secondary resource, have conducted the study to recover P and Mn from steelmaking slag with various methods.

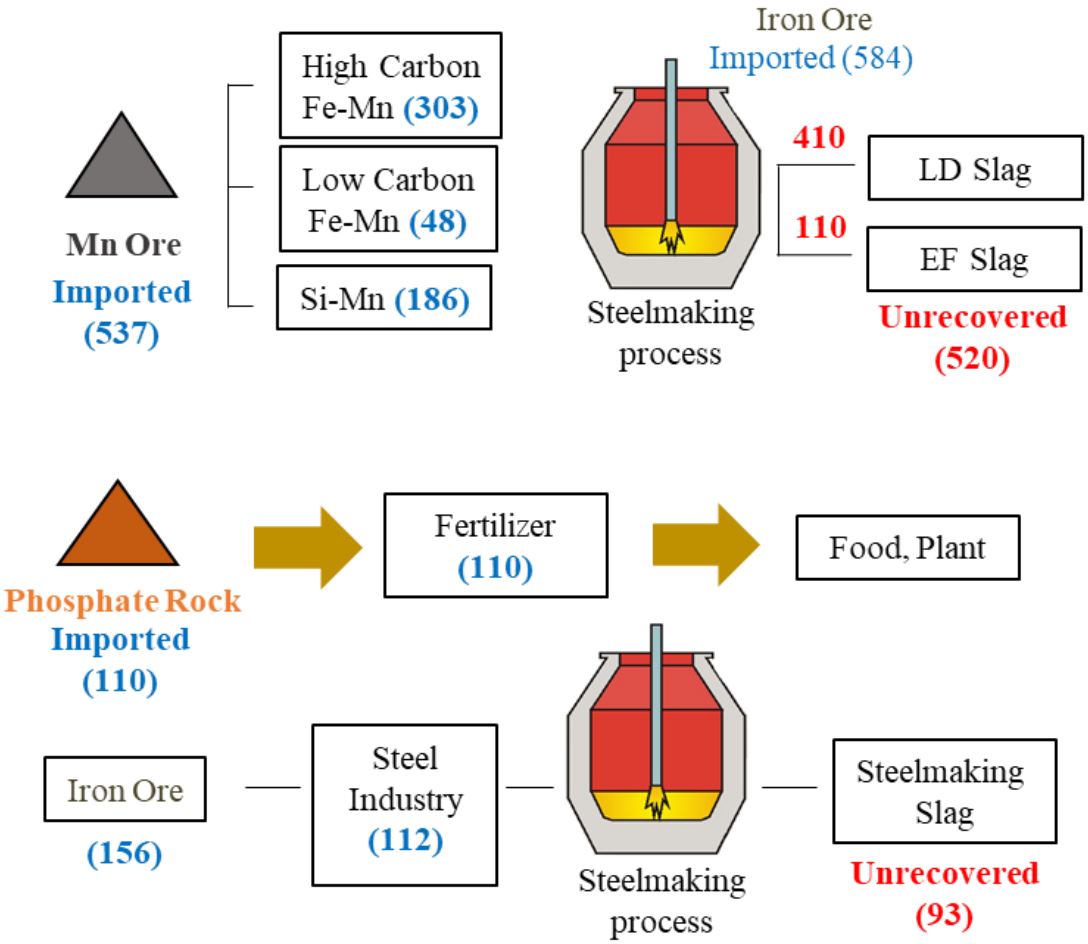

Fig. 1.1 Material flow of P and Mn in Japan (kton/year) [12, 13]

1.3 Various methods to recycle P and Mn from steelmaking slag

Based on the differences in properties between each component or each phase, many studies have been proposed to extract P or Mn from steelmaking slag through physical or chemical separation method. For example, Ono *et al*. [14] and Li *et al*. [15] suggested floating separation and super gravity separation processes respectively focusing on different density between P rich phase and matrix phase in steelmaking slag. Ono *et al*. used slow cooling method for molten slag in order to precipitate the P rich phase, which is relatively low density and has a higher melting point. Preferentially crystallized P rich phase was floated up to top of liquid slag, the steelmaking slag was separated to P-rich area (top) and matrix area (bottom). Li *et al*. applied artificial gravity through strong rotation to the solid liquid coexisting slag in order to enhance the separation speed and ratio.

Magnetic separation process using the difference of magnetic properties between the P rich and Fe rich phases was proposed by Yokoyama *et al*. [16] Kubo *et al*. [17] By this process, powdered steelmaking slag was separated to magentized power (Fe rich phase) and non-magentized powder (P rich phase), and the content of P in non-magentized powder was similar to that of P rich phase in steelmaking slag. Kim *et al*. [18] studied the sulfurization of steelmaking slag using the difference of thermodynamic stability of sulfide between P and Mn. Under the controlled oxygen and sulfur partial pressure, the Mn in steelmaking slag was selectively sulfurized, and phase separation between sulfide phase and oxide phase was achieved. The separated sulfide phase is considered as law material to produce low P content ferromanganese alloy. Teratoko *et al*. [19] reported the dissolution behavior of the solid solution with high P content in acidic solution, and proposed the selective leaching process to separate P from steelmaking slag. As the fundamental study of this process, Numata *et al*. [20] and Du *et al*. [21] invesigated various factors on the difference in the dissolution behavior of P rich phase and Fe rich phase in steelmaking. Miki *et al*. [22] showed the capillary action of FeO and P in steelmaking slag using a CaO sinter as absorber. As the liquid phase of steelmaking slag can be

introduced to the pores in CaO sinter, the sinter absorbed FeO rich liquid and separate P in steelmaking slag selectively. The recovery ratio of FeO and P from steelmaking slag was close to 90%. The proposed technologeis are summarized in **Table 1.2.**

Table 1.2 Proposed technologies to separate and recover P or Mn from steelmaking slag

Method	Researchers	Process Summary
Floatation separation	Ono *et al.* [14]	Slag was separated into two layers by floatation of dicalcium silicate with low density.
Magnetic separation	Yokoyama *et al.*[16] Nagasaka *et al.*[17]	C_2S-C_3P solid solution was separated from Fe_tO-containing matrix phase with the aid of a magnetic field.
Oxidation & Sulfurization	Kim *et al.* [18]	Separation of Mn and P from steelmaking slag by sulfurization using the difference in the thermodynamic stability of sulfide between Mn and P
Selective leaching	Teratoko *et al.* [19] Kitamura *et al.* [20, 21]	In steelmaking slag, C_2S-C_3P solid solution was selectively dissolved in acid solution at a constant pH.
Capillary action	Miki *et al.* [22]	The FeO-rich liquid phase was moved into sintered CaO by capillary action, and separate it from C_2S-C_3P solid solution.
Super gravity separation	Li *et al.* [15]	Super gravity was applied to separate C_2S-C_3P solid solution from slag based on density difference.

1.4 Carbon reduction of steelmaking slag

Carbon reduction is a simply applicable method for recovering Fe, Mn and P from steelmaking slag. Even though, this method requires high temperature, it is noteworthy method due to low costs and simple processes and equipment. In particular, since the steelmaking slag is discharged to a high temperature after process, the heating process is omitted, which is more attractive. Several studies have also been carried out aiming at recovering those resources through carbon reduction, and major studies have been reviewed in sequence. Shiomi *et al*. [23] conducted the experiment to remove P from steelmaking slag using carbon reduction. Artificial steelmaking slag (FeO = 19.5 mass %, CaO/SiO_2 = 1.1 ~ 1.2) was used for experiment, and the mixture of powdered slag and carbon was heated to 1773K ~ 1873K. As a result, a considerable amount of FeO reduction was preferentially observed before the start of P_2O_5 reduction. (**Fig. 1.2)** Based on this phenomenon, the possibility to recover metallic iron in steelmaking slag with low P content was suggested by adjusting the reduction condition (contact method between reductant and slag, the reduction time and temperature etc.). In addition, evaporation phenomena of P in Fe-Si-P alloy (Si = 15 ~ 49 mass %, P = 0.9 ~ 4.5 mass %) was shown under Ar or vacuum atmosphere at 1873K ~ 1973K. The P content in Fe-Si-P decreased to 0.005 mass % from 1.1 mass % at 1873K after 9 mins in vacuum condition.

Takeuchi *et al*. [24] investigated the suggested possibility to recover Fe and P individually from steelmaking slag proposed by Shiomi *et al*. Focusing on the unstability of P in Fe-Si alloy, Si-Fe alloy (Si = 75 mass %) was introduced into the test. The concept of this process is schematically shown in **Fig. 1.3.** The mixture of the Si-Fe alloy, steelmaking slag (T.Fe = 19. 8, CaO/SiO_2 = 0.5 ~ 2.3) and carbon was heated to 1873K by plasma furnace. As the results, most of Fe and P was removed from steelmaking slag by carbon reduction, and about 60% P was separated as P_2 gas. As the ratio of CaO/SiO_2 increased from 0.5 to 1.6, the gasification degree of P increased but higher than 1.6 the degree decreased.

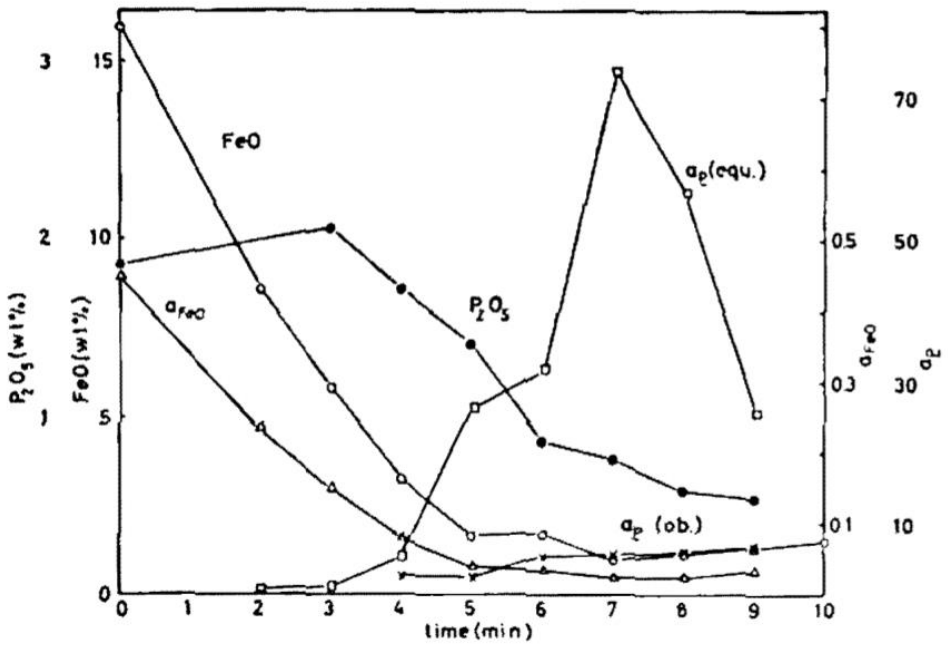

Fig. 1.2 Composition and activity change of Fe and P in slag and metal

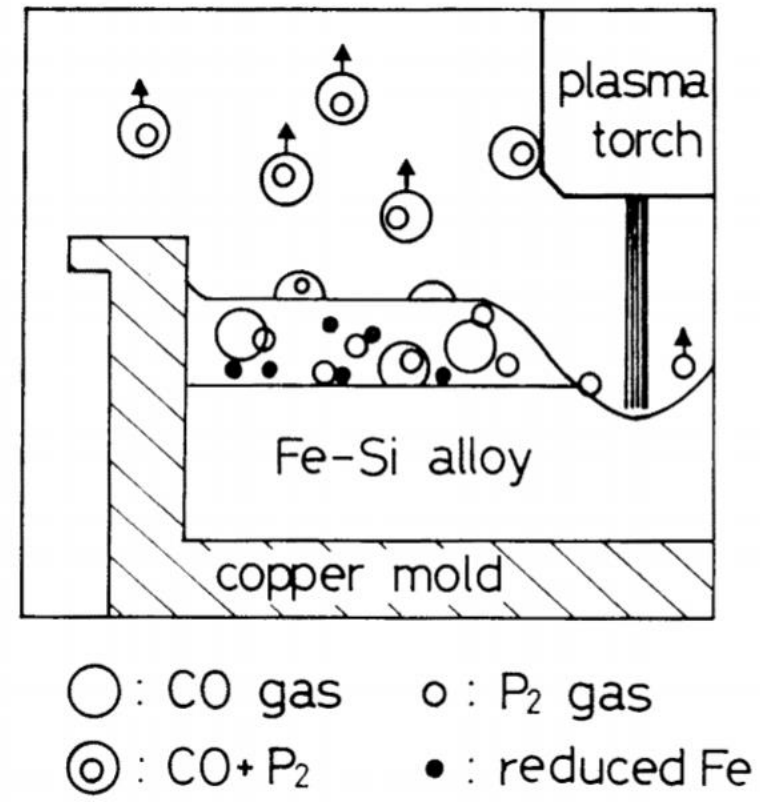

Fig. 1.3 Schematic figure of gaseous dephosphorization from steelmaking slag

Li *et al*. [25] proposed a waste-free steelmaking process which consists of a conceptual slag regenerator though computer simulation. The concept of this process is shown in **Fig 1.4**. Firstly, De-P slag was reduced by smelting reduction in the slag regenerator, and produced high P content metal was assumed as a raw material to produce fertilizer. Secondary, the regenerated slag from 1st step was mixed either totally or partly with De-C slag, and the mixed slag was reused for De-P as flux. By the second step, De-P slag was newly generated, and this slag was reduced again in regenerator. This process was repeated and distribution of P between slag and metal was calculated. For calculation, the distribution ratio of P at each steps were considered thermodynamically from reference data. The result of distribution ratio of P by simulation was shown as a function of the number of regeneration times and the mixed ratio of De-P slag, and the possibility to reuse the regenerated slag was shown. Although their study was limited to a computer simulation, as the used data are reported by the experiment, the result is worthy for the further deliberation.

Morita *et al*. [26] reported the recovery of Fe and P from steelmaking slag by carbon reduction with microwave process. An artificial steelmaking slag (T.Fe = 11.7 mass %, CaO/SiO_2 = 1.57) and graphite powder were mixed and heated to higher than 1873K by microwaves irradiation. By this experiment, FeO and P_2O_5 in steelmaking slag was reduced and formed a lump of Fe-C(sat.)-P alloy, and P content in alloy increased in up to 9.7 mass %. As the graphite ratio increased from 0.5 to 1.5, the recovery ratio of Fe increased, and became constant at a graphite ratio higher than 1.5. When 10 mass % of extra SiO_2 was added to mixture, the result showed considerable improvement in reduction behavior for Fe and P (P in metal 13 mass %), as the increase in the fluidity of slag and the activity coefficient of P_2O_5 in slag (**Fig. 1.5**). For the separation of Fe and P from the alloy, the De-P process was also studied using Na_2CO_3 and K_2CO_3 as flux at 1473K. After De-P process, the P content in Na_2CO_3 based slag increased to up to 16.2 mass % (initial P content in metal is 11.3 mass %) and this slag can be considered as a P resources.

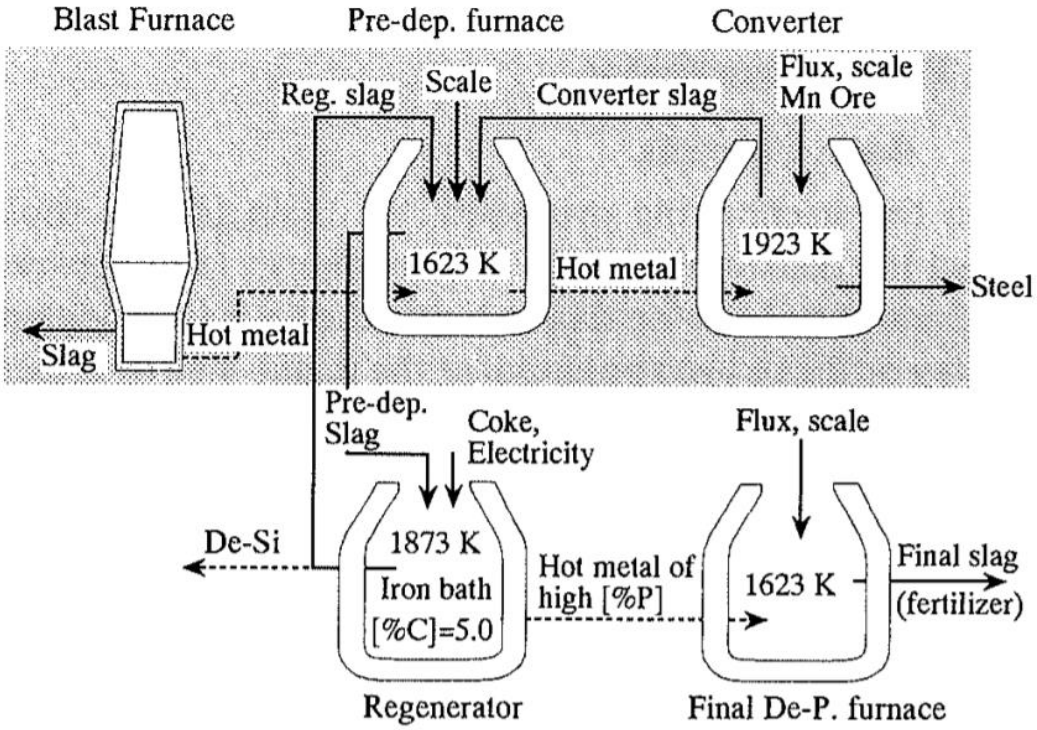

Fig. 1.4 Schematic flow of steelmaking slags recycling process

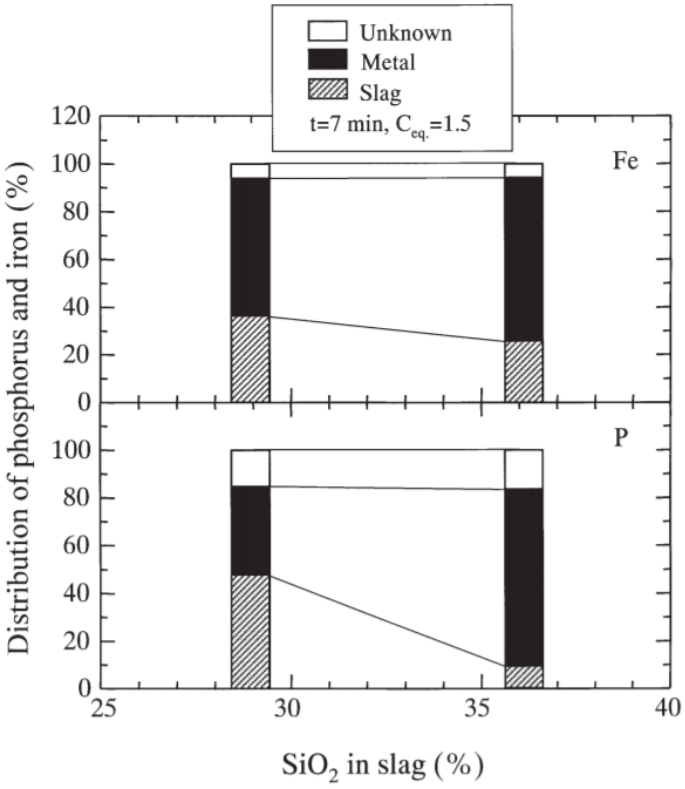

Fig. 1.5 Influence of SiO_2 content on reduction behavior of Fe and P

The effect of temperature (1473K ~ 1873K) and slag composition (CaO/SiO_2 = 1.2 ~ 4.0) on the reduction behavior of Fe_tO and P_2O_5 in steelmaking slag was investigated by Matsui *et al*. [27]. Slag and reductant were added to the MgO crucible and the sample was heated to the target temperature (heating rate of 15k / min) while stirring the sample by impeller (60 rpm). After 40 min, the reduced metal particles, metal droplets and slag were distinguished separately as shown in **Fig.1.6** and mass balance of P was calculated. The reduction ratio of Fe and P was strongly influenced by temperature and basicity. As temperature increases and basicity decreases, the reduction ratio of Fe and P also increased. The reduction behavior of P was analyzed with the equilibrium distribution ratio of P between slag and metal. Recently, Nakase *et al*. [28] showed the influence of Fe_tO content (Fe_tO = 2.0 ~ 18.8 mass %) and basicity (CaO/SiO_2= 0.5 ~ 2.0) on the reduction behavior of Fe and P by carbon reduction of steelmaking slag. The experiment performed as the same method used by Matusi *et al.* The slag and graphite powder in a MgO crucible was heated to the target temperature, and after the reduction, the sample was separated 3 phases (lump metal, magnetized slag and non-magnetized slag). The mass balance of Fe, and P was calculated. According to result, the reduction and evaporation behavior of P was significantly influenced by Fe_tO in slag and about half of P in slag could be removed by evaporation under the optimum condition.

Previous researches mainly focused on the removal of P from steelmaking slag by carbon reduction, but separation of Mn and P was not paid attention. In general, Fe, Mn and P in steelmaking slag are reduced simultaneously by simple carbon reduction and it forms Fe-P-Mn-C alloy. To utilize Mn and P in steelmaking slag as a secondary resource, these elements need to be recovered separately. Especially, Mn is majorly used as source for ferromanganese for steel products. However, P is one of the harmful impurities that lower mechanical and chemical properties of steel product. Therefore, in order to use Mn in steelmaking slag as raw material, P has to be separated.

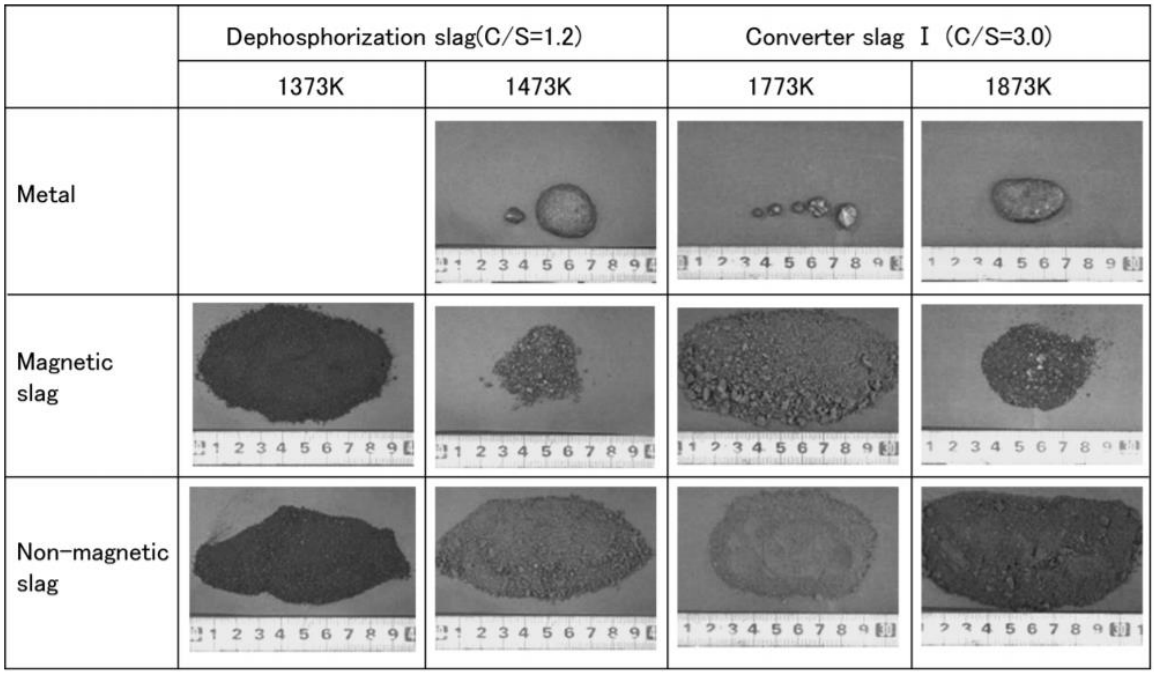

Fig. 1.6 Distinguished slag and metal after reduction experiment

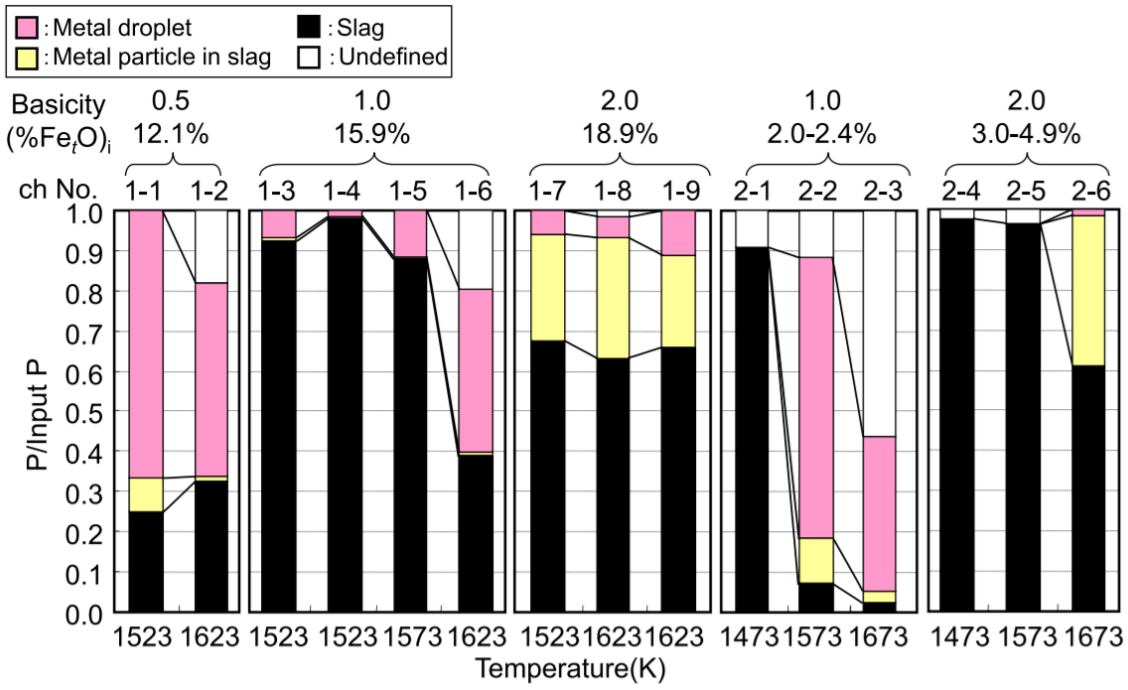

Fig. 1.7 Distribution of P by different Fe_tO content and basicity with temperature

1.5 Concept for separation of P and Mn from steelmaking slag by selective reduction

It is well known that MnO is a basic oxide and P_2O_5 is an acidic oxide, and the standard free energy of formation of these oxides are widely different. In the hot metal De-P process using a flux injection, Mn in hot metal is hardly oxidized during De-P process, because Mn-oxide in slag is much stable than P-oxide. To minimize the loss of Mn at BOF refining process, a highly basic slag is designed. These operations indicate that the selective oxidations of P or Mn are conducted in steelmaking process. Therefore, I have considered the possibility of separation of P and Mn by selective reduction and proposed the process as shown in **Fig. 1.8.**

First step is selective reduction of P for separation between P and Mn in steelmaking slag. By the control of slag basicity as acid, P and Fe is reduced selectively by the carbon reduction at high temperature. After this step, high P containing alloy is produced which is a source for phosphate fertilizer, and the remaining slag containing Mn can be used for ferromanganese production. Second step is the reduction of Mn for slag cleaning. By the control of slag basicity as basic, high Mn containing alloy is produced by the reduction. After this step, cleaned slag is produced which is applicable for sintering process. Therefore, P, Mn and the other resources in steelmaking slag can be recycled entirely.

This study is as a fundamental research focusing on the first step to find optimum conditions for the separation of P and Mn. Factors such as slag basicity (CaO/SiO_2), temperature, reductant amount, and crucible type are likely to affect the reduction behavior of P and Mn from steelmaking slag and need to be elucidated for its feasibility. In addition, if the P and Mn can be efficiently separated by this process, it is possible to apply the optimum condition to other oxides where P and Mn coexisting in which requires separation of them such as Mn-ore.

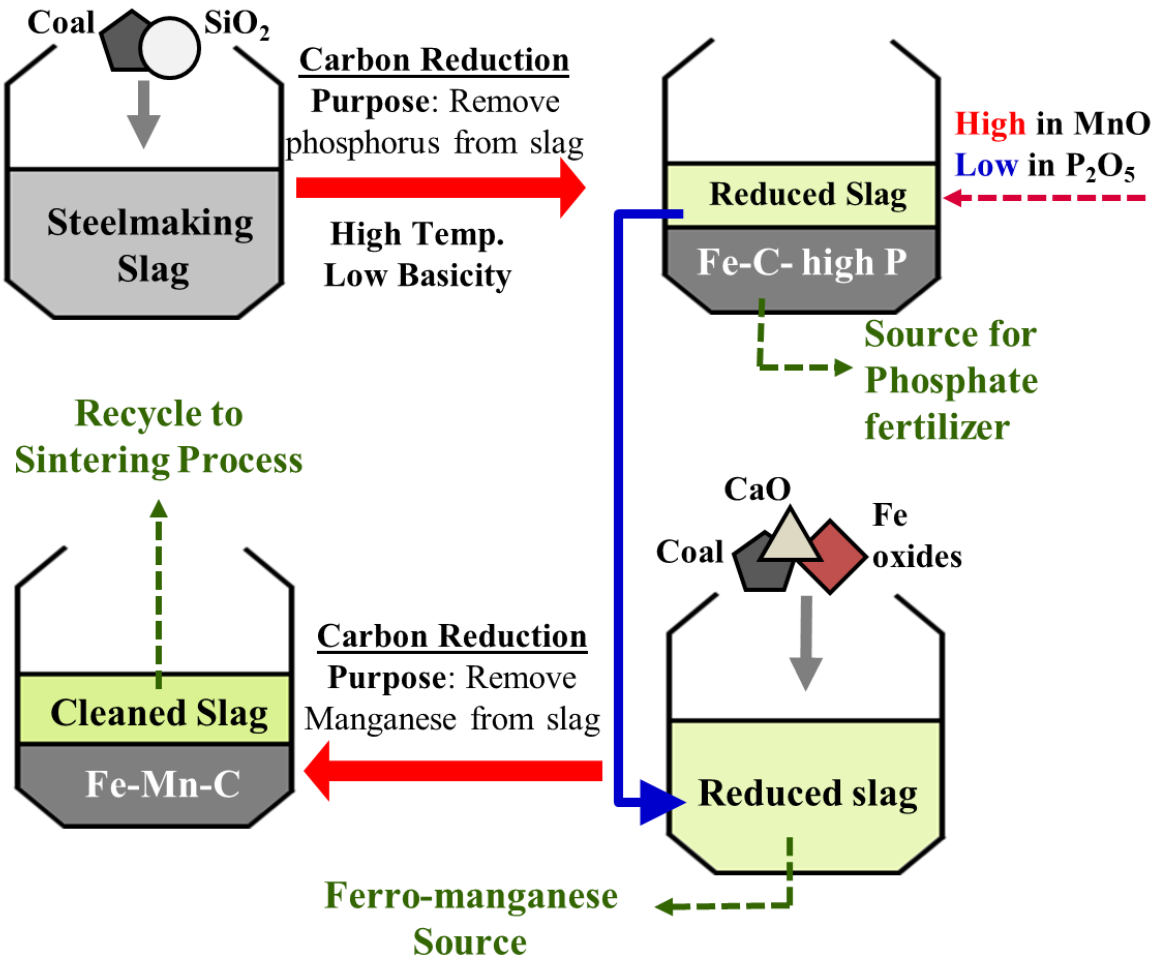

Fig. 1.8 A proposal of selective reduction process of steelmaking process

1.6 Application of selective reduction process for Mn-ore

1.6.1 Importance of low P in ferromanganese

As mentioned earlier, demand for high-performance steel products is growing, and high Mn steel can be a good solution to meet this requirement. The high Mn steel is a steel containing 10 ~ 30 mass % of Mn, and its better mechanical properties and chemical properties than normal steel is well-known. Beside the high Mn steel, Mn is one of the most important elements to increase the strength of steel. On the other hand, P is the most harmful element which causes the embrittlement of steel. In the case of high Mn steel, metallic Mn produced by electrolysis is used to avoid the contamination of P from the alloy. Therefore, the demand of low P containing ferromanganese is increasing. The ferromanganese alloys are produced by smelting reduction using Mn-ore in either electric furnaces or blast furnaces [29].

However, Mn-ore has several impurities, especially P (0.1 ~ 0.3 mass % depends on Mn-ore). During the Mn-ore smelting process, most of the P in Mn-ore is reduced into the ferromanganese alloy, and the content of P in the produced ferromanganese alloy reaches to 0.2 ~ 0.5 mass % depending on the grade of Mn-ore. In particular, ferromanganese alloys are generally added to the molten steel after refining process, most of the P in the ferromanganese alloys is dissolved in the steel and affect the quality of the final product.

The ferromanganese alloy is classified based on their bulk composition and mode of production as ferromanganese (FeMn), silicomanganese (SiMn), and electrolytic manganese metal (EMM). They may further classified based on carbon content, high carbon (HC) medium carbon (MC), and low carbon (LC). The typical composition of ferromanganese materials and relative price index is shown in **Table 1.3**.

Table 1.3 Typical chemical composition (mass %) [30]

Material	Mn	Fe	Si	C	P	Price index Rel. to HC FeMn
HC FeMn	78	Bal.	0.3	6.8	0.2	1.0
MC FeMn	81	Bal	0.3	1.2	0.15	2.4
LC FeMn	82	Bal.	0.6	0.2	0.15	2.7
MC SiMn	68	Bal.	18	1.6	0.15	1.2
LC SiMn	60	Bal.	30	0.05	0.05	1.8
EMM	99.8	0.001	0.002	0.002	0.001	4.2
Mn-ore	25~50	5~15	2~10	-	0.1~0.4	

The electrolytic manganese metal shows the excellent chemical purity but, its price is notably high. The high carbon ferromanganese and medium carbon silicomanganese are provided at substantial lower prices, but the content of P is not adequate for producing high Mn steel.

1.6.2 Removal of P from Mn bearing materials (literature review)

To decrease P content, oxidation refining of ferromanganese alloy was studies. However, when normal De-P process is applied to ferromanganese alloys, a considerable amount of Mn is oxidized. This is because Mn oxide in slag is stable as much as that of P oxide, and as the content of Mn in the ferromanganese alloy is much higher than that of P, the oxidation of Mn is inevitable. Some researchers have studied De-P using BaO based fluxes which have a very high phosphate capacity in order to minimize the loss of Mn. Fujita *et al*. [31] showed high phosphate capacity of BaO-based flux by conducting De-P of high carbon Fe-Mn alloy (5 ~ 60%). In this study, various carbonates of basic

oxides ($BaCO_3$, Na_2CO_3, $CaCO_3$ and Ni_2CO_3) were examined as a flux at 1573K ~ 1773K. The relationship between De-P efficiency and factors such as the melting point of the flux, the carbon content in the ferromanganese alloy, content of SiO_2 in flux was reported, and as the those factors decreases, the De-P efficiency increases.

Sim *et al*. [32] and Watanabe *et al*. [33] reported equilibrium data between BaO-BaF_2-MnO slag and high carbon Fe-Mn alloy at 1573K ~ 1673K. The addition of BaF_2 in BaO based flux, not only decreases melting point of flux, but also increases the phosphate capacity and activity coefficient of MnO. Liu *et al*. [34] investigated the influence of additives (CaO, MgO, SiO_2, CaF_2 and Al_2O_3) for BaO-BaF_2-MnO slag on the distribution of P and Mn between slag and high carbon ferromanganese alloy. The effect of slag composition on phosphate and manganese capacities were calculated. Chaudhary *et al.* [35] conducted De-P of high carbon ferromanganese alloy without significant loss of Mn (less than 5 %) using $BaCO_3$-BaF_2 based flux at 1573 ~ 1623K. By this De-P process, the maximum removal ratio of P was 68%, and the content of P in Fe-Mn alloy was decreased to 0.2 from 0.55 mass %.

Meanwhile, several researchers have focused to separate P from Mn-ore. G.V Rao *et al*. [36], and B.C. Acharya *et al*. [37] showed preferential presence of P at Goethite in Mn-ore by in-situ observation. Using relatively high magnetic property of Goethite among various phases in Mn-ore, magnetic separation process was proposed, in order to increase ratio of Mn/Fe and to decrease P content in Mn-ore simultaneously. Roasted Mn-ore was magnetized, the Mn-ore was separated to magnetized, and non-magnetized ore. The concentration of Mn in non-magnetized ore was enriched to 40% from 32%, the P content also decreased to 0.3% from 0.45%. Recently, Spitzer *et al*. [38] reported production of tailored MnO-SiO_2 slag with low P for SiMn alloy using mixture of Mn-ore and Fe-ore. The mixture of the ores (Fe/Mn ratio 1 or 2), coke (13% ~ 17%/ore mixture) and SiO_2 (14% ~ 24%/ore mixture) was pre-reduced at 1373K for 4h in the solid state. After that, the temperature was

further raised to melt the sample. When the reduced metal and the slag were melted, phase separation was achieved. The Fe and P in ore mixture were reduced to hot metal, and the separated slag was $MnO\text{-}SiO_2$ system with low P content. The slag was used for SiMn alloy production as raw material, and the P content obtained SiMn was lower than 0.02%.

In order to separate P, many studies have focused on the selective oxidation of P from Fe-Mn alloy, but the separation of P by reduction of Mn-ore is only achieved by Spitzer *et al*. Therefore, it is meaningful to apply optimum condition to Mn-ore to separate P in order to establish fundamental database.

1.7 Purpose and contents

The influence of slag basicity (mass % CaO/SiO_2), temperature, carbon mixing ratio, and crucible on the reduction behavior of P and Mn were investigated mainly in Chapter 2 in order to obtained optimum condition. To consider the obtained metal composition from Chapter 2 thermodynamically, activity coefficient of P and Mn in C saturated high p and high Mn alloy was measured in Chapter 3. In Chapter 4, the influence of melting behavior on selective reduction of P and Mn was observed. Based on the obtained result from Chapter 2 ~ 4, the optimum condition of selective reduction process was applied to Mn-ore to separate P. The contents of this thesis are as follows:

- ✓ Chapter 1 presents a background and purpose this thesis.
- ✓ Chapter 2 presents optimum condition of selective reduction of steelmaking slag.
- ✓ Chapter 3 presents measurement of activity coefficient of P and Mn in Fe-P-Mn-C(sat.) alloy.
- ✓ Chapter 4 presents mechanism of the selective reduction of steelmaking slag.
- ✓ Chapter 5 presents application of the selective reduction to the production of low P ferromanganese alloy.
- ✓ Chapter 6 presents the conclusions of this thesis

1.8 Reference

1. Nippon Slag Association (2017) Production and uses of steel slag in Japan, http://www.slg.jp/pdf/Steel%20Slag%202017FY.pdf Accessed 29 August 2018 [Japanese]
2. Horii, K., Kato, T., Sugahara, K., Tsutsumi, N., & Kitano, Y. (2015). Overview of iron/steel slag application and development of new utilization technologies. *Nippon Steel & Sumitomo Technical Report*, *109*.
3. Dippenaar, R. (2005). Industrial uses of slag (the use and re-use of iron and steelmaking slags). *Ironmaking & steelmaking*, *32*(1), 35-46.
4. Yabuta, K., Tozawa, H., & Takahashi, T. (2006). New applications of iron and steelmaking slag contributing to a recycling-oriented Society. *JFE technical report*, *10*(8), 17-23.
5. Kato, T., Kosugi, C., Kiso, E., & Torii, K. (2015). Application of steelmaking slag to marine forest restoration. *Nippon Steel & Sumitomo Metal Tech Rep*, *109*, 79-84.
6. Gao, X., Okubo, M., Maruoka, N., Shibata, H., Ito, T., & Kitamura, S. Y. (2015). Production and utilisation of iron and steelmaking slag in Japan and the application of steelmaking slag for the recovery of paddy fields damaged by Tsunami. *Mineral Processing and Extractive Metallurgy*, *124*(2), 116-124.
7. Bouaziz, O., Allain, S., Scott, C. P., Cugy, P., & Barbier, D. (2011). High manganese austenitic twinning induced plasticity steels: A review of the microstructure properties relationships. *Current opinion in solid state and materials science*, *15*(4), 141-168.
8. Sutou, Y., Kamiya, N., Umino, R., Ohnuma, I., & Ishida, K. (2010). High-strength Fe–20Mn–Al–C-based alloys with low density. *ISIJ international*, *50*(6), 893-899.
9. Lu, Y., Molodov, D. A., & Gottstein, G. (2011). Correlation between microstructure and texture development in a cold-rolled TWIP steel. *ISIJ international*, *51*(5), 812-817.

10. U.S. Department of the Interior U.S. Geological Survey, (2018). Mineral commodity summaries 2018. https://minerals.usgs.gov/minerals/pubs/mcs/2018/mcs2018.pdf#search=%27MINERAL+COMMODITY+SUMMARIES+2018%27 Accessed 31 August 2018.
11. Japan Oil, Gas and Metals National Corporation, (2017) Mineral resources and materials flow 2017. http://mric.jogmec.go.jp/wp-content/ebook/201803/5aa63015/material_flow2017.pdf Accessed 31 August 2018 [Japanese]
12. Nakajima, K., Yokoyama, K., & Nagasaka, T. (2008). Substance flow analysis of manganese associated with iron and steel flow in Japan. *ISIJ international*, *48*(4), 549-553.
13. Matsubae-Yokoyama, K., Kubo, H., Nakajima, K., & Nagasaka, T. (2009). A material flow analysis of phosphorus in Japan: the iron and steel industry as a major phosphorus source. *Journal of Industrial Ecology*, *13*(5), 687-705.
14. Ono, H., Inagaki, A., Masui, T., Narita, H., Mitsuo, T., Nosaka, S., & Gohda, S. (1980). Removal of phosphorus from LD converter slag by floating of dicalcium silicate during solidification. *Tetsu-to-Hagané*, *66*(9), 1317-1326.
15. Li, C., Gao, J., & Guo, Z. (2016). Isothermal Enrichment of P-Concentrating Phase from CaO–SiO2–FeO–MgO–P2O5 Melt with Super Gravity. *ISIJ international*, *56*(5), 759-764.
16. Yokoyama, K., Kubo, H., Mori, K., Okada, H., Takeuchi, S., & Nagasaka, T. (2007). Separation and recovery of phosphorus from steelmaking slags with the aid of a strong magnetic field. *ISIJ international*, *47*(10), 1541-1548.
17. Kubo, H., Matsubae-Yokoyama, K., & Nagasaka, T. (2010). Magnetic separation of phosphorus enriched phase from multiphase dephosphorization slag. *ISIJ international*, *50*(1), 59-64.

18. Kim, S. J., Shibata, H., Maruoka, N., Kitamura, S., & Yamaguchi, K. (2011). Novel recycling process of Mn by sulfurization of molten slag from a by-product of steelmaking process. *High Temperature Materials and Processes*, *30*(4-5), 425-434.
19. Teratoko, T., Maruoka, N., Shibata, H., & Kitamura, S. Y. (2012). Dissolution behavior of dicalcium silicate and tricalcium phosphate solid solution and other phases of steelmaking slag in an aqueous solution. *High Temperature Materials and Processes*, *31*(4-5) 329-338.
20. Numata, M., Maruoka, N., Kim, S. J., & Kitamura, S. Y. (2014). Fundamental experiment to extract phosphorous selectively from steelmaking slag by leaching. *ISIJ International*, *54*(8), 1983-1990.
21. Du, C. M., Gao, X., Ueda, S., & Kitamura, S. Y. (2017). Effects of cooling rate and acid on extracting soluble phosphorus from slag with high P2O5 content by selective leaching. *ISIJ International*, *57*(3), 487-496.
22. Miki, T., & Kaneko, S. (2015). Separation of FeO and P2O5 from steelmaking slag utilizing capillary action. *ISIJ International*, *55*(1), 142-148.
23. Shiomi, S., Sano, N., & Matsushita, Y. (1977). Removal of phosphorus in BOF slags. *Tetsu-to-Hagané*, *63*(9), 1520-1528.
24. Takeuchi, S., Sano, N., & Matsushita, Y. (1980). Separate Recovery of Iron and Phosphorus from BOF Slags by Using Fe-Si Alloys. *Tetsu-to-Hagané*, *66*(14), 2050-2057.
25. Li, H. J., Suito, H., & Tokuda, M. (1995). Thermodynamic analysis of slag recycling using a slag regenerator. *ISIJ international*, *35*(9), 1079-1088.
26. Morita, K., Guo, M., Oka, N., & Sano, N. (2002). Resurrection of the iron and phosphorus resource in steel-making slag. *Journal of Material Cycles and Waste Management*, *4*(2), 93-101.

27. Matsui A, Nakase K, Kikuchi N, Kishimoto Y, Takahashi K, Ishida K (2011). Phosphorus Separation from Steelmaking Slag by High Temperature Reduction with Mechanical Stirring. *Tetsu-to-Hagané 97*(8):416−422.
28. Nakase, K., Matsui, A., Kikuchi, N., & Miki, Y. (2017). Effect of slag composition on phosphorus separation from steelmaking slag by reduction. *ISIJ international*, *57*(7), 1197-1204.
29. Elliott, R., Coley, K., Mostaghel, S., & Barati, M. (2018). Review of Manganese Processing for Production of TRIP/TWIP Steels, Part 2: Reduction Studies. *JOM*, 1-9.
30. Elliott, R., Coley, K., Mostaghel, S., & Barati, M. (2018). Review of Manganese Processing for Production of TRIP/TWIP Steels, Part 1: Current Practice and Processing Fundamentals. *JOM*, 1-11.
31. Fujita, M., Katayama, H., Yamamoto, A. & Matsuo, M. (1988). Dephosphorization of Fe-Mn-C alloy with BaCO3. *Tetsu-to-Hagané* , *74* (5), 816-822.
32. Shim, S. C., Tsukihashi, F., & Sano, N. (1993). Thermodynamic properties of the BaO-MnO flux system. *Metallurgical Transactions B*, *24*(2), 333-337.
33. Watanabe, Y., Kitamura, K., Rachev, I. P., Tsukihashi, F., & Sano, N. (1993). Thermodynamics of phosphorus and sulfur in the BaO-MnO flux system between 1573 and 1673 K. *Metallurgical Transactions B*, *24*(2), 339-347.
34. Liu, X., Wijk, O., Selin, R., & Edström, J. O. (1998). Effects of additives in BaO-BaF2-MnO slag on phosphate and manganese capacities. *ISIJ international*, *38*(1), 36-45.
35. Chaudhary, P. N., Goel, R. P., & Roy, G. G. (2001). Dephosphorisation of high carbon ferromanganese using BaCO3 based fluxes. *Ironmaking & steelmaking*, *28*(5), 396-403
36. Rao, G. V., Acharya, B. C., Murty, B. V. R., Mohanty, J. N., Swamy, Y. V., Chattopadhay, P., & Tripathy, A. K. (1998). Removal of phosphorus and enrichment of manganese from a complex ferruginous manganese ore. *Physical Separation in Science and Engineering*, *9*(2), 109-123.

37. Acharya, B. C., Rao, D. S., & Sahoo, R. K. (1997). Mineralogy, chemistry and genesis of Nishikhal manganese ores of South Orissa, India. *Mineralium Deposita*, *32*(1), 79-93.

38. Hils, G., Newirkowez, A., Kroker, M., Grethe, U., Schmidt-Jürgensen, R., Kroos, J., & Spitzer, K. H. (2015). Conventional and Tailored Mn-Bearing Alloying Agents for the Production of High Manganese Steels. *Steel research international*, *86*(4), 411-421.

Chapter 2 Optimum Condition of Selective Reduction of Steelmaking Slag

By using the difference of thermodynamic properties of P and Mn, the possibility of selectively reduction to separate Mn and P from steelmaking slag was considered. In this chapter, as a fundamental study for the selective reduction of P from steelmaking slag, the effects of slag basicity (mass% of CaO/SiO_2), graphite mixing ratio, temperature, and crucible type are mainly elucidated to determine the optimum condition.

2.1 Experimental method

2.1.1 Sample preparation

Reagent-grade $CaCO_3$, SiO_2, Fe, Fe_2O_3, $Ca_3(PO)_4$, MnO, MgO, and Al_2O_3 were used to synthetize the slag. First, FeO was pre-synthesized through a reaction of Fe with Fe_2O_3 at 1673 K for 1 h in Ar atmosphere, and CaO was calcined from $CaCO_3$ at 1473 K for 12 h in air. The reagents with CaO and FeO were mixed homogenously and pre-melted at 1673 K in an Al_2O_3 crucible for 1 h under Ar atmosphere (flow rate: 100 ml/min). After a given time, the pre-melted slag was quenched in water. The chemical composition of the slag, analyzed by inductively coupled plasma atomic emission spectroscopy (ICP–AES), is shown in **Table 2.1.**

Table 2.1 Composition of synthesized slag by ICP-AES (mass %)

Sample	FeO	CaO	SiO_2	P_2O_5	MnO	MgO	Al_2O_3	Basicity (CaO/SiO_2)
Slag A	23.36	29.87	20.07	4.06	5.61	3.43	13.60	1.49
Slag B	30.24	24.69	20.72	4.22	6.12	3.70	10.32	1.19
Slag C	26.37	25.70	25.54	3.77	6.02	3.67	9.03	1.01
Slag D	25.10	23.10	30.43	3.91	5.54	3.37	8.22	0.76
Slag E	25.95	16.75	33.43	3.90	6.22	3.44	10.31	0.50

The contents of P_2O_5 and MnO were set to about 4 and 6 mass%, which are similar to that of industrial steelmaking slag. The Al_2O_3 content was about 10 mass%, which is higher than that of industrial slag, as an Al_2O_3 crucible was used. For investigating the effect of slag basicity, the ratio of CaO and SiO_2 was varied from 0.5 to 1.5. The synthesized slags were used for each experiment after crushing them into powder (with particle size of smaller than 500 μm).

2.1.2 Experimental set up & Procedure

The graphite powder (with particle size of smaller than 44 μm) was used as a reductant in this experiment. I homogenously mixed 3 g of crushed slag with graphite powder. The amount of mixed graphite powder was set as 100%–200% of the amount required for reducing all FeO, MnO, and P_2O_5 in the slag, which was stoichiometrically calculated by Eqs. (2.1) to (2.3).

$$(FeO) + C(s) = [Fe] + CO(g) \quad \text{(2.1)}$$

$$(MnO) + C(s) = [Mn] + CO(g) \quad \text{(2.2)}$$

$$(P_2O_5) + 5C(s) = 2[P] + 5CO(g) \quad \text{(2.3)}$$

The experiment was performed using a vertical type of resistance furnace equipped an alumina reaction tube (Inner diameter: 42 mm, Height: 1000 mm) shown in **Fig. 2.1**. Basically, a dense Al_2O_3 crucible (Inner diameter: 19 mm, Height: 45 mm) was used, and a dense MgO crucible of the same size was applied for comparison to investigate the influence of the crucible.

Before the sample was sent in, the furnace was heated to the target temperature (1673, 1773, and 1873 K) and Ar gas (purity: 99.9999%) was injected (flow rate: 300 ml/min) into the reaction tube for 30 min for oxygen removal. Subsequently, the mixture of slag and graphite powder loaded in the crucible was charged into the heated furnace, and this moment was set as the start of the experiment. A typical temperature change of the sample with time is shown in **Fig. 2.2**

To reach the target temperature, it generally took 7 to 9 min. The experimental time was 20, 40, and 80 min and the inner atmosphere of the furnace was completely controlled by Ar gas (flow rate: 500

ml/min) during the experiment. After the experiment, the sample with the crucible was unloaded from the furnace and quenched in water immediately. The sample was separated into slag and metal, and the compositions of each phase were analyzed by ICP–AES. The carbon content in the metal was analyzed by the combustion method using a combustion infrared spectrometer (CIP).

2.1.3 Mass balance of P and Mn

The mass of the slag was calculated by CaO balance assuming that the mass of CaO in the slag did not change during the experiment. The mass of the metal was determined by the change in FeO content in the slag. The equations for the calculations of the slag and metal are expressed as Eq. (2.4) and (2.5), respectively.

$$W_{slag} = 100 \times W_{CaO}^{Initial} / (\text{mass\% CaO}) \quad \text{……..…….. (2.4)}$$

$$W_{Metal} = (W_{FeO}^{Initial} - W_{slag} \times (\text{mass\% FeO})/100) \times (M_{Fe} / M_{FeO}) \quad \text{……..…. (2.5)}$$

where W_{Slag} and W_{Metal} indicate the masses of slag and metal after the experiment (g), $W_{CaO}^{Initial}$ and $W_{FeO}^{Initial}$ indicate the masses of CaO and FeO in the initial slag, (mass% CaO) and (mass% FeO) indicate the concentration of each oxide in the slag after the experiment, and M_{Fe} and M_{FeO} indicate the atomic weight of Fe and the molecular weight of FeO.

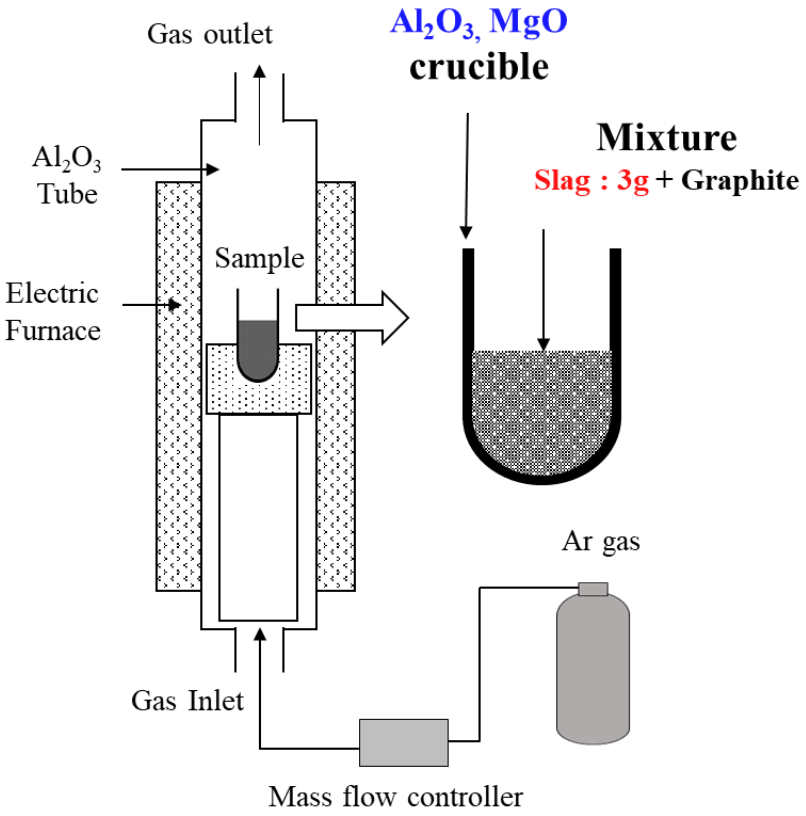

Fig. 2.1 Experimental setup

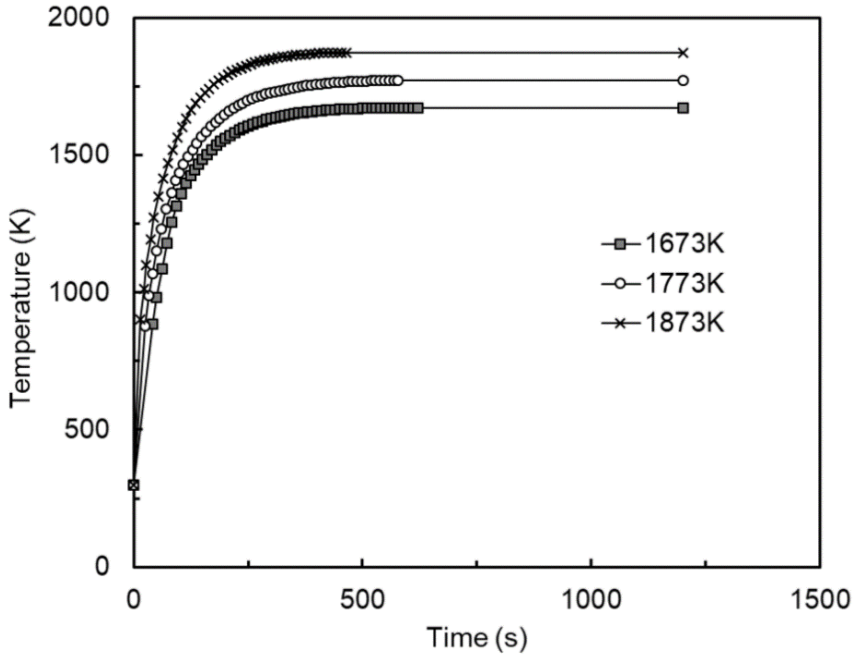

Fig. 2.2 Typical temperature change of the sample with time.

2.2 Result

2.2.1 General reduction behavior of slag

Fig. 2.3 shows a cross-section of the sample after 20 min reduction at 1773 K. As shown in this figure, the metal is easily separated from the slag. Through the shape of the cross-section, the slag and metal are considered to be in the molten state before quenching. When 3 g of slag is used for the reduction, the diameter of the reduced metal reaches 4 ~ 6 mm (0.5 ~ 0.7 g). The top of the sample is covered by the residual graphite powder. However, as the graphite powder is lost during the quenching procedure, it is not observed in this figure.

A typical composition change of the slag and metal for Slag B at 1773 K with time is shown in **Fig. 2.4** for Slag B at 1773K. In the Fig. 2.4-(a), preferential reduction of FeO is observed, and then, P_2O_5 and MnO are gradually reduced with time during the initial 20 min. The content of Al_2O_3 in the slag is significantly increased with time owing to the dissolution of Al_2O_3 from the crucible. Since the considerable content Al_2O_3 is difficult to ignore, the role of Al_2O_3 on the selective reduction is need to be clarified. This part will present in detail following Chapter 4.

Corresponding to the change in the slag composition, the contents of Mn and P in the metal phase gradually increase with time (Fig. 2.3-(b)). In this figure, the initial value of carbon is plotted as 4 mass%, considering the saturated value of the hot metal without the presence of Mn and P. The carbon content decreases continuously due to the change in solubility due to an increase in Mn and P contents.

The changes in slag composition are shown in **Fig. 2.5** on the phase diagram of SiO_2-CaO-Fe_tO and SiO_2-CaO-Al_2O_3 systems. Comparing with the actual temperature change of sample, shown in Fig. 2.1, slag was considered to be liquid during the initial 20 mins. This indicated that except the initial heating period, the reduction has been occurred at the interface between molten slag and hot metal, besides the interface of molten slag and graphite powder floating on the surface.

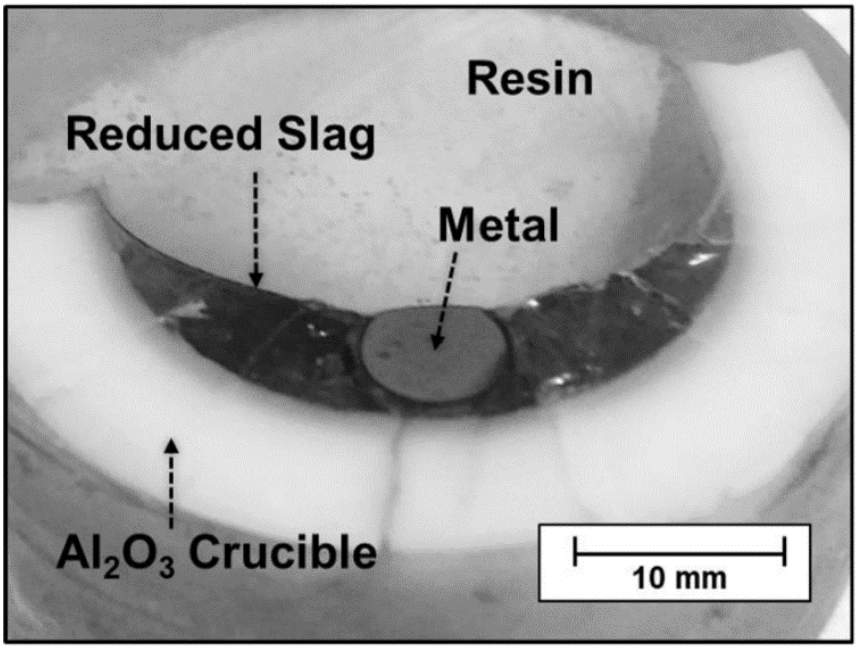

Fig. 2.3 A typical cross-section image of sample after 20 mins reduction at 1773K

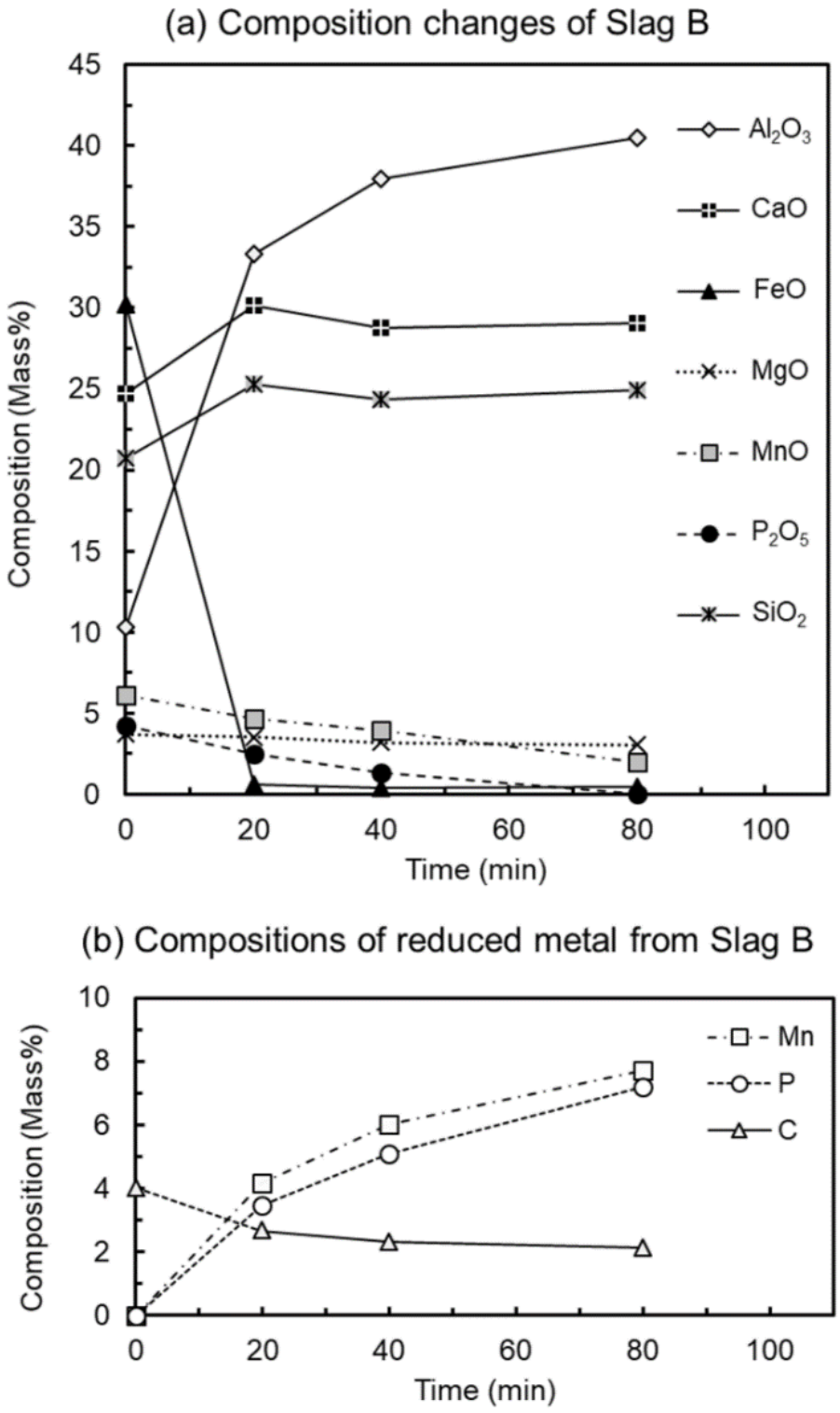

Fig. 2.4 Composition changes of Slag B and its reduced metal (1773K, graphite mixing ratio: 200%)

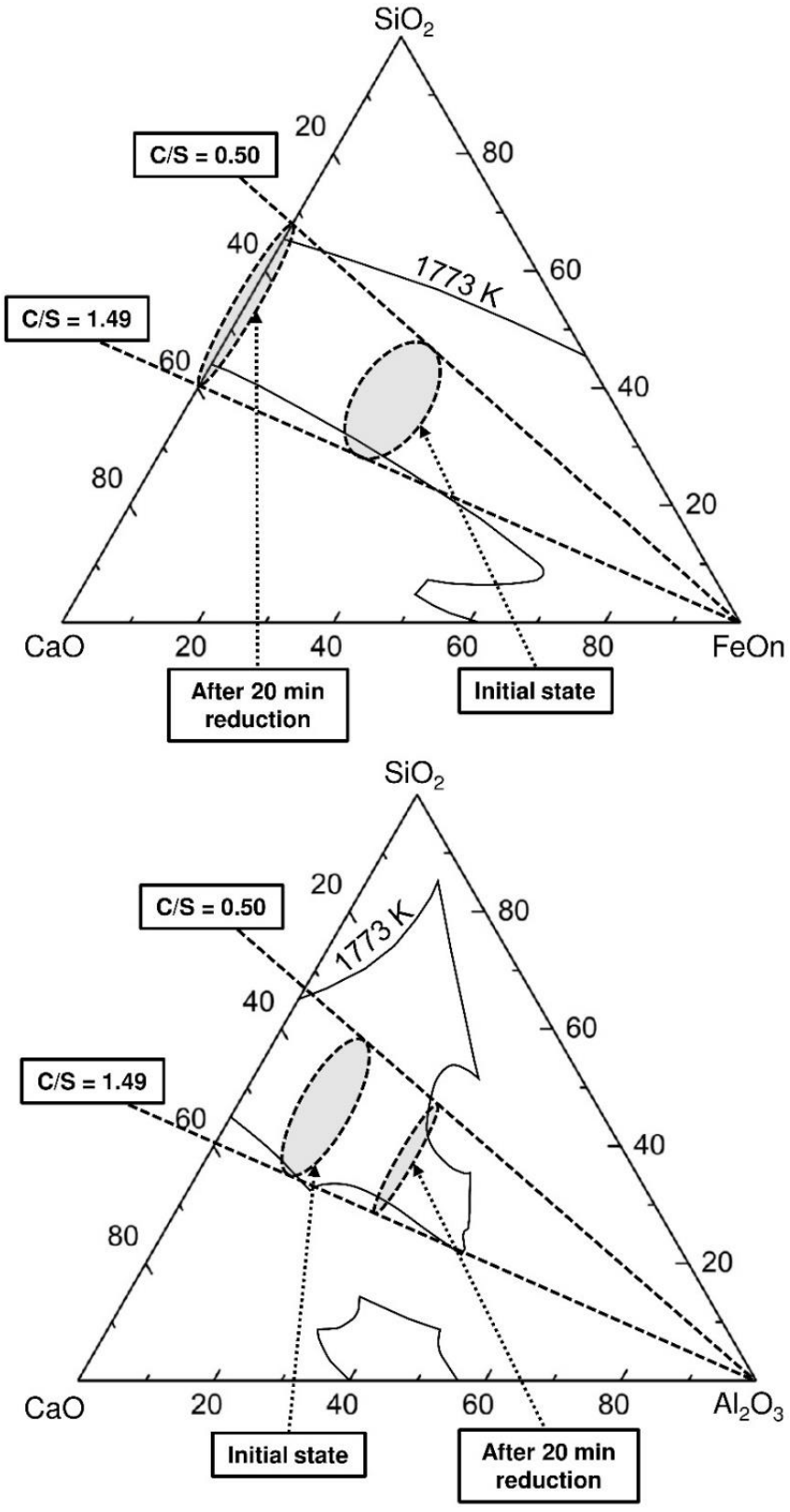

Fig. 2.5 The composition changes of slags in SiO_2-CaO-Fe_tO and SiO_2-CaO-Al_2O_3 phase diagrams [1]

2.2.2 Influence of slag basicity (CaO/SiO_2 mass %)

Fig. 2.6 shows the change in Mn and P contents with reduction time in each phase for the slag with varying basicity at 1773 K. Regarding the reduction rate of MnO shown in Fig. 2.6-(a), with an increase in slag basicity, the reduction is enhanced and Slag A (C/S = 1.49) shows the fastest reduction rate. A small increase in MnO content is observed in Slags D and E for 20 min, which is attributable to the rapid reduction of other components in the slag. On the contrary, regarding the reduction rate of P_2O_5, as shown in Fig. 2.6-(b), with a decrease in slag basicity, the reduction rate increases and Slag D (C/S = 0.76) and Slag E (C/S = 0.50) show the most rapid decrease. The content of P_2O_5 in these slags is lower than 0.20 mass% after 20 min. Corresponding to the composition change in the slag phase, Slag A shows the greatest Mn content in the metal phase (Fig. 2.6-(c)), while Slags D and E show the greatest P content (Fig. 2.6-(d)).

The partition ratios of Mn and P are shown in **Fig. 2.7**. The result shows that a decrease in slag basicity from 1.49 to 0.50 suppresses MnO reduction and enhances P_2O_5 reduction. At 20 min reduction of Slags D and E, more than 95 mass% of Mn remains in the slag, while more than 95 mass% of P is reduced into metal. The separation between Mn and P is achieved when the slag basicity is lowered below 0.76 at 1773 K. When the reduction time is increased to 40 min for Slags D and E, the residual mass of P in the slag is lowered further, while the reduced mass of Mn in the metal increases.

In this experiment, the selective reduction of P, suppressing the reduction of Mn, is achieved using the acid slag. However, the reduction of MnO gradually occurs through the elongation of the reduction time. Therefore, the optimum condition should be determined not only by the equilibrium condition but also by the kinetics of the reduction reaction.

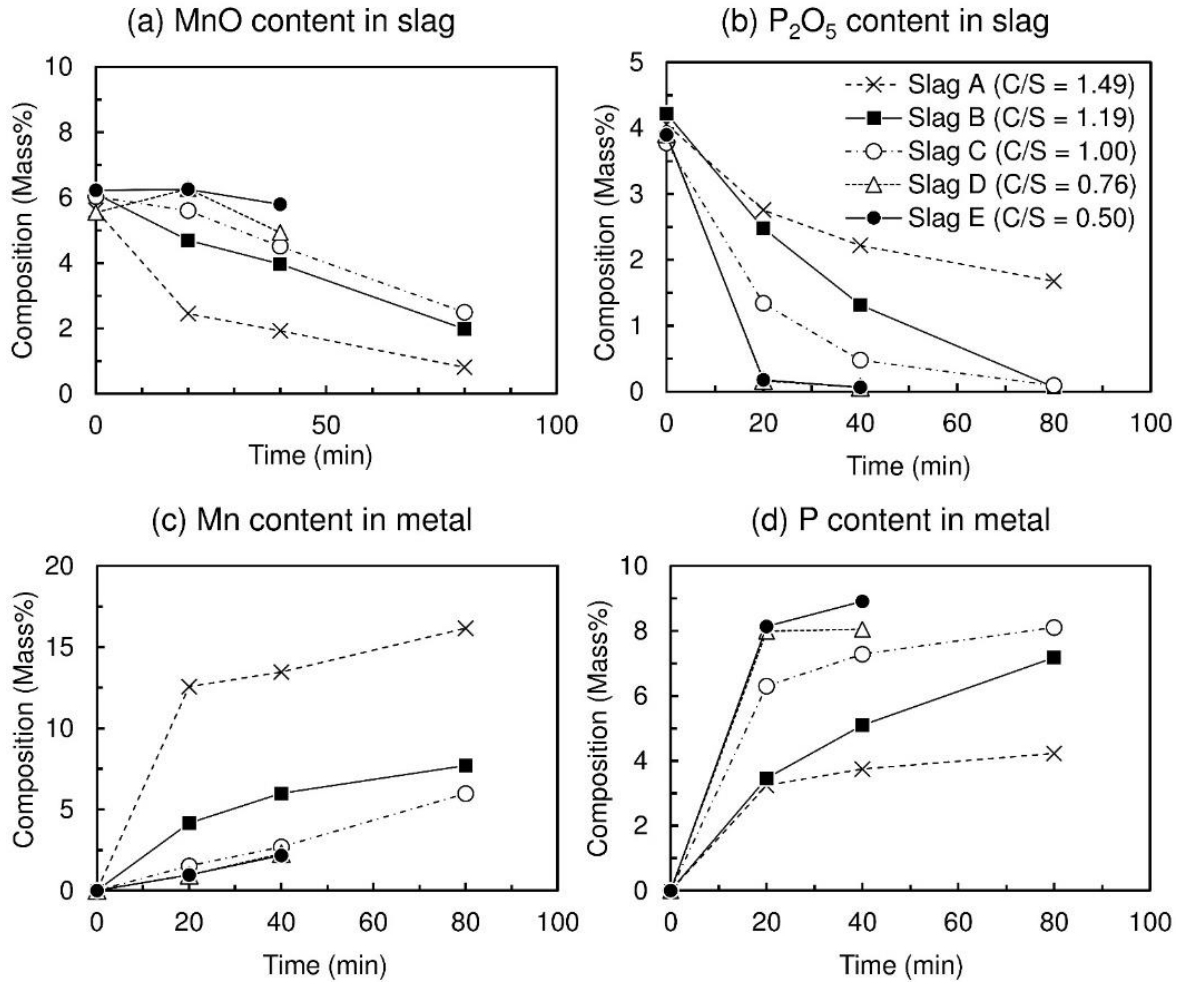

Fig. 2.6 The changes of P and Mn contents in each phase with reduction time by different slag basicity (1773K, graphite mixing ratio: 200%)

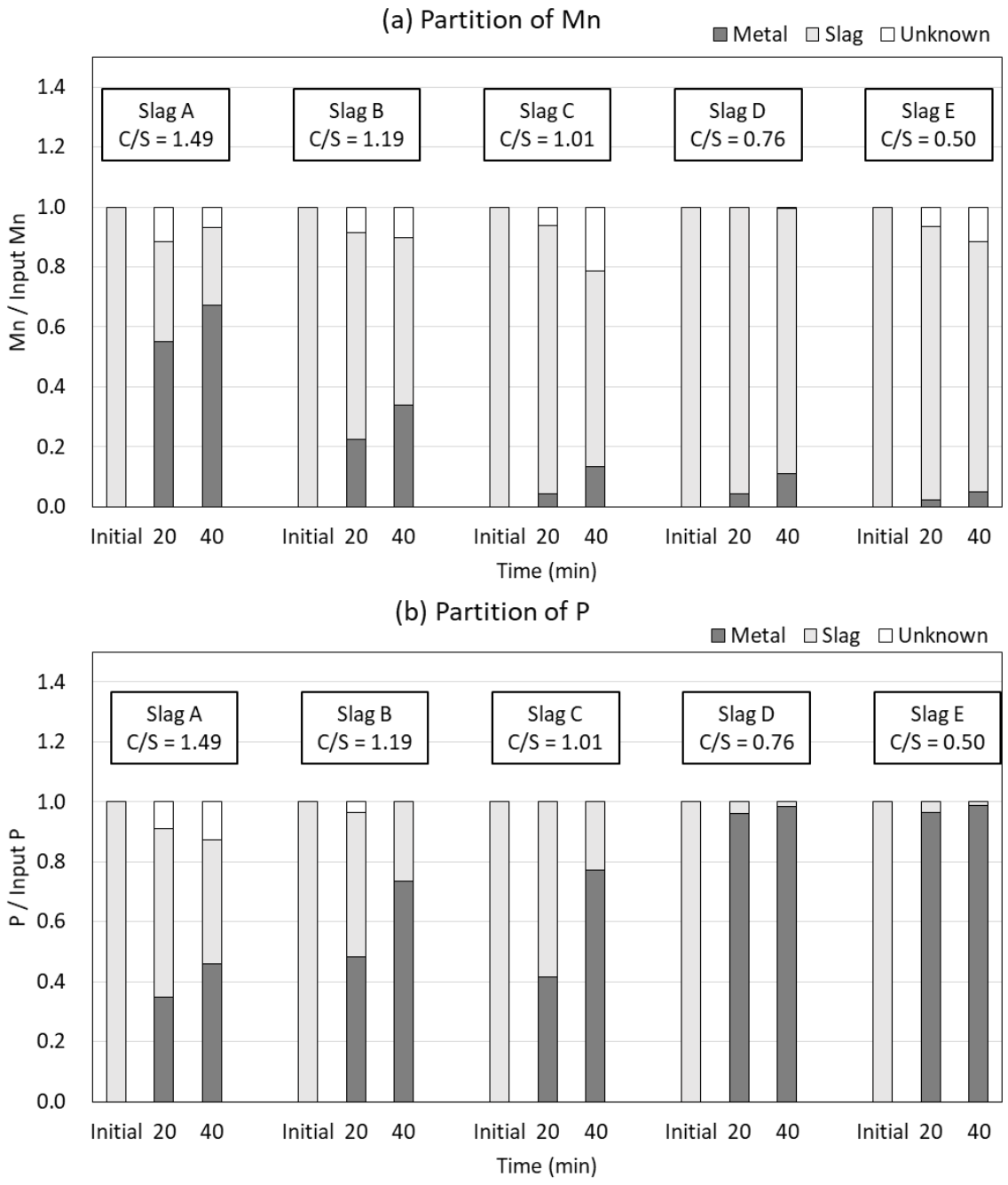

Fig. 2.7 The partitions of Mn and P with reduction time by different slag basicity

2.2.3 Influence of temperature

The influence of temperature was investigated using Slag D (C/S=0.76) and the graphite mixing ratio was 200%. **Fig. 2.8** shows the changes of P and Mn contents in each phases with reduction time by different temperature. It was clear that the rapid reduction of MnO was observed at 1873K (Fig. 2.7-(a)) and the reduction rate of P_2O_5 at 1673K was significantly slow (Fig. 2.7-(b)). The content of P_2O_5 at 1673K was 1.64 mass % in slag after 20 mins, and still about 0.5 mass % of P_2O_5 was observed in slag even after 40 mins. The changes of P and Mn contents in metal (Fig. 2.7-(c) and (d)), exhibited a consitent tendency with the composition change in slag.

Fig. 2.9 shows the result of partitions of Mn and P at each temperature. At 1873K, the partition of Mn into metal gradually increased with time (Fig. 2.9-(a)). On the other hand, at 1673K, the partition of P in slag was still high after 20 mins and the reduction rate was remarkably decreased (Fig. 2.9-(b)).

Therefore, for the reduction of P_2O_5, low temperature treatment is not appropriate. However, when the temperature increased, the reduction rate of MnO was gradually increased. To conduct the efficient separation of P and Mn, the optimum reduction time should be determined for each temperature.

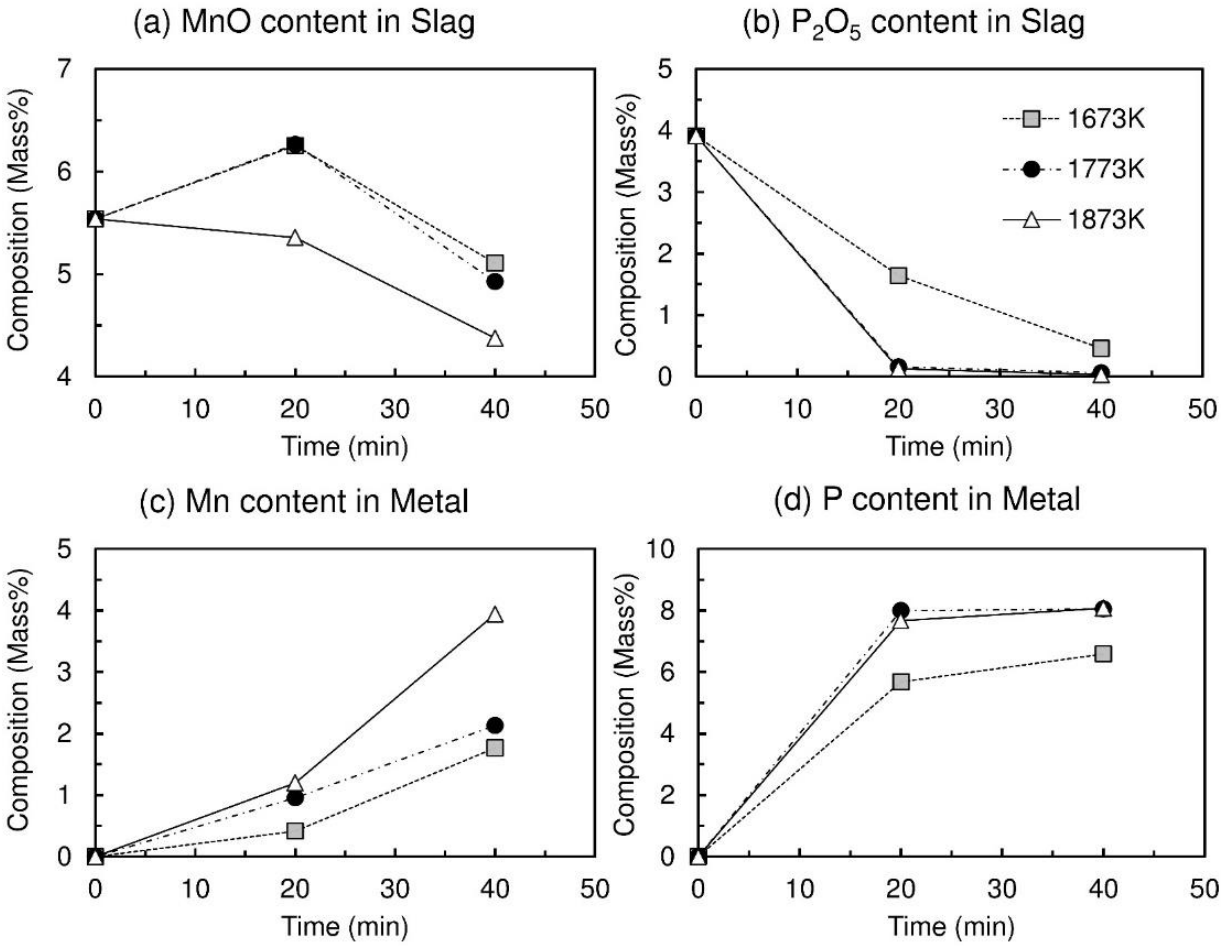

Fig. 2.8 The contents changes of P and Mn in each phase with reduction time by different reduction temperature (Slag D, graphite mixing ratio: 200%)

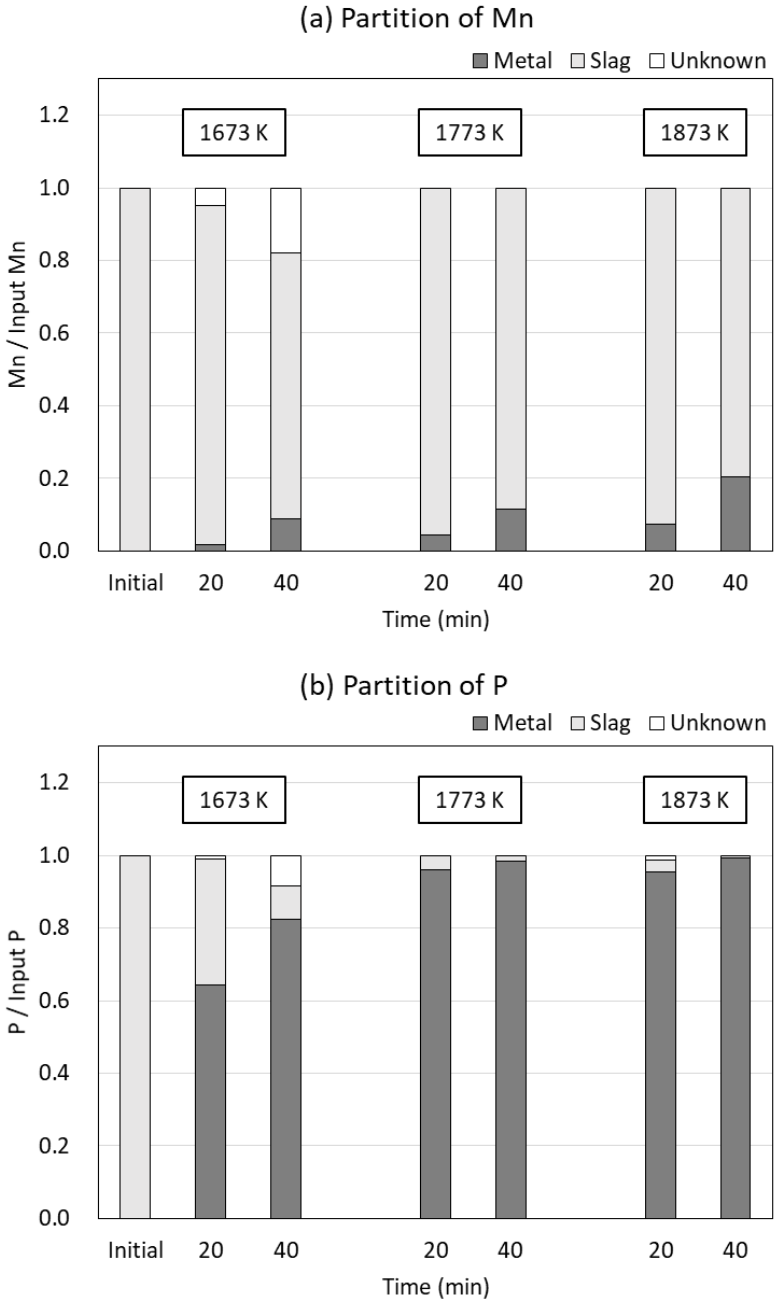

Fig. 2.9 The partitions of P and Mn with reduction time by different temperature

2.2.3 Influence of graphite mixing ratio

Fig. 2.10 illustrates the effect of graphite mixing ratio on the reduction behavior of Slag D. As the graphite mixing ratio changes, the reduction trend differs significantly. When the graphite mixing ratio decreases from 200% to 150%, the reduction of MnO is effectively suppressed during the initial period of reduction, but the reduction rate of P_2O_5 does not change much. The decreases in FeO and C concentrations in the metal are almost the same. On the other hand, when the graphite mixing ratio decreases to 100%, the reduction of FeO does not fully proceed and about 5 mass% of FeO remains in the slag even after 40 min. Furthermore, the carbon content is lower than that in the other conditions. Considering the difference of P content in the metal, in this case, the formed hot metal is not saturated with carbon. The content of P_2O_5 in the slag does not decrease much and the rate of increase of P in the metal is very low. In addition, the content of Mn in the metal does not increase. As the reduction behavior is much influenced by the mixing ratio of graphite, the reaction would mainly occur at the interface of slag and graphite powder.

2.2.4 Influence of different crucible (Al_2O_3, MgO)

Since, Al_2O_3 crucible was used, Al_2O_3 content in slag increased to about 30 mass % or more in the above experiments. Al_2O_3 is a neutral oxide in slag and lower the melting temperature. Therefore, to keep liquid state after the reduction of FeO, Al_2O_3 would have an important role. To clarify the effect of Al_2O_3, the experiments of Slag D and E were conducted using MgO crucible. The influence of crucible was summarized in **Fig. 2.11**. The considerable dissolution of MgO was also observed and the MgO content in slag reached about 25 mass % or more. Compared to the result of Al_2O_3 crucible, when MgO crucible was applied, the reduction rate of MnO was enhanced, but that of P_2O_5 was decreased a little. This behavior is similar to that by the increase in slag basicity. Based on the phase diagram of CaO-SiO_2-MgO [1] system, the liquid slag was formed during the experiment using MgO crucible. The difference of the crucible would be attributed to the slag basicity.

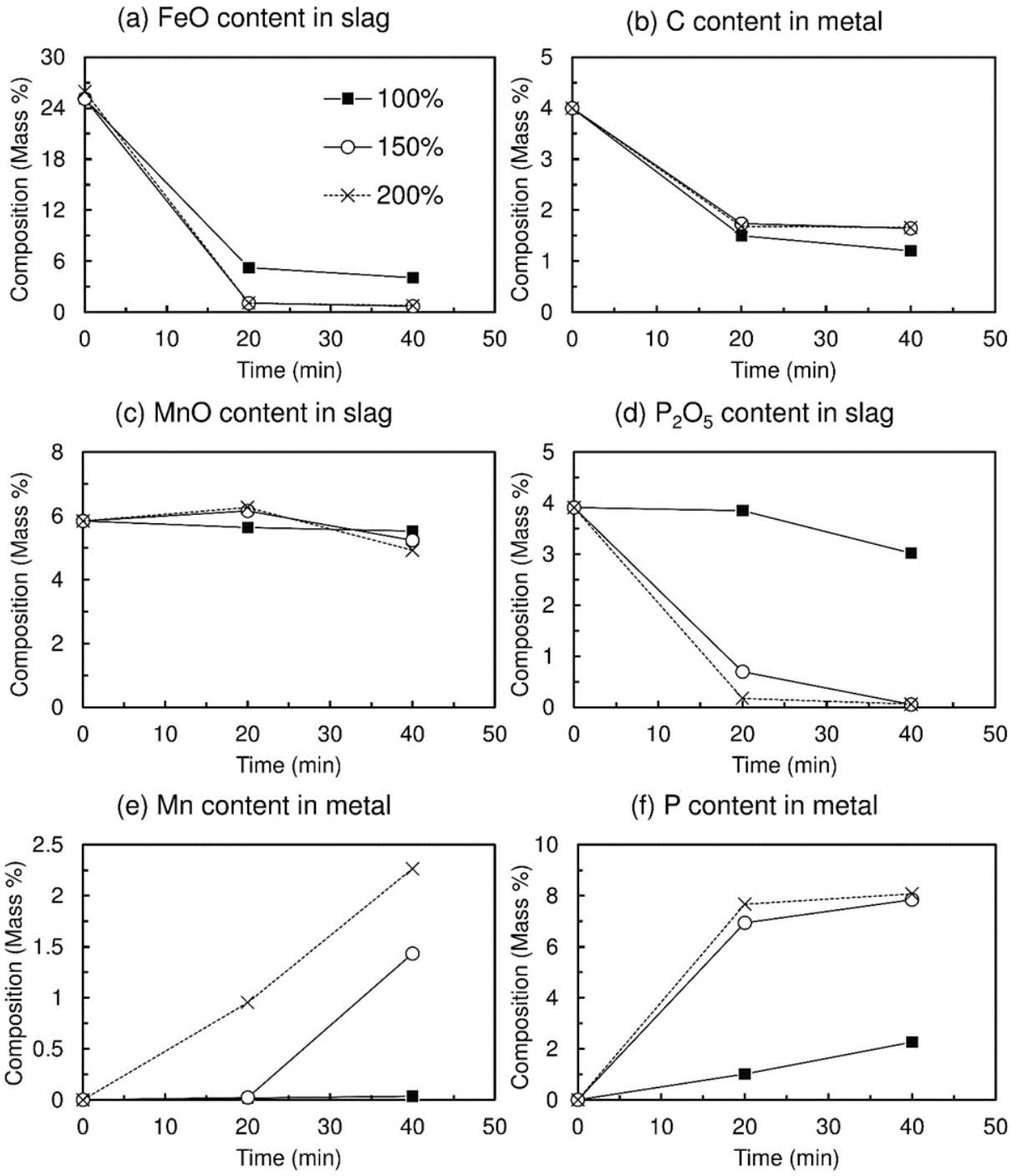

Fig. 2.10 The contents changes of P and Mn in each phase with reduction time by different graphite mixing ratio (Slag D, 1773K)

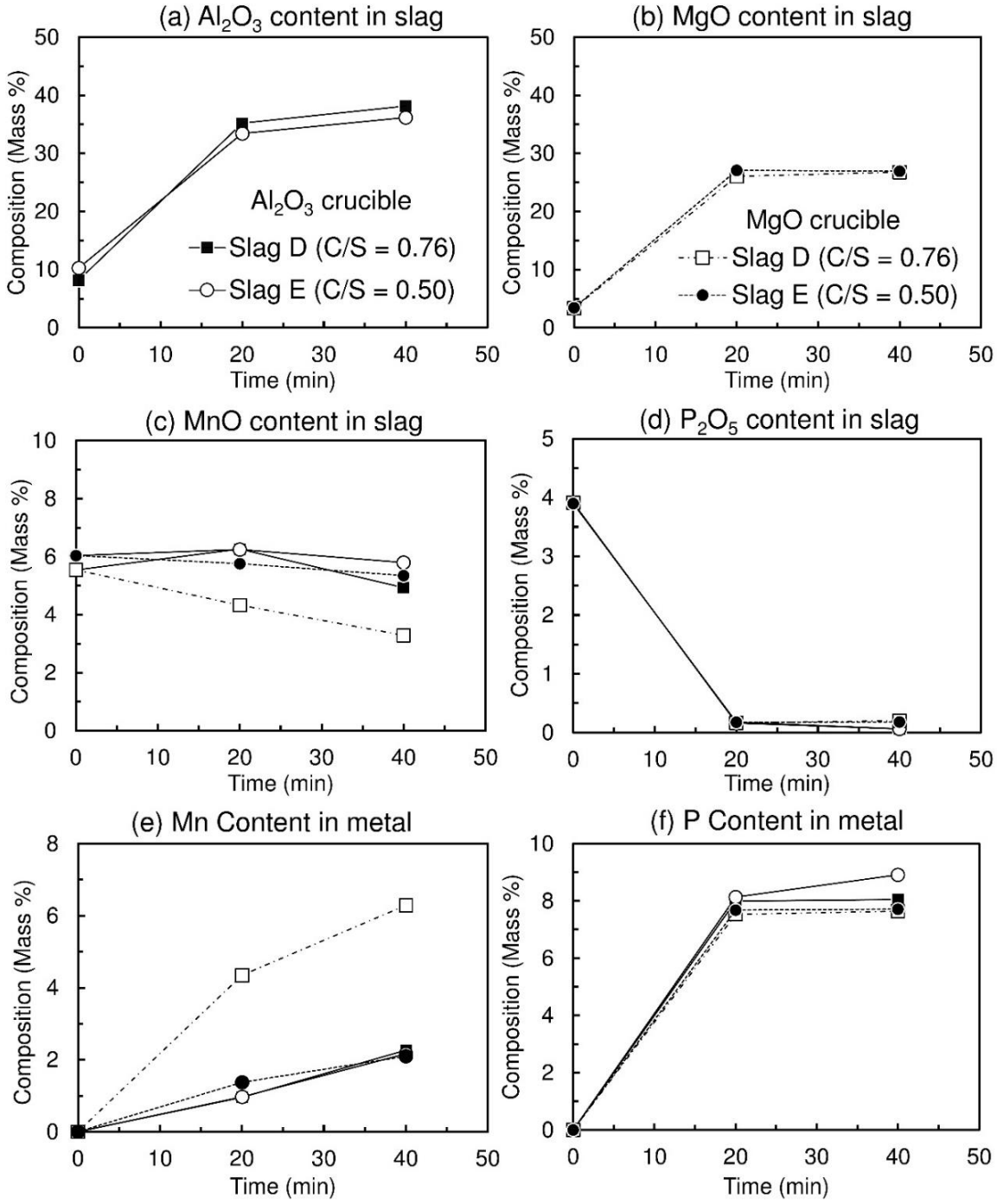

Fig. 2.11 The contents changes of P and Mn in each phase with reduction time by different crucible (1773K, graphite mixing ratio: 200%)

2.3 Discussion

In this experiment, although the mixture of solid slag and graphite were loaded in the crucible, the slag and the formed metal were liquid state from the early stage of the reduction. Therefore, except the very initial stage, most of the experimental period graphite powders floated on the surface of molten slag. In this case, the reduction of slag can occur at the interface of molten slag and graphite powders floating on the slag. According to the result which show the influence of mixing ratio of graphite (Fig. 2.10), the main reaction site can be considered as the interface of graphite powders floating on the slag surface.

The reduction rates of P and Mn (R; mol/s) are calculated and shown in **Fig. 2.12** in the case of Slag C. The reduction rate was calculated by Eq. (2.6) and (2.7).

$$R_P = (d\,W_P / M_P)/dt \quad \ldots\ldots\ldots\ldots (2.6)$$

$$R_{Mn} = (d\,W_{Mn} / M_{Mn})/dt \quad \ldots\ldots\ldots (2.7)$$

where, W is mass of P and Mn in metal (g) , M is atomic weight (g/mol), *t* is the reaction time (s). In this figure, the relation between the average reduction rates between each experimental time was plotted with the average experimental time. The reduction rate of P decreased with time, but that of Mn did not change much and lower than that of P. In most of the experiments, the reduction rate of Mn was low and the concentration change during the experiment was small. So, for the kinetic analysis, the reduction rate of P was used.

Fig. 2.13 shows the influence of P content in slag on the reduction rate. For this analysis, the results of Slag B and C were used as these slags showed the intermediate reduction rate. As the decrease in the P_2O_5 content in slag, the reduction rate decreased linearly. As the reduction occurred at the interface of floating graphite powder, mainly, the reduction rate was not affected by the P content in metal and the mass transfer of P_2O_5 in slag can be considered as a rate controlling step.

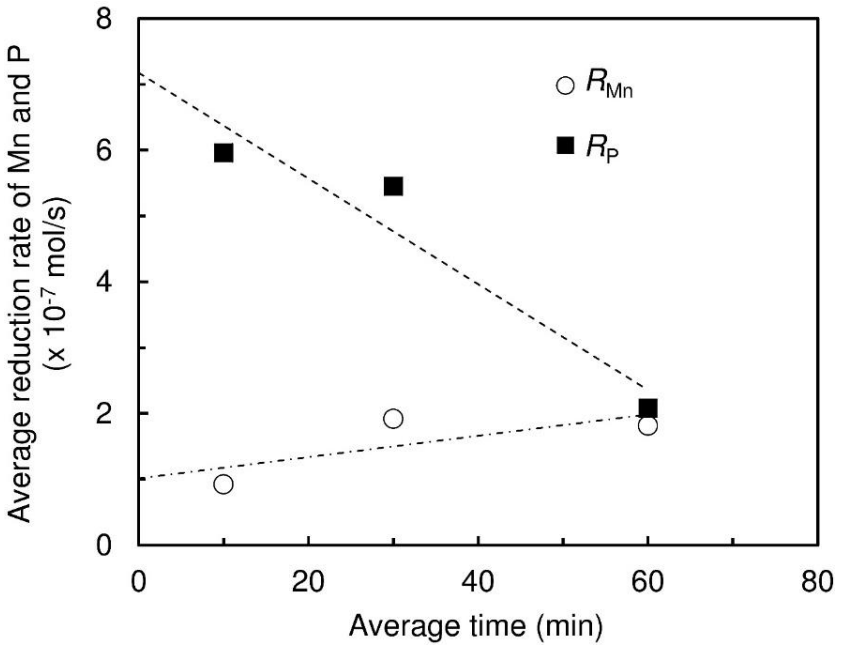

Fig. 2.12 The change of the reduction rates of P and Mn in slag C with time

(1773 K, graphite mixing ratio: 200%)

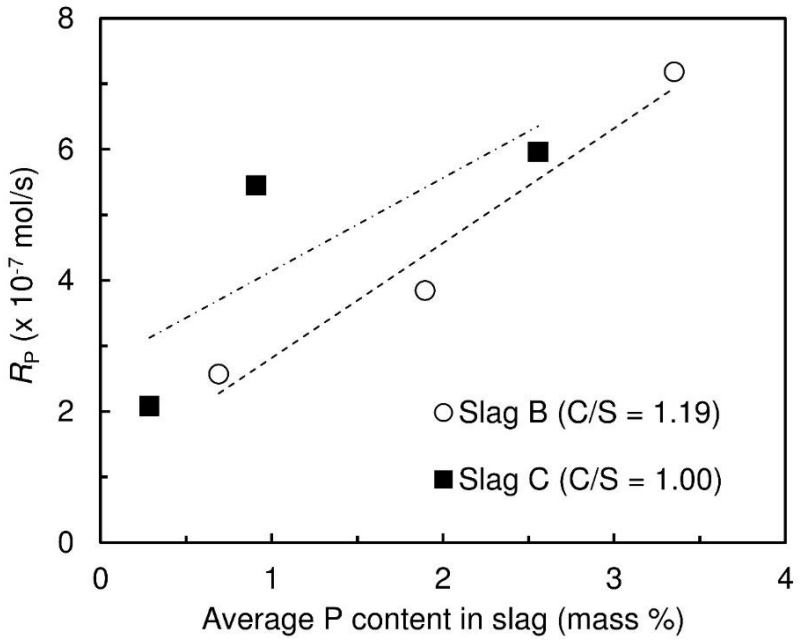

Fig. 2.13 Influence of P content in slag on the reduction rate of P

(1773 K, graphite mixing ratio 200%)

The decreasing rate of P in slag can be expressed as Eq. (2.8), where, k_P(1/min) is a rate constant. Through the relation shown in Fig. 2.13, k_P was evaluated and its temperature dependency was discussed.

$$d(\%P)/dt = R_P \times 60 \times M_P \times 100/W_{slag} = k_P\,(\%P) \quad \ldots\ldots\ldots (2.8)$$

As most of the reaction finished before 20 mins, the rate constant for each temperature was evaluated using the P content in slag during the initial 20 mins. The results are summarized in the form of Arrhenius equation as shown in **Fig 2.14** and the Eq. (2.9) was obtained.

$$\ln k_P = 2.1895/T + 10.11 \quad \ldots\ldots\ldots\ldots (2.9)$$

Using this equation, the activation energy was calculated as about 181kJ/mol. The activation energy of the diffusion of P in a molten slag with compositions of 40~43mass%CaO–30~35mass%SiO_2–21mass%Al_2O_3 is about 188 kJ/mol [2]. Therefore, the rate controlling step can be considered as the mass transfer in the slag phase.

Fig. 2.15 shows the influence of basicity on the reduction rate of P and Mn. The distribution ratio of each element (L) between slag and metal phase is calculated in Eq. (2.10) using the result at 20 mins. In these equations, (%X) and [%X] indicate the concentration of element X in slag and metal phase, respectively. The influence of basicity for each crucible is shown in **Fig. 2.16**.

$$L_P = (\%P)/[\%P],\ L_{Mn} = (\%Mn)/[\%Mn] \quad \ldots\ldots\ldots\ldots\ldots (2.10)$$

In the case of Al_2O_3 crucible, about the behavior of Mn as the increase in basicity, the reduction rate increased and the distribution ratio decrease. On the contrary, about the behavior of P, the opposite trends were found. When MgO crucible was used, the behavior of P was not changed much but the reduction rate of Mn increased, and the distribution ratio decreased. Therefore, for the selective reduction suppressing the reduction of MnO, the crucible made of neutral oxide (Al_2O_3) was favorable comparing with that made of basic oxide crucible (MgO).

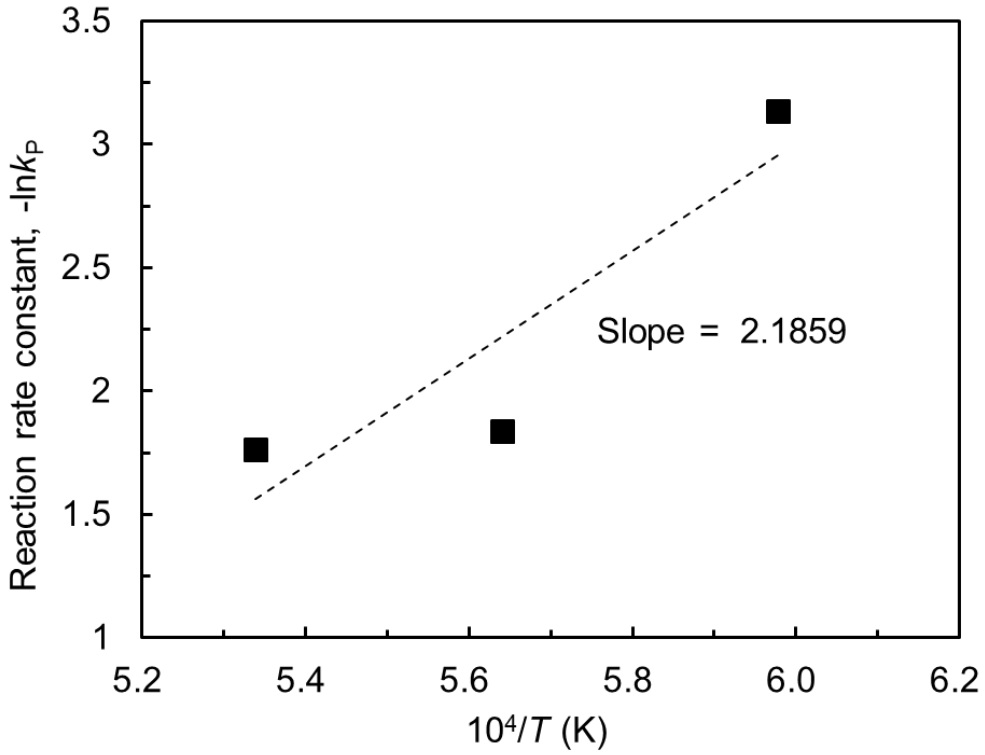

Fig. 2.14 Temperature dependence of the rate constant calculated by Eq. (2.8)

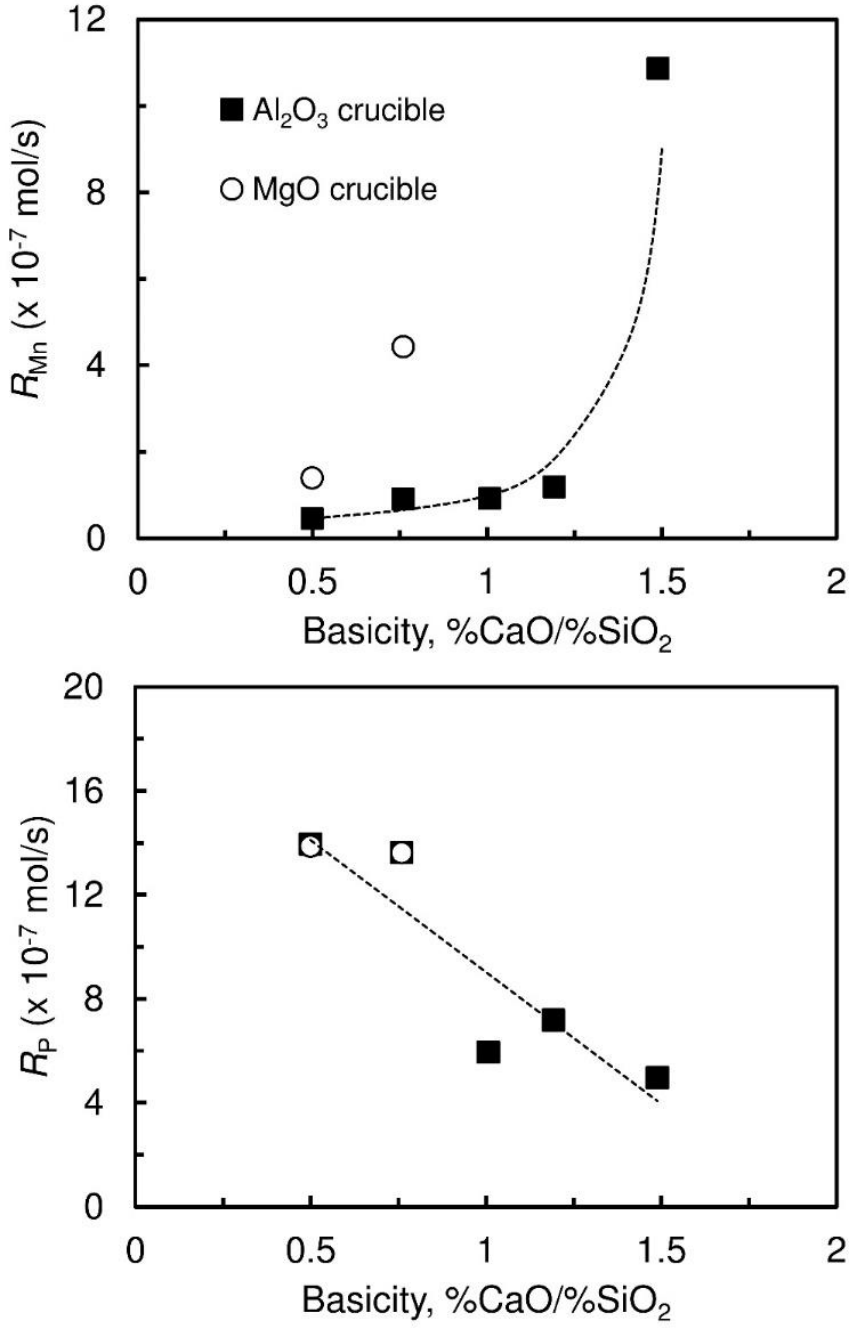

Fig. 2.15 The influence of basicity on the reduction rates of P and Mn

(1773 K, graphite mixing ratio 200%)

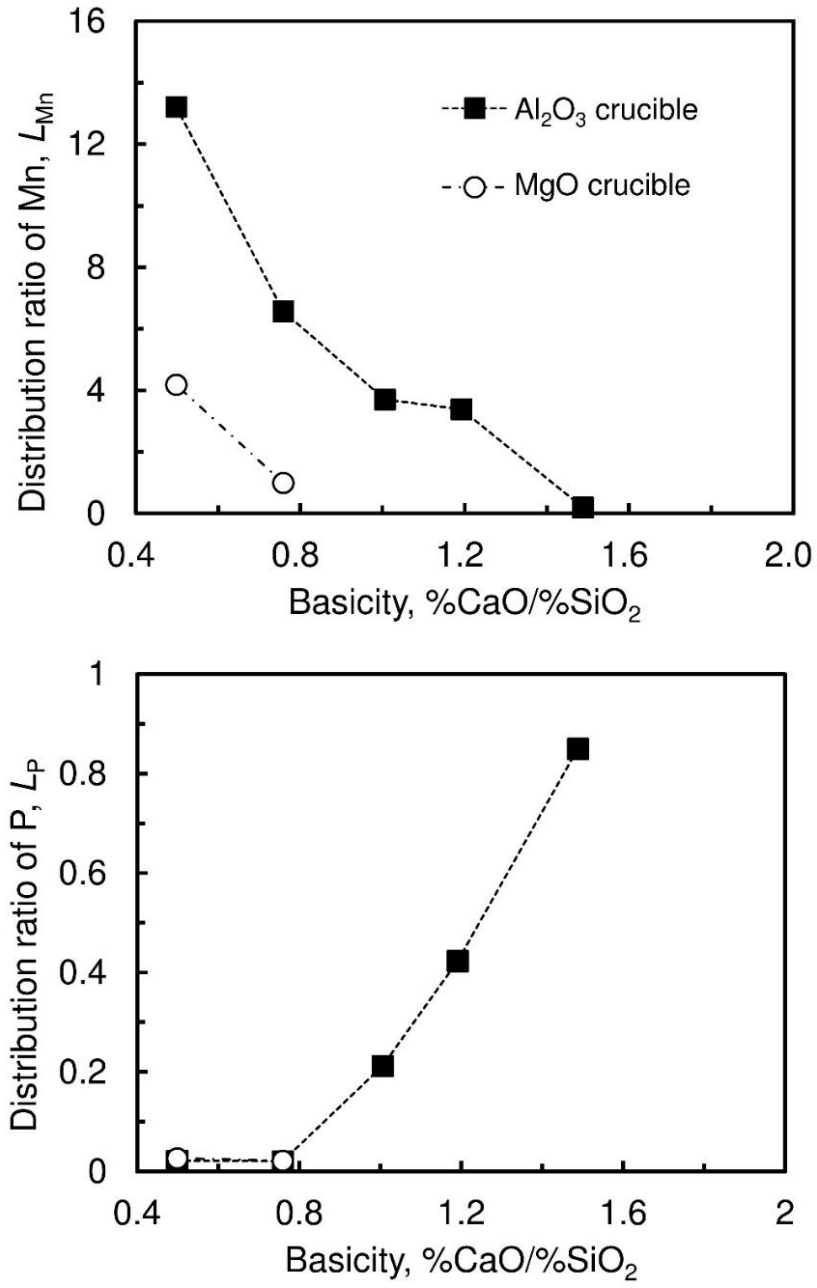

Fig. 2.16 The influence of basicity on the distribution ratio of P and Mn

The target value of distribution ratio for the selective reduction is considered. The assumed composition of typical industrial steelmaking slag is shown in **Table 2.2.** After the control the basicity of slag by SiO_2 addition, the selective reduction of this slag was calculated as a first step. As a second step, the reduction of the residual slag of the first step is calculated to produce ferromanganese alloy.

Table 2.2 Typical steelmaking slag composition (mass %)

FeO	CaO	SiO_2	P_2O_5	MnO	MgO	Al_2O_3
17.9	45.1	22.0	1.90	5.7	3.7	3.7

In the first step, 97% of FeO is assumed to be reduced, and the slag composition is calculated by changing the distribution ratios of P and Mn. In the second step, FeO, MnO and P_2O_5 in the residual slag is considered to be completely reduced and produce ferro-manganese alloy. In this case, the carbon concentration in the ferro-manganese alloy is assumed as 7.0%. The result is shown in **Fig. 2.17**. Since L_P and L_{Mn} obtained by the experiment are 0.02-0.085, 0.2-13 respectively, Mn concentration in the ferro-manganese is sufficiently high in this condition, but the concentration of P is estimated to be about 0.9%. As the limitation of P content in the high carbon ferro-manganese is generally about 0.2%, the target value of L_P should be 0.004 or less. This calculation indicates that the further improvement to suppress the reduction of P during the selective reduction is necessary.

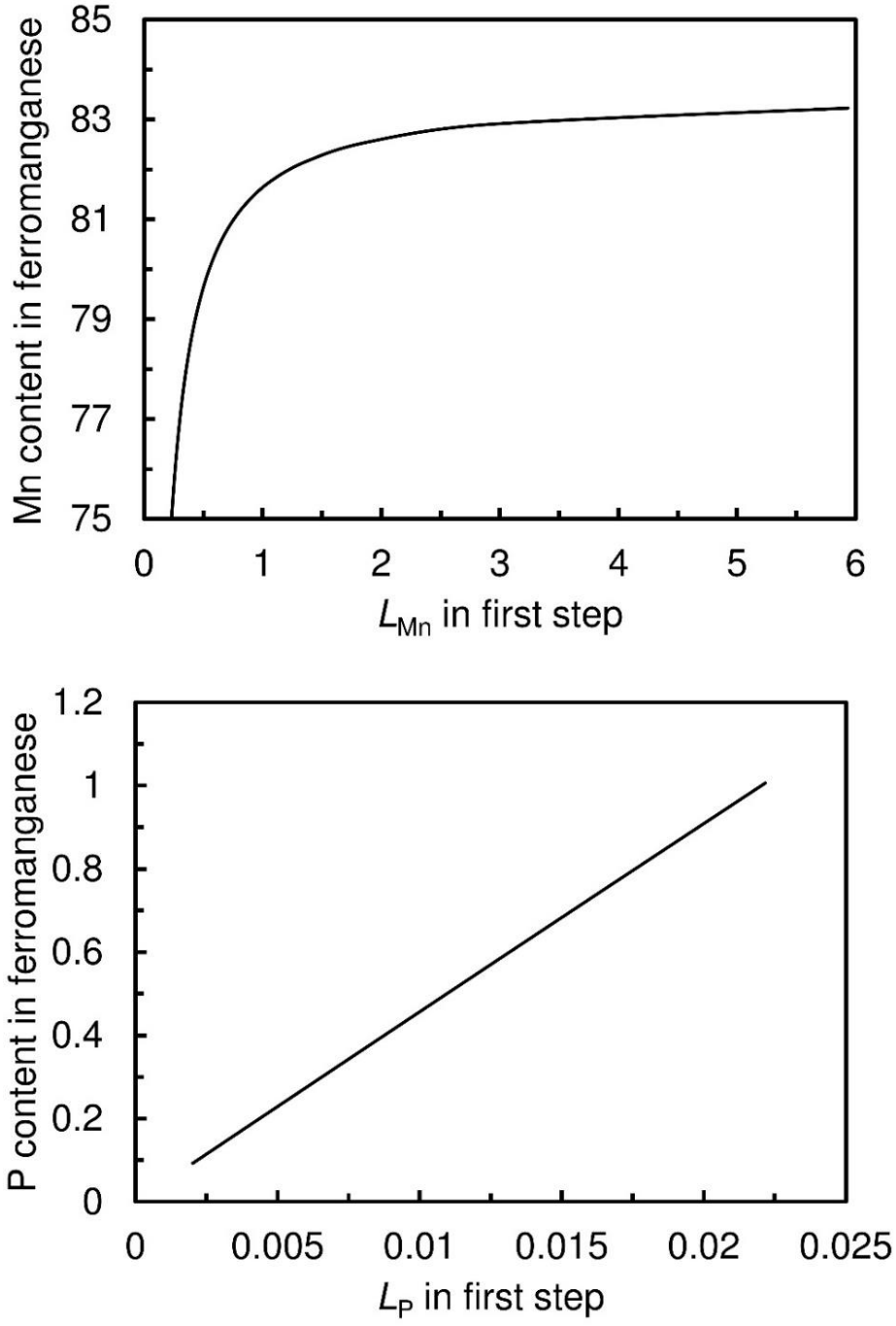

Fig. 2.17 The estimated content of P and Mn in ferromanganese alloy.

From equation (2.2) and (2.3), the relation between P and Mn is represented by equation (2.12).

$$2[P] + 5MnO(l) = 5[Mn] + P_2O_5(l) \quad \ldots\ldots\ldots\ldots\ldots \quad (2.12)$$

The equilibrium constant K of the reaction is represented by equation (2.13) [3,4].

$$\log K = \log\left(\frac{a_{Mn}^5}{a_P^2} \times \frac{a_{P_2O_5}}{a_{MnO}^5}\right) = \log\left(\frac{[\%Mn]^5}{[\%P]^2} \times \frac{f_{Mn}^5}{f_P^{\,2}} \times \frac{a_{P_2O_5}}{a_{MnO}^5}\right) = -16.17\ (1773\ K) \quad \ldots\ldots\ldots \quad (2.13)$$

If the activity of oxide in slag is calculated by the regular solution model [5], and the activity coefficient of the solute element in the molten metal is assumed as unity, the value of $[\%Mn]^{2.5}/[\%P]$ can be calculated. By using the experimental results of Slag D at 1773K after 20 mins reduction, the calculated value is about 0.03. However, this value obtained by the experiment is about 190, which does not agree at all. This means that the activity coefficient in dilute solution, which generally used to analyze steelmaking reactions, cannot be used for this system. It is necessary to measure the activity coefficients of P and Mn in high Mn high P molten metal.

2.4. Summary

In this study, as a fundamental study for selective reduction of P from steelmaking slag, the effect slag basicity, graphite mixing ratio, temperature and crucible type were conducted to find the optimum condition. The following conclusions were obtained from this study.

(1) Decreasing in slag basicity from 1.49 to 0.50 suppressed the reduction rate of Mn while enhanced the reduction rate of P. When slag basicity was lower than 0.76 at 1773K, the selective reduction of P was achieved.

(2) The influence of temperature on the reduction rate of P and Mn was investigated. By the relation between the rate constant for the reduction of P_2O_5 in slag and temperature, the activation energy was evaluated. The obtained value was close to the activation energy for diffusion of P in slag.

(3) The reduction behavior of FeO, MnO and P_2O_5 were influenced by the mixing ratio of graphite. The reduction reaction is considered to occur at the interface between slag and graphite powder mainly.

(4) By difference of crucible, the reduction rate and the distribution ratio of Mn was changed but those of P were not changed much.

2.5 Reference

1. Verein Deutscher Eisenhüttenleute: *Slag atlas 2nd Edition*., Verlag Stahleisen GmbH, Düsseldorf, 1995, Germany
2. The Japan Institute of Metals (2000) Metals Handbook, 6th edition, Maruzen, Tokyo, Japan [Japanese].
3. Turkdogan, E. T., & Pearson, J. (1953). Activities of constituents of iron and steelmaking slags. *Journal of the Iron and Steel Institute*, *12*, 398-402.
4. The Japan Society for the Promotion of Science, the 19th Committee on Steelmaking: *Steelmaking Data Sourcebook (Revised Edition)*, 1988, Gordon and Breach Science Publications, New York
5. Ban-Ya, S. (1993). Mathematical expression of slag-metal reactions in steelmaking process by quadratic formalism based on the regular solution model. *ISIJ international*, *33*(1), 2-11.

Chapter 3 Measurement of Activity Coefficient of P and Mn in Fe-P-Mn-C(sat.) alloy

In chapter 2, Fe and P were selectively reduced from steelmaking slag when the carbon reduction was performed at a high temperature (1773 K) and the slag basicity was adjusted to low values ($CaO/SiO_2 < 0.76$). This process was used to obtain the Fe-P-Mn-C (sat.) alloy with a high content of P (up to 9 mass %), a low content of Mn (up to 2 mass %), and an oxide residue with high contents of MnO and low P_2O_5. In discussion, the distribution ratio of P and Mn between alloy and slag were estimated by using a regular solution model to calculate the activities of oxides and by assuming the activity coefficients of solute elements in the alloy as unity. However, significant differences existed between the values obtained in the calculations and those obtained in the experiments. This was potentially because the activity coefficients of P and Mn in the Fe-P-Mn-C (sat.) alloy were not properly evaluated.

Table 3.1 lists several reported expressions for the activity coefficients of P and Mn and the interaction parameters between P and Mn [1-7]. As shown in the table, the applicable composition range of these thermodynamic data are not significantly suitable for the alloy system that is obtained from the selective reduction process as previously mentioned. Additionally, differences exist in the interaction parameters obtained via different measuring methods. Therefore, it is necessary to measure the activities of P and Mn in the Fe-Mn-P-C (sat.) alloy, and this specifically holds when the content of P is high. Furthermore, the activities of P and Mn in this type of alloy system are important for the selective reduction process of steelmaking slag and also useful in the reduction process of Mn ore to produce ferromanganese alloy.

Therefore, in the chapter 3, the activity coefficients of P and Mn in the Fe-P-Mn-C(sat.) alloy (2.5 < [mass % P] < 15.2, 2.9 < [mass % Mn] < 12.8) were measured by equilibrating the Fe-P-Mn-C(sat.) alloy with Ag at 1673 K.

Table 3.1 Reported equilibrium data for P and Mn in Fe-based alloy system

Alloy system (Temp.)	Activity coefficients of P and Mn in the alloy system		Interaction parameter	Ref.
	P	Mn		
Fe-P (1573–1873 K)	$\log\psi_{\mathrm{P}} = 0.982X_{\mathrm{P}}$ ($0 < X_{\mathrm{P}} < 0.33$)	-	-	[1]
	$\log\psi_{\mathrm{P}} = -2.32 + 7.96X_{\mathrm{P}}$ ($0.33 < X_{\mathrm{P}} < 0.5$)	-	-	
Fe-P-C(sat.) (1773 K)	$\log\gamma_{\mathrm{P}} = 1.85X_{\mathrm{P}} + 1.85X_{\mathrm{P}}^2 + 3.21X_{\mathrm{P}}^3 + 2.05X_{\mathrm{C}} + 2.05X_{\mathrm{C}}^2 + 2.34X_{\mathrm{C}}^3 + 7.33X_{\mathrm{P}}X_{\mathrm{C}}$ ($X_{\mathrm{P}} < 0.33$, $X_{\mathrm{C}} < 0.17$)	-	-	
Fe-P-C (C: up to sat.) (1673 K)	$\log\gamma_{\mathrm{P}} = 1.41X_{\mathrm{P}} + 1.41X_{\mathrm{P}}^2 + 1.70X_{\mathrm{P}}^3 + 2.36X_{\mathrm{C}} + 2.36X_{\mathrm{C}}^2 + 2.65X_{\mathrm{C}}^3 + 3.77X_{\mathrm{P}}X_{\mathrm{C}}$ ($X_{\mathrm{C}} < 0.12$)	-	-	[2]
Fe-Mn-C (C: up to sat.) (1736-1823 K)	-	$\log\psi_{\mathrm{Mn}} = (-15830/T + 7.93)y_{\mathrm{C}} + (-23980/T + 15.24)y_{\mathrm{Mn}}y_{\mathrm{C}} + (96920/T + 59.32)y_{\mathrm{C}}^2$ ($0.15 < X_{\mathrm{Mn}} < 0.45$)	-	[3]
Fe-Mn-C(sat.) (1813 K)	-	$\log\gamma_{\mathrm{Mn}} = e^{-2.3\times3X_{\mathrm{Mn}}X_{\mathrm{C}}/(1-X_{\mathrm{C}})^2}$ ($X_{\mathrm{Mn}} < 0.3$)	-	[4]
Fe-P-Mn (1673 K)	$\log\gamma_{\mathrm{P}} = 1.41X_{\mathrm{P}} + 1.41X_{\mathrm{P}}^2 + 1.70X_{\mathrm{P}}^3 - 3.11X_{\mathrm{Mn}} - 3.11X_{\mathrm{P}}X_{\mathrm{Mn}}$ ($X_{\mathrm{Mn}} < 0.23$)	-	$\varepsilon_{\mathrm{P}}^{\mathrm{Mn}} = -7.17 \pm 1.16$ ($e_{\mathrm{P}}^{\mathrm{Mn}} = -0.032 \pm 0.005$)	[5]
Fe-P-Mn (1788–1923 K)	-	-	$\varepsilon_{\mathrm{P}}^{\mathrm{Mn}} = 0$	[6]
Fe-P-Mn-C(sat.) (1573–1673 K)	$\log f_{\mathrm{P}} = -0.0029[\%\mathrm{Mn}] - 386/T + 0.891$ ([%P] < 1.0)	-	$e_{\mathrm{P,\,C\ sat.}}^{\mathrm{Mn}} = -0.0029$	[7]

Chapter 3

3.1 Principle for measuring the activity coefficients of P and Mn in Fe-P-Mn-C(sat.) alloy

When the Fe-P-Mn-C (sat.) alloy is equilibrated with Ag, the activity of Mn (a_{Mn}) between the two metal phases is expressed as shown in Eq. (3.1) by using pure Mn as a reference. Given that Eq. (3.1) is expressed as Eq. (3.2), if the activity coefficient of Mn in Ag is known, then the activity coefficient of Mn in the Fe-P-Mn-C(sat.) alloy is obtained by using the measured equilibrium contents of Mn in the alloy and Ag. Therefore, Eq. (3.3) as proposed by H. Schenck *et al* [8]. is used to calculate the activity coefficient of Mn in Ag. Here, X_{Mn} denotes the mole fraction of Mn in the metal phases; X_{Ag} denotes the mole fraction of Ag in the Ag phase; γ_{Mn} denotes the Raoultian activity coefficient of Mn in the metal phases; and *T* denotes temperature in Kelvin. To calculate the activity coefficient of Mn in Ag, Eq. (3.3) is used as follows;

$$a_{\mathrm{Mn\ [in\ Fe-P-Mn-C\ (sat.)]}} = a_{\mathrm{Mn\ [in\ Ag]}} \quad \text{..... (3.1)}$$

$$\gamma_{\mathrm{Mn\ [in\ Fe-Mn-P-C\ (sat.)]}} = (X_{\mathrm{Mn\ [in\ Ag]}}/X_{\mathrm{Mn\ [in\ Fe-Mn-P-C\ (sat.)]}})\gamma_{\mathrm{Mn\ [in\ Ag]}} \quad \text{.... (3.2)}$$

$$\gamma_{\mathrm{Mn\ [in\ Ag]}} = (^{33300}/_{T} - 14.46)X_{\mathrm{Ag}}^{2} + (^{39400}/_{T} - 16.73)X_{\mathrm{Ag}}^{3} \quad \text{..... (3.3) [8]}$$

By using the references of dilute solutions of Fe and Ag, the distribution reaction of P between the Fe-P-Mn-C(sat.) alloy and Ag is expressed as shown in Eq. (3.4). This is different from the case of Mn since the dilute solution is used as the reference state as opposed to a pure substance. This is because the pure substance for phosphorus typically corresponds to P_2 gas and fugacity is presented. Therefore, the use of a dilute solution is more convenient for calculation purposes.

$$\mathrm{P\ (in\ Fe\text{-}P\text{-}Mn\text{-}C(sat.)}, X) = \mathrm{P\ (in\ Ag}, X) \quad \log K = -7184/T + 0.54 \text{..... (3.4) [1]}$$

$$\ln\gamma^{\mathrm{H}}_{\mathrm{P\ [in\ Fe-P-Mn-C\ (sat.)]}} = \left(X_{\mathrm{P\ [in\ Ag]}}/X_{\mathrm{P\ [in\ Fe-P-Mn-C\ (sat.)]}}\right)K^{-1} \quad \text{..... (3.5)}$$

Based on Henry's law, the activity coefficient is unity for an infinite dilute solution. As the content of P in Ag is extremely low, the activity coefficient of P in Ag can be assumed as unity, and subsequently the equilibrium constant K of Eq. (3.4) is rearranged as Eq. (3.5). Therefore, the activity coefficient of P in the alloy is determined by measuring the equilibrium distribution of P between the alloy and Ag. Here, $\ln\gamma^{\mathrm{H}}_{\mathrm{P\,[in\,Fe-P-Mn-C\,(sat.)]}}$ denotes the Henrian activity coefficient of P in the alloy; and X_{P} denotes the mole fraction of P in metal phases.

Based on the aforementioned principles, the activity coefficients of both P and Mn in the alloy are simultaneously determined by equilibrating it with Ag. It should be noted that the interaction between P and Mn in Ag can affect the results. However, this interaction is not considered in the calculation because the interaction parameter between P and Mn in Ag is not available.

3.2 Experimental method

3.2.1 Raw materials

To prepare the Fe-P-Mn-C(sat.) alloy, reagent grade metallic Fe, metallic Mn, Fe_3P, and graphite powder were mixed in various ratios, and they were melted in carbon crucibles under an Ar atmosphere at 1673 K for 1 h. The temperature of the hot zone in the furnace was calibrated before loading the samples. Subsequently, the crucible and molten alloy were withdrawn and quenched via a He gas spray. Prior to the melting, a few additional graphite powders were added at the surface of the mixture to ensure carbon saturation and to prevent surface oxidation during cooling. After quenching, each prepared alloy was crashed into briquettes, and its composition was analyzed via inductively coupled plasma-atomic emission spectrometry (ICP-AES). The composition range for P and Mn in the

alloy prior to the equilibrium experiments corresponded to 2 ~ 15 mass % and 5 ~ 20 mass %, respectively. With respect to the Ag, high purity Ag (99.99 %) was used, and the Ag was also analyzed by ICP-AES prior to the equilibrium experiments to confirm that both P and Mn were not present as impurities.

3.2.2 Equilibrium experiment

The experimental apparatus is shown in **Fig. 3.1**. In each experiment, 4 g of Ag and 2 g of the prepared alloy briquettes were installed in a carbon crucible, and the surface of loaded metals was covered with a few additional graphite powders as per the previously mentioned reason. Subsequently, the alloy and Ag were reacted until equilibrium under the Ar atmosphere at 1673 K.

After reaching an equilibrium, the crucible and metal sample were carefully removed and cooled by the He gas spray with a low flow rate to minimize suspensions in either the alloy or Ag phase. After cooling, the alloy and Ag samples away from the interface were cut and polished, and subsequently the P and Mn contents in both phases were analyzed by ICP-AES. Additionally, the C content of alloy sample was measured via a combustion infrared spectrometer (CIP).

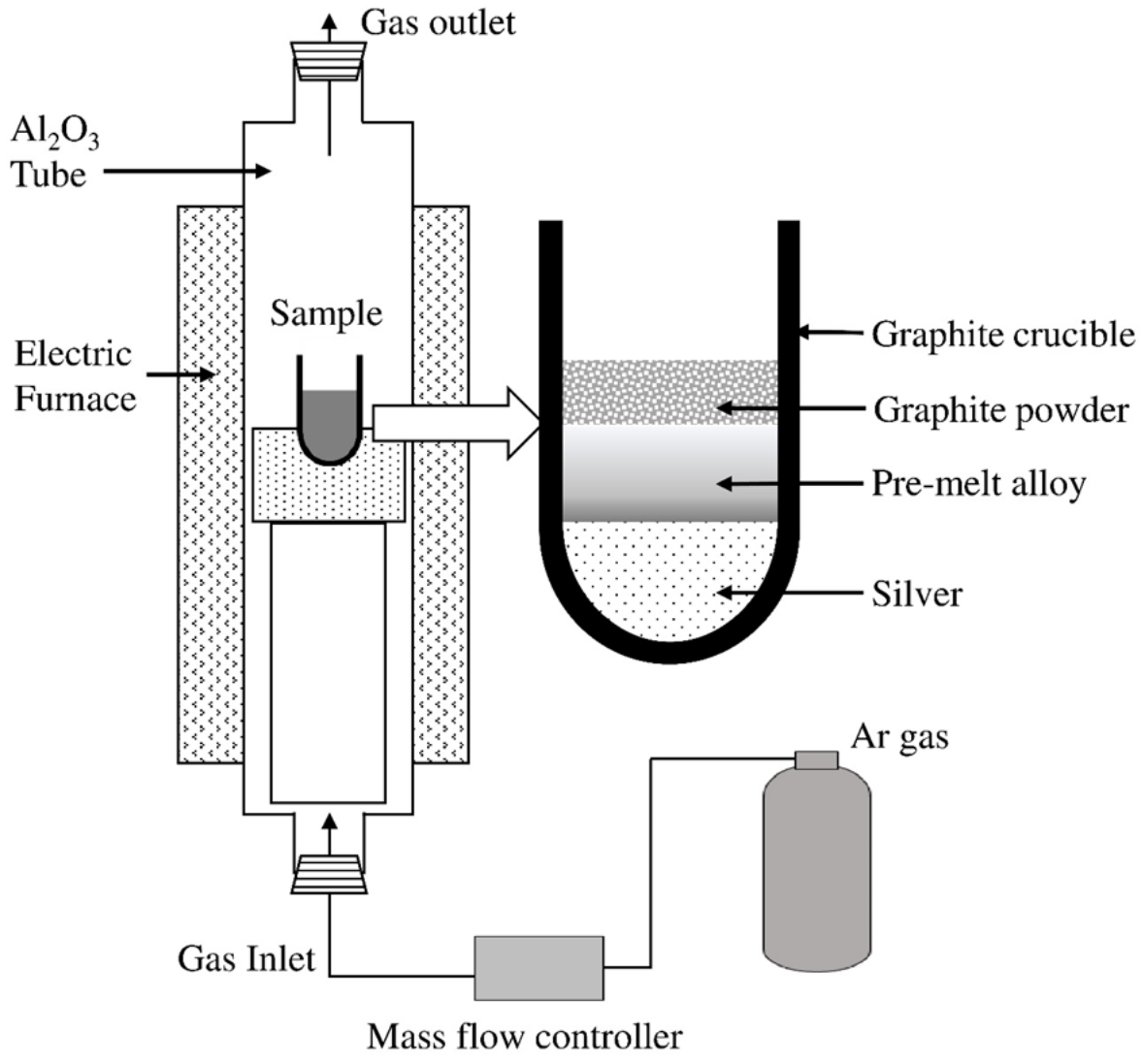

Fig. 3.1 Experimental setup

3.3 Results and Discussion

Fig 3.2 illustrates determination of equilibrium time. The reaction time to reach the equilibrium was measured via preliminary experiments in which the P and Mn contents in alloy and Ag became stable after 2 ~ 3 hours. Therefore, the equilibrium time was set as 4 hours. Furthermore, the weight losses after different reaction times were also measured, and the results indicated that the weight loss was low and negligible under the experimental conditions in the current study. This indicated that the gasification of P, Mn and Ag during the high temperature reaction did not significantly affect the results.

The equilibrium compositions of P and Mn in the alloy and Ag are summarized in **Table 3.2**. The P and Mn contents in the alloy vary from 2.5 mass % to 15.2 mass % and 2.9 mass % to 12.8 mass%, respectively. The observed Mn content in the alloy increases with increases in the P content. In the Ag, the Mn content is approximately 1000 times that of P. Therefore, the equilibrium Ag phase is considered as Ag–Mn binary, and the effect of P on the activity coefficient of Mn in Ag appears as less significant and can be potentially neglected. Furthermore, the P content in Ag is extremely low, and thus the assumption wherein the Henrian activity coefficient of P in Ag corresponds to unity appears reasonable. Nevertheless, given the high difference in the contents of P and Mn in Ag, the interaction between P and Mn in Ag (as mentioned in section 3.2) can be potentially ignored and does not significantly affect the results.

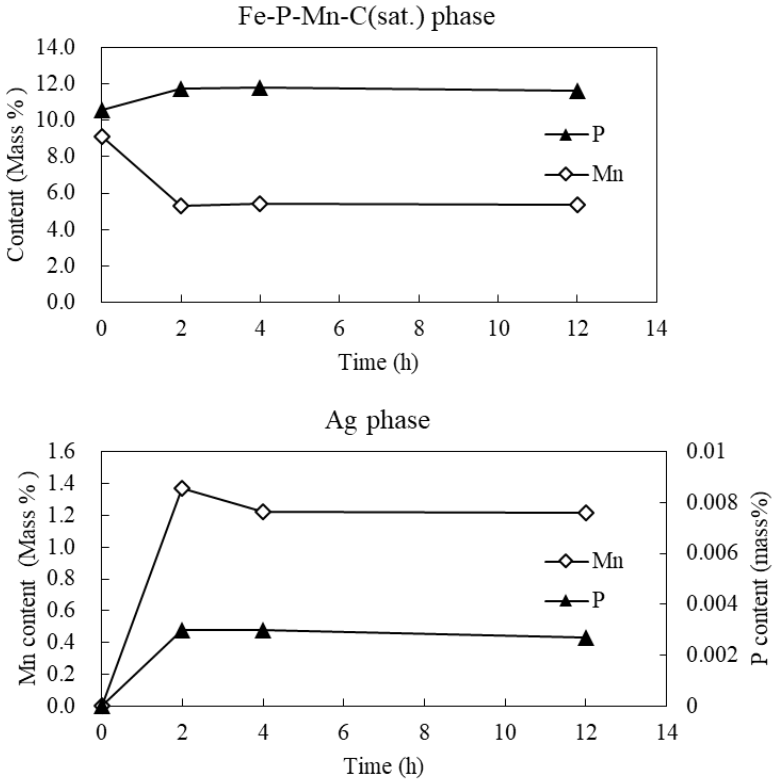

Fig. 3.2 Determination of equilibrium time

Table 3.2 Equilibrium chemical compositions of the Fe-P-Mn-C(sat.) alloy and Ag

No.	Fe-P-Mn-C(sat.) alloy						Ag			
	[%Mn]	[%P]	[%C]	X_{Mn}	X_P	X_C	[%Mn]	[%P]	X_{Mn}	X_P
1	2.88	9.70	1.81	2.6E-02	1.5E-01	7.4E-02	0.94	1.0E-03	1.8E-02	3.6E-05
2	4.55	2.51	3.90	4.0E-02	3.9E-02	1.6E-01	1.66	5.9E-04	3.2E-02	2.0E-05
3	5.13	5.54	2.96	4.5E-02	8.7E-02	1.2E-01	1.76	1.2E-03	3.4E-02	4.1E-05
4	5.15	11.62	1.52	4.6E-02	1.8E-01	6.1E-02	1.21	2.3E-03	2.3E-02	8.1E-05
5	6.34	15.16	1.03	5.6E-02	2.4E-01	4.1E-02	1.32	1.4E-02	2.6E-02	4.9E-04
6	8.47	11.31	1.79	7.4E-02	1.8E-01	7.2E-02	2.41	3.7E-03	4.6E-02	1.2E-04
7	12.81	11.26	1.81	1.1E-01	1.8E-01	7.3E-02	3.63	9.3E-03	6.9E-02	3.1E-04

3.3.1 Activity coefficient of Mn in the Fe-P-Mn-C(sat.) alloy

By using the data shown in Table 3.2, the activity coefficient of Mn in the Fe-P-Mn-C(sat.) alloy ($\gamma_{\text{Mn [in Fe−P−Mn−C(sat.)]}}$) at 1673 K is calculated, and its relationship with the mole fraction of P in alloy is shown in **Fig. 3.3**. In this figure, the activity coefficient of Mn for the Fe-Mn-C(sat.) ternary system is also plotted from references [4, 9]. The aforementioned reported data are measured at different temperatures. Thus, a conversion is performed by using Eq. (3.6) as follows:

$$RT\ln\gamma = constant \quad \text{..... (3.6)}$$

As presented in Fig. 3.3, the activity coefficient of Mn in Fe-P-Mn-C(sat.) alloy decreases linearly with increases in the P content, and the linear relation is maintained when X_{Mn} is lower than 0.06. Additionally, the interception of the linear relation is close to the activity coefficient of Fe-Mn-C(sat.) alloy as reported by Ohtani *et al.* [4]. Therefore, within a composition range of $0 < X_{\text{Mn}} < 0.06$, a linear expression of the $\gamma_{\text{Mn [in Fe−P−Mn−C(sat.)]}}$ that uses the first order of interaction parameters is expressed as shown in Eq. (3.7).

$$\ln\gamma_{\text{Mn [in Fe−P−Mn−C(sat.)]}} = \ln\gamma^{0}_{\text{Mn, C sat.}} + \varepsilon^{\text{C}}_{\text{Mn}}X_{\text{C}} + \varepsilon^{\text{Mn}}_{\text{Mn}}X_{\text{Mn}} + \varepsilon^{\text{P}}_{\text{Mn}}X_{\text{P}} \quad \text{..... (3.7)}$$

Here, $\gamma^{0}_{\text{Mn, C sat.}}$ denotes the activity coefficient of Mn in C saturated alloy, and a reported value of 0.42 is used [4]. Additionally, $\varepsilon^{i}_{\text{Mn}}$ denotes the interaction parameter of element *i* with respect to Mn in the C saturated alloy, and the values used in the calculation are summarized in **Table 3.3**. Furthermore, X_{C} and X_{P} denote the measured C solubility and P content of the Fe-P-Mn-C(sat.) alloy, respectively.

Table 3.3 Interaction parameters of C saturated alloy used in the calculation

$\varepsilon_{\mathrm{Mn}}^{\mathrm{C}}$	-0.47	M. Ohtani *et al.* [4]
$\varepsilon_{\mathrm{Mn}}^{\mathrm{Mn}}$	0	M. Hino and K. Ito [10]
$\varepsilon_{\mathrm{P}}^{\mathrm{P}}$	4.26	S. Banya *et al.* [1]

Eq. (3.8) is obtained by rearranging Eq. (3.7), and the relation between the right side and left side of the equation is calculated by using experimental data as shown in **Fig. 3.4**.

$$\ln\gamma_{\mathrm{Mn\ [in\ Fe-P-Mn-C\ (sat.)]}} - \ln\gamma_{\mathrm{Mn,\ C\ sat.}}^{0} - \varepsilon_{\mathrm{Mn}}^{\mathrm{C}} X_{\mathrm{C}} = \varepsilon_{\mathrm{Mn}}^{\mathrm{P}} X_{\mathrm{P}} \quad \ldots\ldots\ldots\ldots\ldots\ldots\ldots \quad (3.8)$$

As shown in Fig. 3.4, a linear regression is obtained by fixing the interception as zero, and the $\varepsilon_{\mathrm{Mn}}^{\mathrm{P}}$ in Fe-P-Mn-C(sat.) alloy is obtained from the slope. The value is expressed as follows:

$$\varepsilon_{\mathrm{Mn}}^{\mathrm{P}} = -4.72 \pm 0.27, (X_{\mathrm{Mn}} < 0.06, X_{\mathrm{P}} < 0.25, 1673\ \mathrm{K}) \quad \ldots\ldots\ldots\ldots\ldots\ldots\ldots \quad (3.8)$$

As shown in **Table 3.1**, Ban-ya *et al.* [5] report that the $\varepsilon_{\mathrm{Mn}}^{\mathrm{P}}$ at 1673 K corresponds to -7.17±1.16 up to a Mn mole fraction of 0.23 in the Fe-P-Mn alloy. Schenck *et al.* [6] obtain the $\varepsilon_{\mathrm{Mn}}^{\mathrm{P}}$ as zero in the range of 1788 K–1923 K. Shim *et al.* [7] reveal that the $\varepsilon_{\mathrm{Mn}}^{\mathrm{P}}$ in a C saturated system is -0.64 ($e_{\mathrm{P,C\ sat.}}^{\mathrm{Mn}} = -0.0029$) at 1573 K–1673 K. A comparison with the aforementioned extant studies indicates that the value of $\varepsilon_{\mathrm{Mn}}^{\mathrm{P}}$ measured in the study is close to that obtained by Banya *et al*., and the differences in the reported values is attributed to the differences in experimental method. By using the measured $\varepsilon_{\mathrm{Mn}}^{\mathrm{P}}$ and the interaction parameters shown in Table 3.3, the activity coefficient of Mn in Fe-P-Mn-C (sat.) alloy are derived as shown in Eq. (3.9):

$$\ln\gamma_{\mathrm{Mn\ [in\ Fe-P-Mn-C(sat.)]}} = -4.72X_{\mathrm{P}} - 0.47X_{\mathrm{C}} - 0.87 \ (X_{\mathrm{Mn}} < 0.06, X_{\mathrm{P}} < 0.25, 1673\ \mathrm{K}) \ldots\ldots \quad (3.9)$$

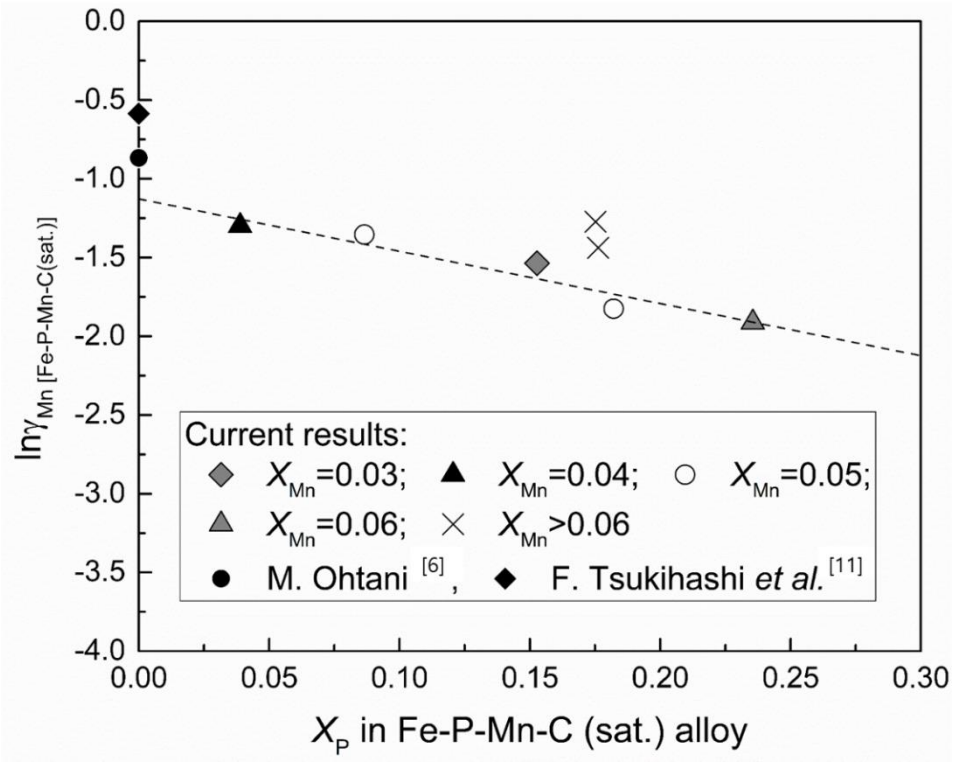

Fig. 3.3 Calculated activity coefficient of Mn in Fe-P-Mn-C(sat.) alloy

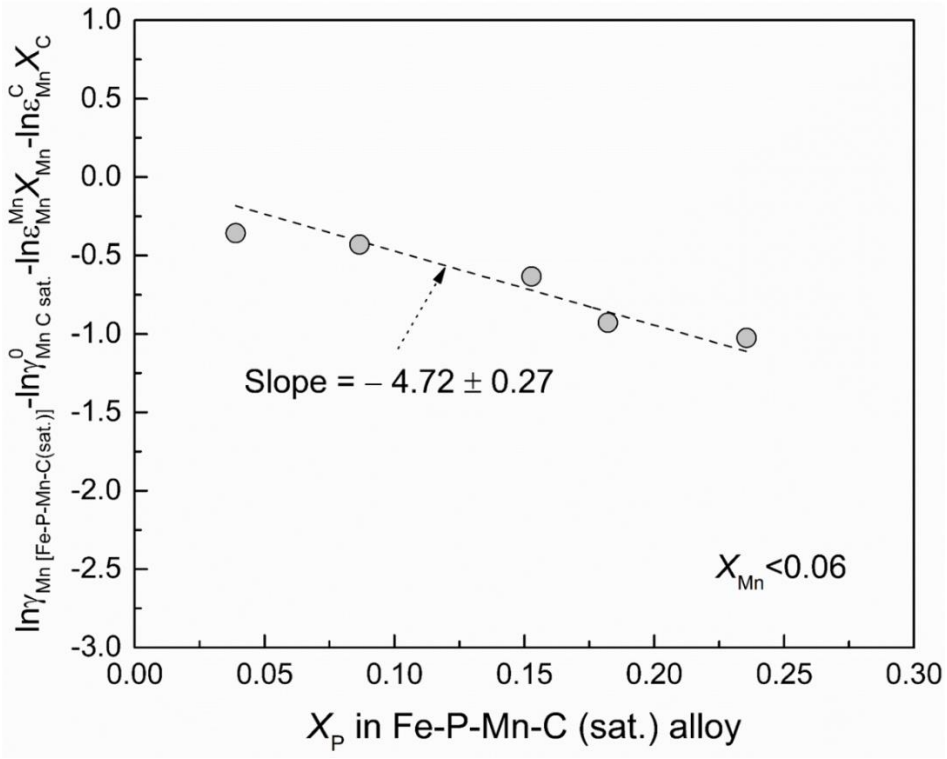

Fig. 3.4 Measured interaction parameter between P and Mn in C saturated alloy

3.3.2 Carbon solubility in the Fe-P-Mn-C(sat.) alloy

Current experiments are conducted under C saturation condition, and thus the activity of C corresponds to unity. Subsequently, the activity coefficient of C is expressed as shown in Eq. (3.10). Therefore, the interaction parameter between P and C is defined in Eq. (3.11) as follows:

$$\gamma_{\mathrm{C}} = \frac{1}{X_{\mathrm{C}}} \quad \text{…….} \quad (3.10)$$

$$\varepsilon_{\mathrm{C}}^{\mathrm{P}} = \frac{\partial \ln \gamma_{\mathrm{C}}}{\partial X_{\mathrm{P}}} \quad \text{…….} \quad (3.11)$$

Fig. 3.5 shows the relationship between the activity coefficient of C and mole fraction of P in Fe-P-Mn-C(sat.) alloy. A linear regression is obtained while fixing the interception by the C solubility in the Fe-Mn-C(sat.) alloy from reference data [4]. Therefore, the interaction parameter $\varepsilon_{\mathrm{C}}^{\mathrm{P}}$ is obtained from the slope and given in Eq. (3.12). Banya *et al.* [1] indicates that the $\varepsilon_{\mathrm{C}}^{\mathrm{P}}$ of a Fe-P-C (sat.) alloy is 10.6 ± 0.6, and this is close to the value obtained in the study.

$$\varepsilon_{\mathrm{C}}^{\mathrm{P}} = 6.09 \pm 0.15, (X_{\mathrm{Mn}} < 0.06, X_{\mathrm{P}} < 0.25, 1673\ \mathrm{K}) \quad \text{……} \quad (3.12)$$

By using the obtained $\varepsilon_{\mathrm{C}}^{\mathrm{P}}$ and the $\varepsilon_{\mathrm{C}}^{\mathrm{Mn}}$ as shown in Table 3, the activity coefficient of C is assumed as given in Eq. (3.13).

$$\ln \gamma_{\mathrm{C\ [in\ Fe-P-Mn-C(sat.)]}} = \ln \gamma_{\mathrm{C}}^{0} + \varepsilon_{\mathrm{C}}^{\mathrm{C}} X_{\mathrm{C}} + \varepsilon_{\mathrm{C}}^{\mathrm{P}} X_{\mathrm{P}} + \varepsilon_{\mathrm{C}}^{\mathrm{Mn}} X_{\mathrm{Mn}} \quad \text{……} \quad (3.13)$$

Subsequently, Eq. (3.14) is obtained by combining Eq. (3.13) with Eq. (3.10).

$$1/X_{C\ [in\ Fe-P-Mn-C(sat.)]} = \gamma_{\mathrm{C}}^{0} \times \mathrm{e}^{(\varepsilon_{\mathrm{C}}^{\mathrm{C}} X_{\mathrm{C}})} \times \mathrm{e}^{(\varepsilon_{\mathrm{C}}^{\mathrm{P}} X_{\mathrm{P}} + \varepsilon_{\mathrm{C}}^{\mathrm{Mn}} X_{\mathrm{Mn}})} = A\mathrm{e}^{(\varepsilon_{\mathrm{C}}^{\mathrm{P}} X_{\mathrm{P}} + \varepsilon_{\mathrm{C}}^{\mathrm{Mn}} X_{\mathrm{Mn}})} \quad \text{……} \quad (3.14)$$

Here, γ_{C}^{0} denotes the activity coefficient of Fe-C(sat.) alloy system. Both the γ_{C}^{0} and the self-interaction parameter of C ($\varepsilon_{\mathrm{C}}^{\mathrm{C}}$) in C saturation alloys are not constant, and thus we assumed a

parameter A to present terms including γ_C^0 and ε_C^C as shown in Eq. (3.14). Subsequently, **Fig. 3.6** is obtained by using experimental results from the current study.

As shown in **Fig. 3.6**, a linear relationship with an interception of zero is obtained, and thus the parameter A is indicated as a constant, and its value is determined as 0.19 ± 0.00 from the slope. Therefore, the C solubility in the Fe-P-Mn-C(sat.) alloy at 1673 K is expressed as given in Eq. (3.15) as follows:

$$X_{C\,[in\ Fe-P-Mn-C(sat)]} = 0.19\ \mathrm{e}^{-\,(6.09\,X_P\,-0.47\,X_{Mn})} \quad \ldots\ldots\ldots\ldots\ldots\ (3.15)$$

By using the Eq. (3.15), the C solubility is calculated, and the results are shown in **Fig. 3.7**. The C solubility mainly changes with the molar ratio of P, and the effect of the molar ratio of Mn is negligible. This is because the interaction parameter ε_C^P exceeds ε_C^{Mn}. Additionally, the calculated value when X_P reaches zero is in agreement with the C solubility of Fe-Mn-C (sat) alloy as reported by Ohtani *et al*. [4].

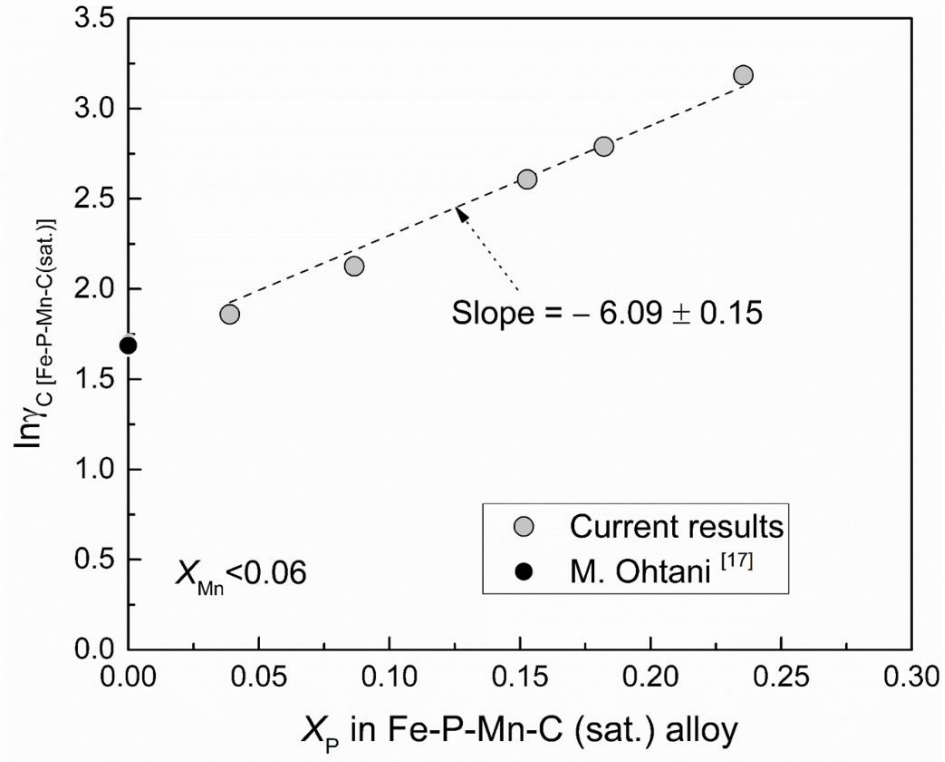

Fig. 3.5 Relation between activity coefficient of C and mole fraction of P in Fe-P-Mn-C(sat.) alloy

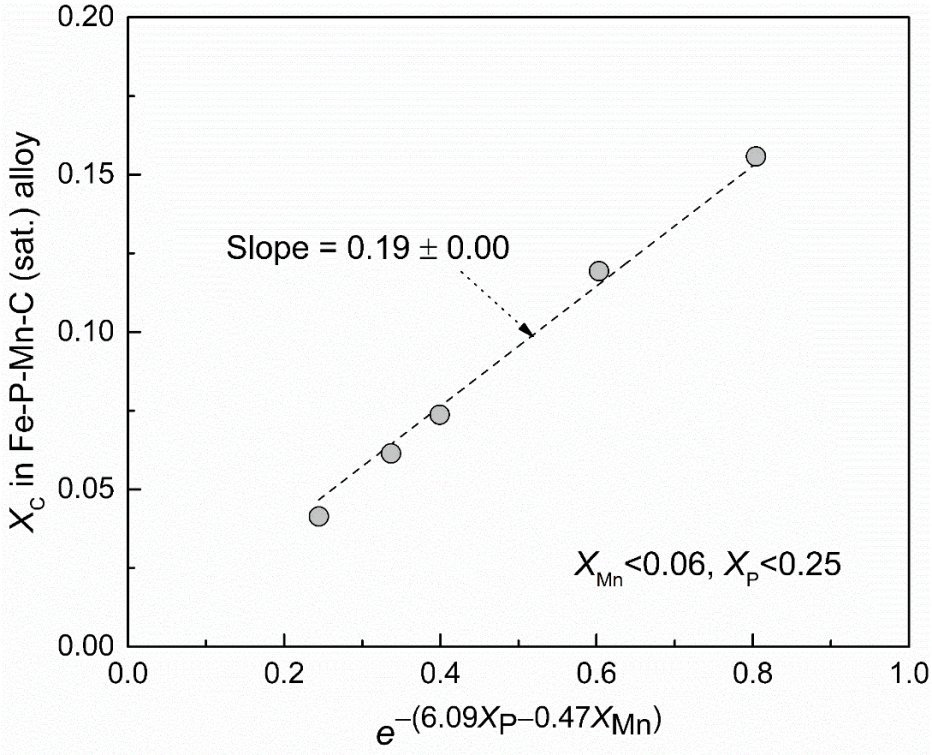

Fig. 3.6 Measurement of unknown constant A

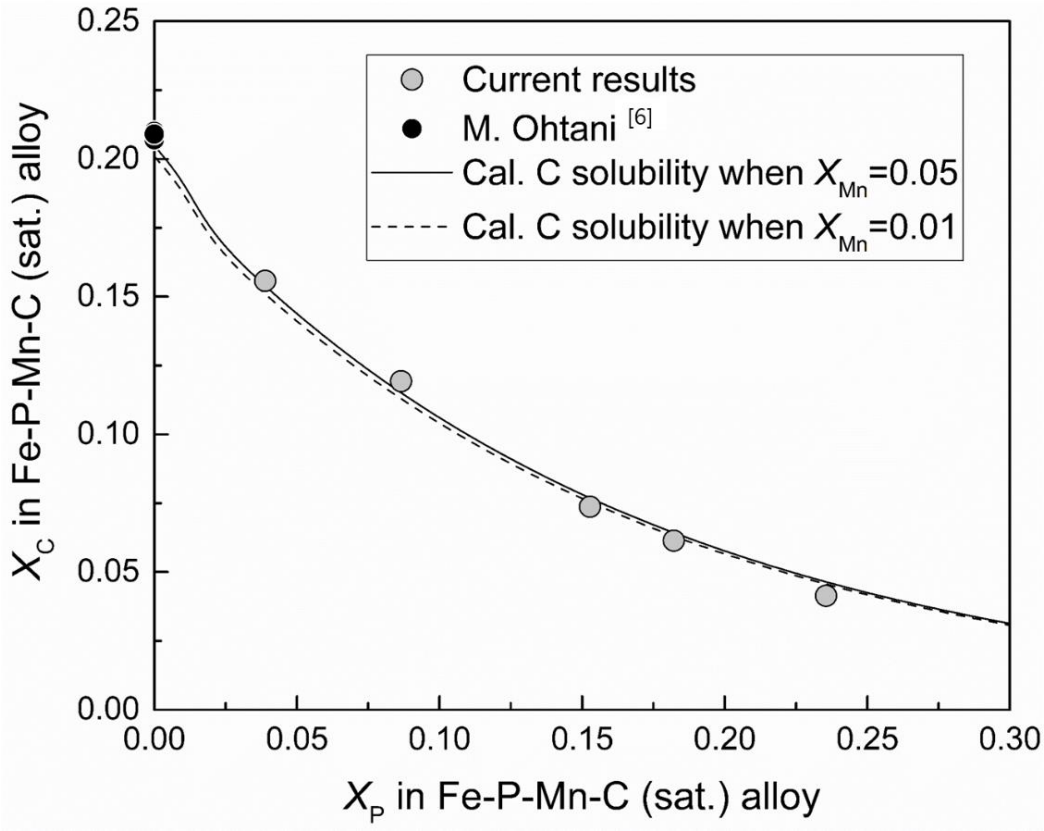

Fig. 3.7 Influence of P and Mn on C solubility in Fe-Mn-P-C(sat.) alloy at 1673K

3.3.3 Activity coefficient of P in Fe-P-Mn-C(sat.) alloy

Fig. 3.8 shows the measured activity coefficient of P ($\gamma^{\mathrm{H}}_{\mathrm{P\,[in\,Fe-P-Mn-C(sat.)]}}$) in the Fe-P-Mn-C(sat.) alloy as a function of the molar fraction of P in the alloy. The results indicate that the activity coefficient is not regressed by a linear relation, and thus other considerations are necessary to express the activity coefficient of P.

Ban-ya *et al.* [2] propose the Henrian activity coefficient of P in Fe-P-C (up to sat.) alloy at 1673 K as expressed in Eq. (3.16). While applying the equation to the Fe-P-Mn-C (sat.) alloy, I assume that the effect of Mn is expressed as Eq. (3.17) by using $\varepsilon_{\mathrm{P}}^{\mathrm{Mn}}$. Higher orders of interaction parameter between P and Mn in C saturated alloy are unavailable, and the composition range of X_{Mn} in the experiments in the current study are excessively low to discuss the relation between $\ln\gamma^{\mathrm{H}}_{\mathrm{P}}$ and X_{Mn}. Thus, only the first order interaction parameter $\varepsilon_{\mathrm{P}}^{\mathrm{Mn}}$ is considered for Eq. (3.17) as follows:

$$\log\gamma^{\mathrm{H}}_{\mathrm{P\,[in\,Fe-P-C]}} = 1.41X_{\mathrm{P}} + 1.41X_{\mathrm{P}}^2 + 1.70X_{\mathrm{P}}^3 + 2.36X_{\mathrm{C}} + 2.36X_{\mathrm{C}}^2 + 2.65X_{\mathrm{C}}^3 + 3.77X_{\mathrm{P}}X_{\mathrm{C}} \quad (3.16)$$

$$\ln\gamma^{\mathrm{H}}_{\mathrm{P\,[in\,Fe-P-Mn-C(sat.)]}} - \ln\gamma^{\mathrm{H}}_{\mathrm{P\,[in\,Fe-P-C]}} = \varepsilon_{\mathrm{P}}^{\mathrm{Mn}}X_{\mathrm{Mn}} \quad \text{……..…….. (3.17)}$$

Eq. (3.18) shows another assumption by using the first order interaction parameters to express the Henrian activity coefficient of P.

$$\ln\gamma^{\mathrm{H}}_{\mathrm{P\,[in\,Fe-P-Mn-C\,(sat.)]}} = \varepsilon_{\mathrm{P}}^{\mathrm{Mn}}X_{\mathrm{Mn}} + \varepsilon_{\mathrm{P}}^{\mathrm{P}}X_{\mathrm{P}} + \varepsilon_{\mathrm{P}}^{\mathrm{C}}X_{\mathrm{C}} \quad \text{…….. (3.18)}$$

In the calculation, the assumed equation is used, and the $\varepsilon_{\mathrm{P}}^{\mathrm{Mn}}$ and $\varepsilon_{\mathrm{P}}^{\mathrm{C}}$ values obtained in the current study and the reported $\varepsilon_{\mathrm{P}}^{\mathrm{P}}$ value are used (see Table 3.3) [1]. Additionally, the C solubility (X_{C}) is calculated by using Eq. (3.15).

The result calculated by using either Eq. (3.17) or Eq. (3.18) is shown in Fig. 3.8. With respect to the calculation of Eq. (3.17), X_{Mn} is set as 0.05 since the value is close to the experimental results shown in Table 3.2. The comparison between the experimental results and calculation indicate that both equations accurately describe the activity coefficient of P in Fe-P-Mn-C (sat.) alloy when the X_P value is lower than 0.2.

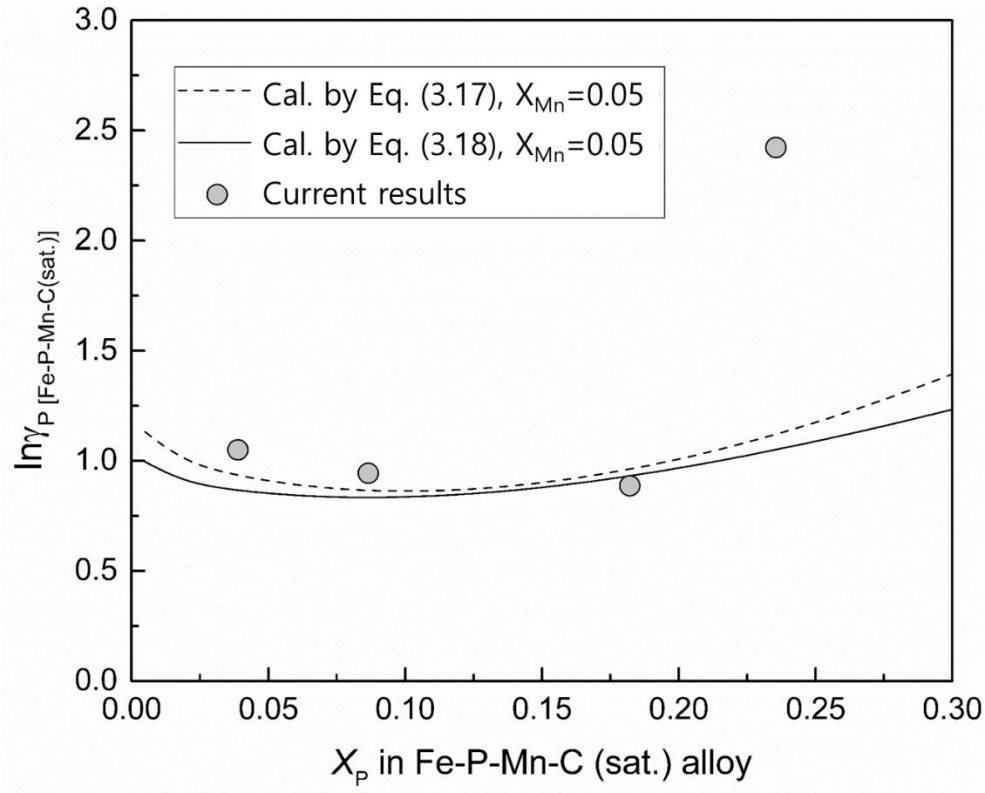

Fig. 3.8 Measured activity coefficient of P in Fe-P-Mn-C(sat.) alloy by different method

3.4. Application of the thermodynamic data to the experimental results of selective reduction of steelmaking slag

In extant studies, artificial steelmaking slag with various basicity was synthesized and mixed with graphite powder in an Al_2O_3 crucible and the reduction was conducted at 1773 K for a period ranging from 20 to 80 min. The graphite powder was used as a reductant, and the amount of mixed graphite powder was set as 200% of the amount required to completely reduce the FeO, MnO, and P_2O_5 present in the slag.

The relation of P and Mn between alloy and slag is expressed as Eq. (3.19), and Eq. (3.20) was obtained by rearranging the equilibrium constant.

$$P_2O_5(l) + 5[Mn] = 2[P] + 5MnO(l)$$

$$\log K = 26950/T + 0.97 \quad \text{..... (3.19) [11, 12]}$$

$$\frac{X_{Mn}^5(\gamma_{Mn}^H)^5}{X_P^2(\gamma_P^H)^2} = \frac{a_{MnO}^5}{a_{P_2O_5}}\frac{1}{K} \quad \text{..... (3.20)}$$

In Eq. (3.20), the left part of the equation was obtained by using the activity coefficient of P and Mn measured in current study and metal composition reported in chapter 2. The Eq. (3.18) was used to calculate the Henrian activity coefficient of P, and Eq. (3.21) (which was obtained by converting Eq. (9)) was used to calculate the Henrian activity coefficient of Mn.

$$\ln\gamma_{Mn\ [in\ Fe-P-Mn-C(sat.)]}^H = -4.72X_P - 0.47X_C \quad \text{..... (3.21)}$$

With respect to the right part of Eq. (3.20), the slag compositions obtained from a chapter 2 was used to calculate the activities of P_2O_5 and MnO by using regular solution model (R.S.M.) [13]. The results after 40 mins of reduction was used in the calculation with respect to both the metal and slag

compositions. The results at 40 mins were selected because the reduction of P_2O_5 stopped, the reduction rate of Mn was slow, and the system was considered as close to equilibrium. The metal compositions and calculated ratio of $a_{\mathrm{MnO}}^{5}/a_{\mathrm{P_2O_5}}$ are listed in **Table 3.4**. Subsequently, if the calculated left part is close to the calculated results of the right part, then it is considered that the measured activity coefficient of P and Mn is applicable to describe the P and Mn distribution in the selective reduction process of steelmaking slag.

Fig. 3.9 shows the comparison between the calculated results of the left and right parts of Eq. (3.20) by using the aforementioned method. With the exception of Slag B, the calculations using the activity coefficients of P and Mn in metal were close to the calculation using equilibrium constant *K* and the activities of P_2O_5 and MnO in the slag. Therefore, the activity coefficient of P and Mn was considered as applicable for the selective reduction process of steelmaking slag. In the case of Slag B, the main difference between calculations was attributed due to the high X_{Mn} content in the alloy (which exceeded 0.05), and thus the activity coefficient was not accurately expressed.

Therefore, if the slag composition during the selective reduction process is obtained, then the relation between X_{Mn} and X_{P} in metal is estimated by using the activity coefficient of P and Mn measured in the study. **Fig. 3.10** shows an example by using the results of Slag E. In Fig. 3.10, the lines were calculated by Eq. (3.20). The activities of P_2O_5 and MnO were calculated via the regular solution model by using the measured slag composition, and the activity coefficients of P and Mn in the alloy were calculated by Eq. (3.18) and Eq. (3.21). As shown in Fig. 3.10, from 20 mins to 40 mins, the difference between the measured metal composition and those estimated by using slag composition decreased. At 40 mins, the measured metal composition was close to the estimated value.

Table 3.4 Calculated $a_{MnO}^5/a_{P_2O_5}$ by regular solution model and experimental result for the alloy

Slag No.	$\log[a_{MnO}^5/a_{P_2O_5}]$ by R.S.M. (after 40 mins)	Metal comp. (after 40 mins)		
		[%Mn]	[%P]	[%C]
Slag B (C/S = 1.19)	4.04	2.69	7.29	2.31
Slag C (C/S = 1.00)	4.80	2.52	7.66	2.01
Slag D (C/S = 0.76)	5.49	2.27	8.04	1.65
Slag E (C/S = 0.50)	7.86	2.17	8.91	1.68

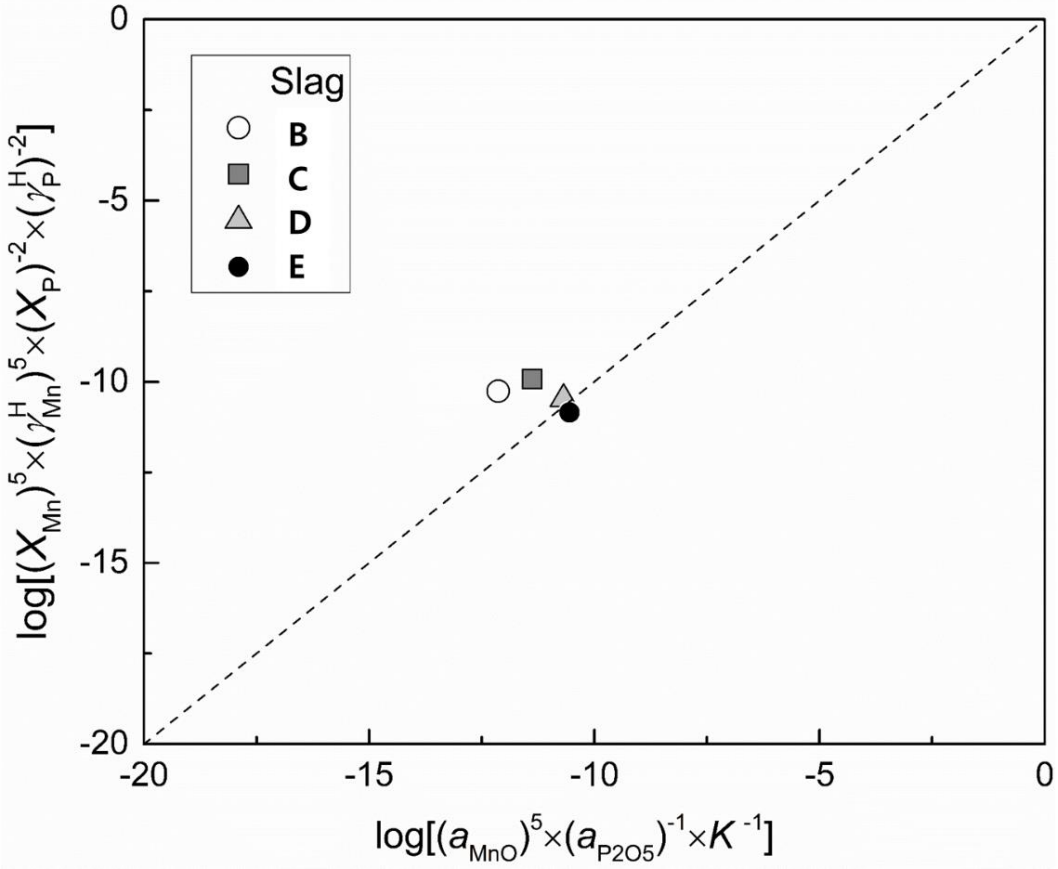

Fig. 3.9 Comparison between the left and right part of Eq. (3.20)

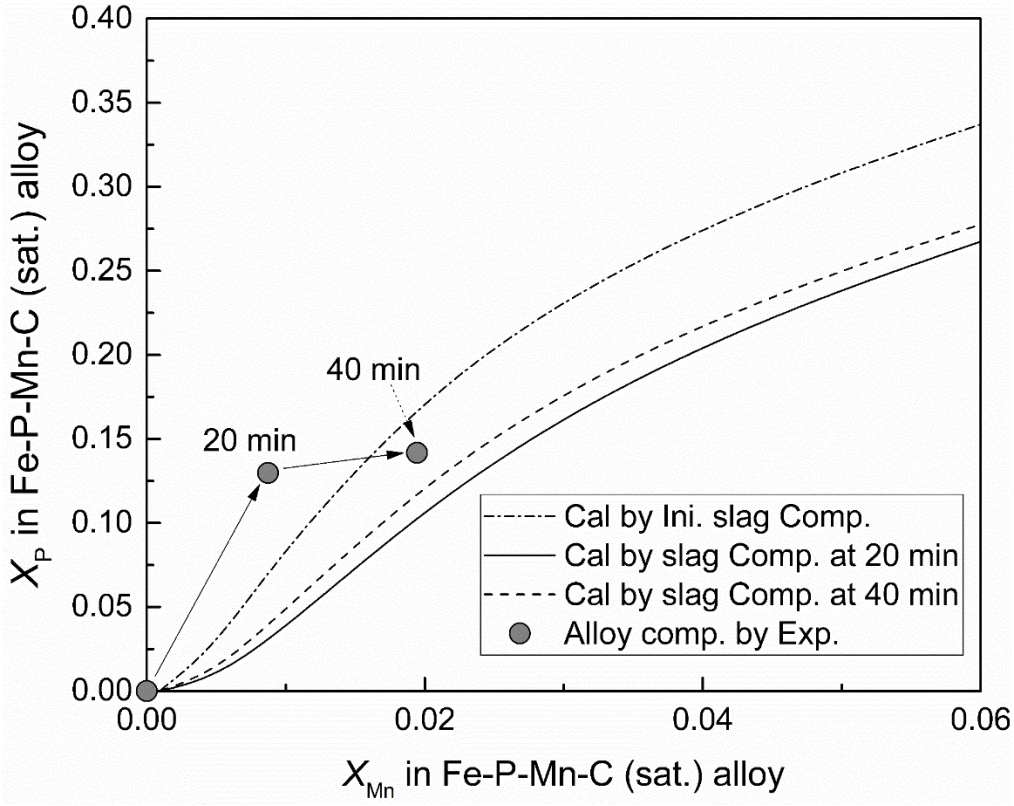

Fig. 3.10 Calculated equilibrium distribution of P and Mn between slag and alloy

3.5. Summary

In the study, in order to accurately describe the activity of P and Mn in a Fe-P-Mn-C(sat.) alloy, the activity coefficients for P and Mn in this type of an alloy system were measured by equilibrating Fe-P-Mn-C(sat.) alloy with Ag by using a graphite crucible at 1673 K, and a few conclusions were obtained as follows,

1. When $0 < X_{\mathrm{Mn}} < 0.06$ and $0 < X_{\mathrm{P}} < 0.25$, a liner relationship was obtained between the activity coefficient of Mn and the mole fraction of P. Thus, the interaction parameter between P and Mn in a Fe-P-Mn-C(sat.) alloy is determined as follows:

$$\varepsilon_{\mathrm{Mn}}^{\mathrm{P}} = -4.72 \pm 0.27, (1673\ \mathrm{K})$$

Subsequently, the activity coefficient of Mn is obtained as follows:

$$\ln\gamma_{\mathrm{Mn\ [in\ Fe-P-Mn-C\ (sat.)]}} = -4.72X_{\mathrm{P}} - 0.47X_{\mathrm{C}} - 0.87\ (1673\ \mathrm{K})$$

2. A linear relation between the activity coefficient of C and the mole fraction of P was observed under the current experimental conditions. Therefore, the interaction parameter between C and P is obtained as follows:

$$\varepsilon_{\mathrm{C}}^{\mathrm{P}} = 6.09 \pm 0.15, (X_{\mathrm{Mn}} < 0.06, X_{\mathrm{P}} < 0.25, 1673\ \mathrm{K})$$

Additionally, the C solubility of Fe-P-Mn-C(sat.) alloy is obtained as follows:

$$X_{C\ [in\ Fe-Mn-P-C(sat.)]} = 0.19\mathrm{e}^{-(6.09X_{\mathrm{P}} - 0.47X_{\mathrm{Mn}})}$$

3. The following equations were indicated as accurate in terms of describing the activity coefficient of P in the Fe-P-Mn-C(sat.) alloy when X_{P} was lower than 0.2.

$$\ln\gamma_{\mathrm{P\ [in\ Fe-P-Mn-C(sat.)]}}^{\mathrm{H}} - \ln\gamma_{\mathrm{P\ [in\ Fe-P-C]}}^{\mathrm{H}} = \varepsilon_{\mathrm{P}}^{\mathrm{Mn}} X_{\mathrm{Mn}} = -4.72 X_{\mathrm{Mn}}$$

$$\ln\gamma_{\mathrm{P\ [in\ Fe-P-Mn-C\ (sat.)]}}^{\mathrm{H}} = -4.72 X_{\mathrm{Mn}} + 4.26 X_{\mathrm{P}} + 6.09 X_{\mathrm{C}}$$

4. A comparison to the results for the selective reduction of steelmaking slag in a previous study indicated that the activity coefficients of P and Mn obtained in the study are applicable.

3.6 Reference

1. Ban-Ya, S., & Suzuki, M. (1975). Activity of Phosphorus in Liquid Fe-P and Fe-P-C Alloys. *Tetsu-to-Hagané, 61*(14), 2933-2942.
2. Ban-Ya, S., Maruyama, N., & Fujino, S. (1983). The Effects of C, Si, Al, and B on the Activity of Phosphorus in Liquid Iron. *Tetsu-to-Hagané, 69*(8), 921-928.
3. Enokido, H., Moro-Oka, A., & Ichise, E. (1995). Thermo-chemical activities of liquid Fe-Mn-C alloy. *Tetsu-to-Hagané, 81*(6), 619-624.
4. Ohtani, M. (1957). Activities of Mn and C in molten Fe-Mn-C alloys. *Tetsu-to-Hagané, 43*(11), 1211-1215.
5. Ban-Ya, S., Maruyama, N., & Kawase, Y. (1984). Effects of Ti, V, Cr, Mn, Co, Ni, Cu, Nb, Mo, and W on the Activity of Phosphorus in Liquid Iron. *Tetsu-to-Hagané, 70*(1), 65-72.
6. Schenck, H., Steinmetz, E., & Gitizad, H. (1969). Die Phosphoraktivität im flüssigen Eisen und ihre Beeinflussung durch Nickel, Mangan und Chrom. *Archiv für das Eisenhüttenwesen, 40*(8), 597-602.
7. Shim, S. C., Morita, K., & Sano, N. (1994). Thermodynamics of phosphorus in carbon-saturated manganese-based alloys. *Steel research, 65*(12), 523-527.
8. Schenck, H., & Neumann, F. (1958). Aktivität des Mangans in flüssigen Eisen-Mangan-

Kohlenstoff-Lösungen. *Archiv für das Eisenhüttenwesen, 29*(5), 263-267.

9. Tsukihashi, F., Matsumoto, F., Hyodo, T., Yukinobu, M., & Sano, N. (1985). Phosphorus and Manganese Distribution between Carbon-saturated Iron and Na_2O-SiO_2 Melts and Nitrogen Solubility in the Melts. *Tetsu-to-Hagané, 71*(7), 823-830.
10. Mitsutaka, H., & Kimihisa, I. (2010). Thermodynamic data for steelmaking: Tohoku University Press, Sendai.
11. Turkdogan, E., & Pearson, J. (1953). Activities of constituents of iron and steelmaking slags. *Journal of the Iron and Steel Institute, 12*, 398-402.
12. The Japan Society for the Promotion of Science, the 19th Committee on Steelmaking: *Steelmaking Data Sourcebook (Revised Edition)*, 1988, Gordon and Breach Science Publications, New York.
13. Ban-Ya, S. (1993). Mathematical expression of slag-metal reactions in steelmaking process by quadratic formalism based on the regular solution model. *ISIJ international, 33*(1), 2-11.

Chapter 4 Mechanism of the Selective Reduction of Steelmaking Slag

In chapter 2, a continuous dissolution of Al_2O_3 from crucible during reduction was observed, and its content exceeded nearly 40% after 20 min. It is necessary to understand the role of Al_2O_3 on the selective reduction of P from steelmaking slag. In this chapter, the experiment of different initial Al_2O_3 contents in slag was conducted in order to control dissolution behavior of Al_2O_3. In addition, the experiment using different crucibles shown in Chapter 2 was analyzed to clarify the effect of Al_2O_3.

4.1 Experimental Method

4.1.1 Slag preparation

Chemical regents of SiO_2, $Ca_3(PO)_4$, MnO, MgO, Al_2O_3, and synthetic CaO and FeO were used as raw materials to prepare synthetic slag. CaO was synthesized by calcination of $CaCO_3$ for 12 hours at 1473 K in air. To prepare FeO, regents of Fe and Fe_2O_3 were reacted for 1 hour in a Fe crucible at 1673 K under Ar atmosphere. These chemicals were well mixed, and melted using an Al_2O_3 crucible for 1 hour at 1673 K under Ar atmosphere (flow rate: 100 ml/min). After given time, the synthesized slags were quenched by water, the synthesized slags were crushed to powders with sizes of less than 500 μm for reduction experiments. The compositions of the slags were confirmed by inductively coupled plasma atomic emission spectroscopy (ICP–AES). The analyzed chemical compositions of the slags are shown in **Table 4.1**.

Table 4.1 Synthesized slag composition (mass %)

Sample	FeO	CaO	SiO_2	P_2O_5	MnO	MgO	Al_2O_3	Basicity (CaO/SiO_2)
Slag F	25.40	21.47	28.41	3.94	6.31	3.43	11.04	0.76
Slag G	25.95	16.75	33.43	3.90	6.22	3.44	10.31	0.50
Slag H	23.70	16.29	31.46	4.12	5.92	3.16	15.36	0.52
Slag I	23.56	14.58	28.99	4.20	5.87	3.15	19.64	0.50
Slag J	23.64	13.25	26.31	3.88	5.97	2.78	24.17	0.50

In Table 4.1, the contents of P_2O_5 and MnO were set to 4 and 6 mass % respectively, which are similar to the industrial steelmaking slag. The Al_2O_3 content was varied from 10 to 25 mass % for investigating the influence of its content in slag on the selective reduction of P. The ratio of CaO and SiO_2 was set from 0.5 to 0.76, because good separation between P and Mn were achieved in this range of basicity according to previous chapter.

4.1.2 Experimental method

3g of crushed slag was mixed homogenously with graphite powder which was used as a reductant. The amount of graphite powder was set as 200% of the amount required for reducing all of the FeO, MnO, and P_2O_5 in slag, which was stoichiometrically calculated using Eqs. (4.1) to (4.3).

$$(FeO) + C(s) = [Fe] + CO(g) \quad \text{..... (4.1)}$$

$$(MnO) + C(s) = [Mn] + CO(g) \quad \text{..... (4.2)}$$

$$(P_2O_5) + 5C(s) = 2[P] + 5CO(g) \quad \text{..... (4.3)}$$

The experiment was performed using a vertical type of resistance furnace equipped with an alumina reaction tube (Inner diameter: 42 mm, Height: 1000 mm). A dense Al_2O_3 crucible (Inner diameter: 19 mm, Height: 45 mm) was used. In each experiment, the furnace was firstly heated to 1773K under Ar atmosphere (purity: 99.9999%). Subsequently, the crucible which contained the mixture of slag and graphite powder was charged into the hot zone of furnace. This moment was set as the start of the experiment. Because the crucible was charged at high temperature, several minutes were required until the slag sample reached to 1773 K. A typical temperature change of the sample with time is shown in **Fig. 4.1**.

The temperature of sample passed thought 1673K after 4 min, and it reached to 1773K before 10 min. After a given heating time, the crucible together with sample was quickly taken out from the furnace and then cooled by helium gas injection immediately. For the experiments using the slag with different initial Al_2O_3 contents, the reaction time was set as 10 min and 20 min. In addition, to understand the reaction mechanism, short reaction time of less than 5 min was set for the slag which initially containing 10% (Slag G) and 20% of Al_2O_3 (Slag I). For the experiments using different crucibles, the reaction time was set as 5 min, 10 min, and 20 min respectively. The chemical composition of the slag and the metal generated after reduction were analyzed by ICP-AES, and the cross-section of the sample was observed by EPMA. The carbon content in the metal was analyzed by the combustion method.

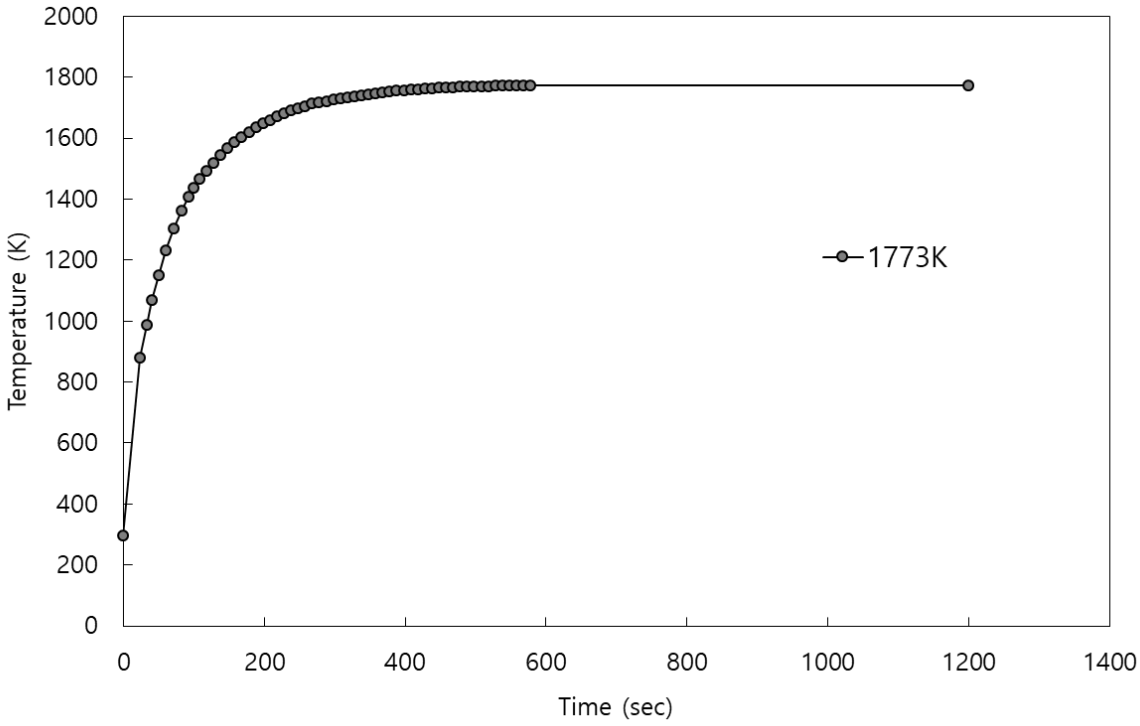

Fig. 4.1 Typical heating profile of the sample after it charged to the heated furnace

4.2 Result

4.2.1 Reduction behavior of slag

Fig. 4.2 shows the change in the composition of slag and metal during reduction of Slag F as an example. In Fig. 4.2 (a), clear decreases in both FeO and P_2O_5 content were observed, and the MnO content changed little. On the opposite, the content of Al_2O_3 continuously increased as the reduction time due to crucible dissolution. Because CaO, SiO_2 and MgO were unlikely to be reduced under current experimental conditions, the changes in their contents were small. In Fig. 4.2 (b), both the content of P and Mn increased with reaction time, and the increase of P was larger than that of Mn. The carbon content in metal decreased slightly from its initial value. This initial content of carbon is assumed as 4 mass % considering the carbon saturation of hot metal. Because P and Mn were the major compositions of metal phase after reduction, the reduction behaviors of these two elements was focused in the followings.

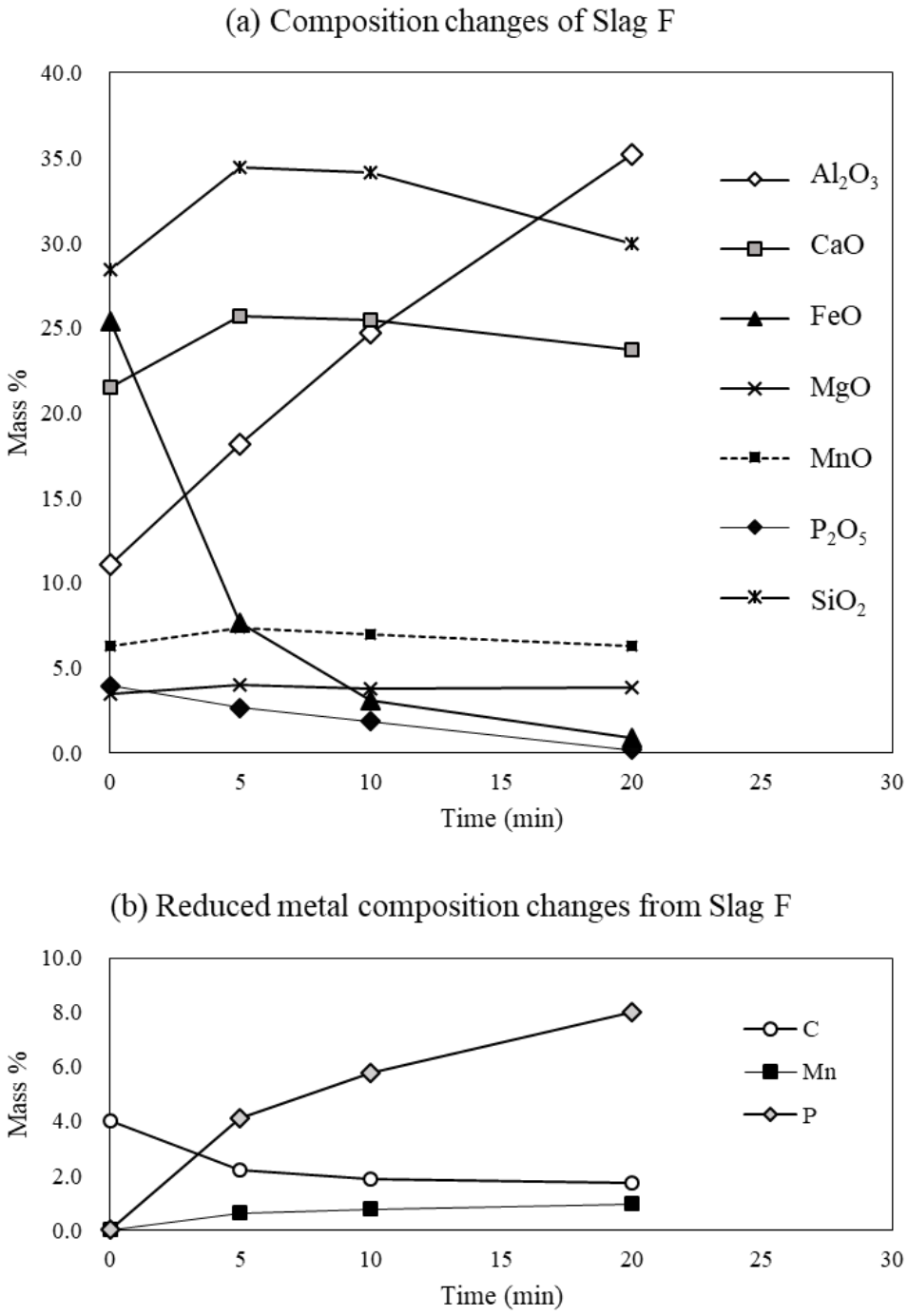

Fig. 4.2 Reduction behavior of Slag F and the change in metal composition at 1773 K

4.2.2 Influence of initial Al_2O_3 content on the reduction behavior

Fig. 4.3 shows the comparison on the reduction of MnO and P_2O_5 from slag of different initial contents of Al_2O_3. When the initial content of Al_2O_3 in slag was 10% (Slag G) and 15% (Slag H), the MnO contents in slag were not decreased after reduction, and as a result the Mn contents in reduced metal were low. When the initial Al_2O_3 content was further increased to 20% (Slag I) and 25% (Slag J), the reduction of MnO from slag became intense and a significant reduction of MnO was observed for Slag J. In the case of P, the P_2O_5 content in slag became smaller with the increase in the initial Al_2O_3 content at 10 min, while it reached to the similar content after 20 min for all samples. Therefore, an increase in the initial Al_2O_3 content enhanced both the reduction of MnO and P_2O_5 from slag. Considering the separation of P and Mn during reduction, the initial content of Al_2O_3 should be controlled at low level.

The mass balance of P and Mn were calculated using the experimental results shown in Fig. 4.3. In the calculation, the weight of slag was calculated by Eq. (4.4) using the mass of CaO which was not to be reduced. For metal weight, it was calculated by Eq. (4.5) using the change in the FeO content in the slag.

$$W_{slag} = 100 \times W_{CaO}^{Initial} / (\text{mass\% CaO}) \quad \cdots\cdots (4.4)$$

$$W_{Metal} = (W_{FeO}^{Initial} - W_{slag} \times (\text{mass\% FeO})/100) \times (M_{Fe} / M_{FeO}) \cdots\cdots (4.5)$$

Here, W_{Slag} and W_{Metal} indicate the masses of slag and metal after the experiment (g); $W_{CaO}^{Initial}$ and $W_{FeO}^{Initial}$ indicate the masses of CaO and FeO in the initial slag; (mass % CaO) and (mass % FeO) indicate the concentration of each oxide in the slag after the experiment; and M_{Fe} and M_{FeO} indicate the atomic weight of Fe and the molecular weight of FeO.

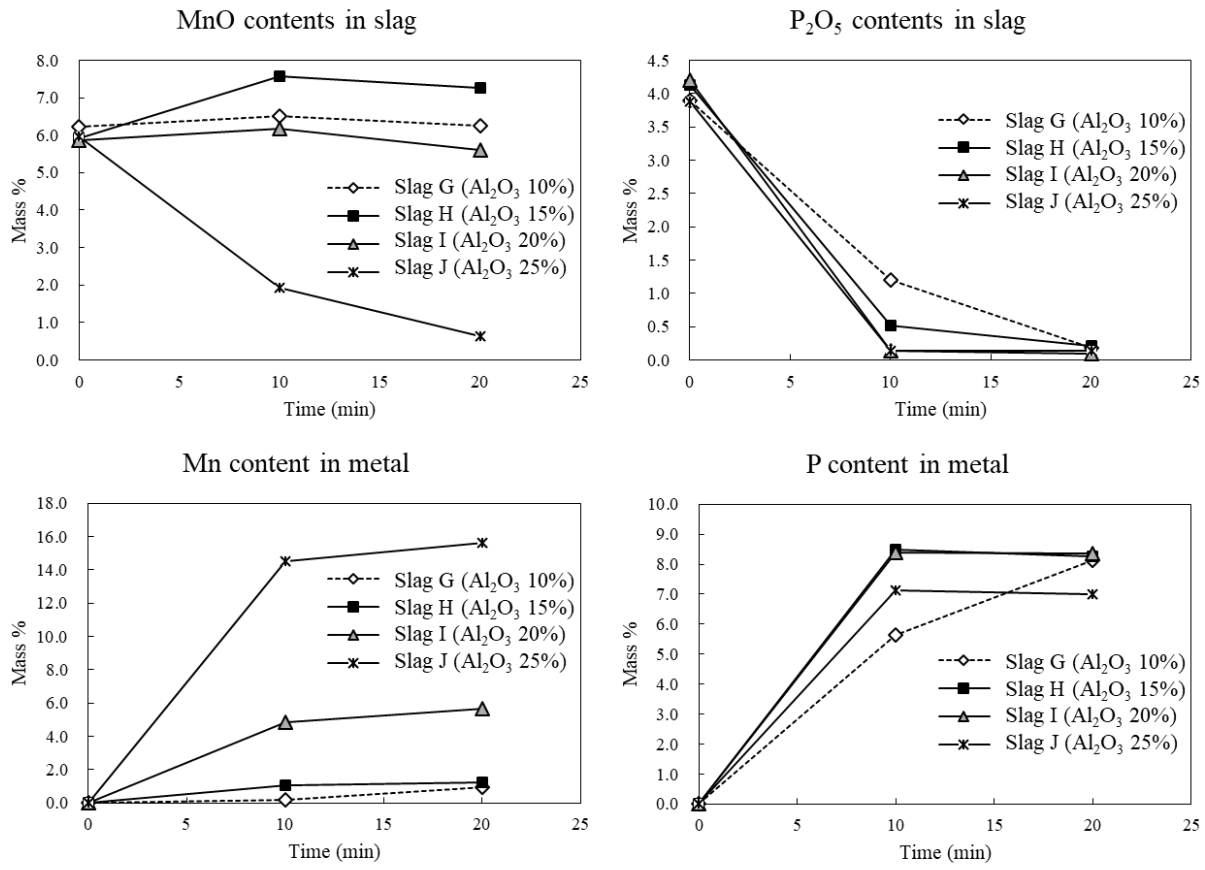

Fig. 4.3 Changes in the P and Mn content in each phase with reduction time for slag with different initial content of Al_2O_3

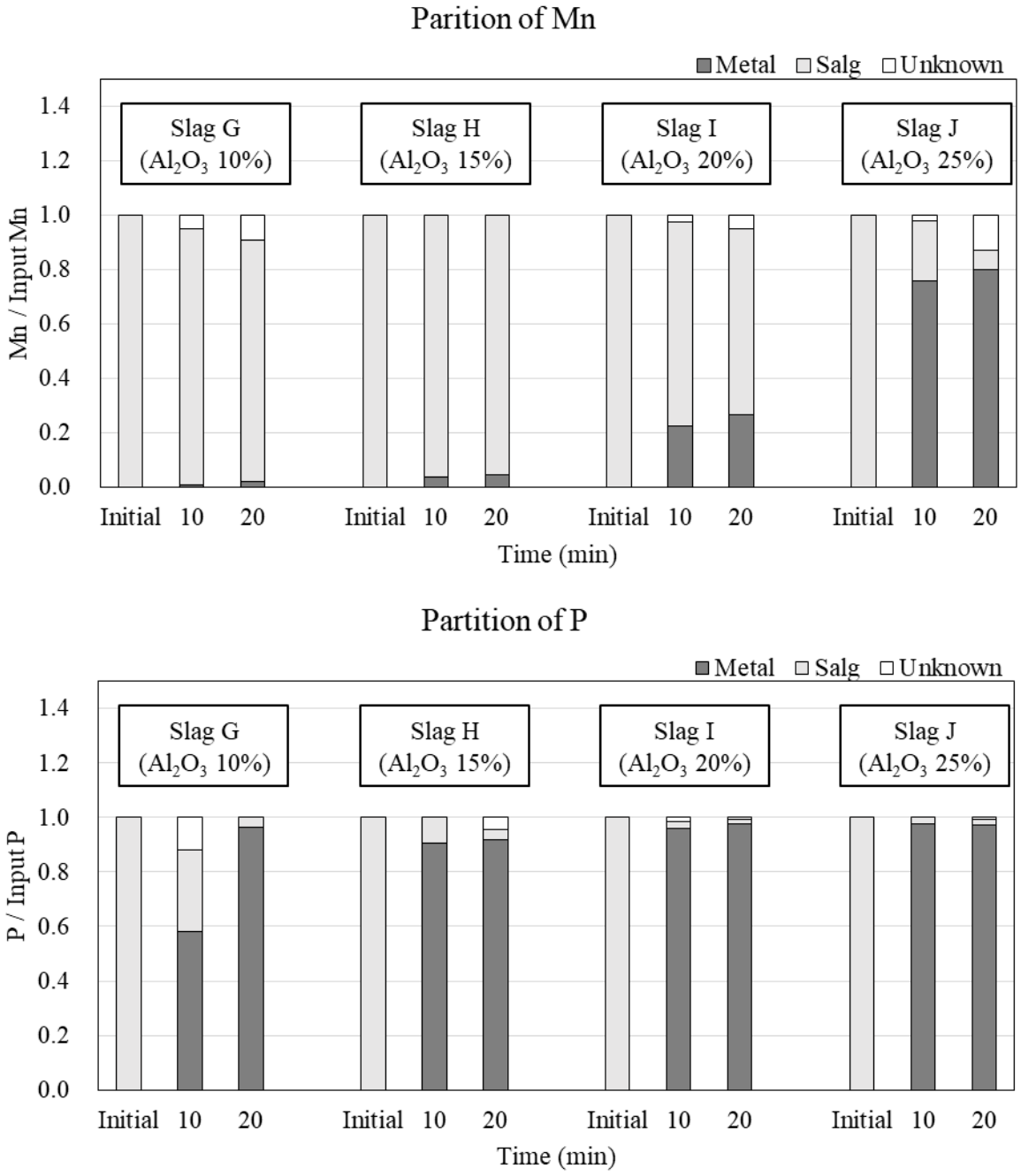

Fig. 4.4 The partitions of Mn and P with reduction time

The calculated results for partitions of P and Mn are shown in **Fig. 4.4.** In all cases, both the unknown part of P and Mn are insignificant after reduction. Hence, most of the P and Mn were concentrated in the reduced metal and the vaporizations of them were little. It can be seen that the partition ratios (slag/metal) of both P and Mn decreased with the increase in the initial Al_2O_3 content. Especially in the cases of Slag I (Al_2O_3 = 20 mass %) and Slag J (Al_2O_3 = 25 mass %), partition of Mn into metal is increased significantly. The changes in the partition of Mn in Slag I and J were large during the early stage (0 ~ 10 min), but those in the late stage (10 ~ 20 min) were small. In chapter 2, the reduction of MnO gradually occurred through the reduction time. This indicated that a significant amount of MnO was reduced at early stage. To clarify the mechanism of Mn reduction in the initial stage, detail experiment with shorter reduction time was conducted.

4.2.3 Melting behavior of slag and composition changes by different initial Al_2O_3 content in slag

Even though sample does not reach to target temperature, short time reduction within 5 min was conducted for Slag G (Al_2O_3 = 10 mass %) and I (Al_2O_3 = 20 mass %). **Fig. 4.5** shows the cross-sections of Slag G (Al_2O_3 = 10 mass %) after different reduction time. When the initial Al_2O_3 content in slag was 10%, molten slag was observed within 1 min. Inside the molten slag, lots of pores were observed which were formed due to the generation of CO gas by reduction. When the reduction time was elongated from 1 to 3 min, the diameter of reduced metal particle was increased, and these particles were observed majorly on top of the molten slag. If the reduction is further elongated, the reduced metal particles would agglomerate and grow up to bigger size, and then it might sink into the bottom of the crucible. Through this observation, the reduction reaction was considered to occur between the molten slag and the solid graphite particle which floated on top of the molten slag, mainly.

Fig. 4.6 shows the compositional change of Slag G (Al_2O_3 = 10 mass %) analyzed by EPMA. The content of FeO decreased rapidly in comparison with other components, and the content of P_2O_5 gradually decreased. The MnO content was almost constant within 5 min. This result indicated that the Fe and P was selectively reduced. In addition, the continuously dissolution of Al_2O_3 crucible was also observed. Comparing to the melting behavior of slag as shown in Fig. 4.5, a selective reduction of P could be achieved when the slag was melted.

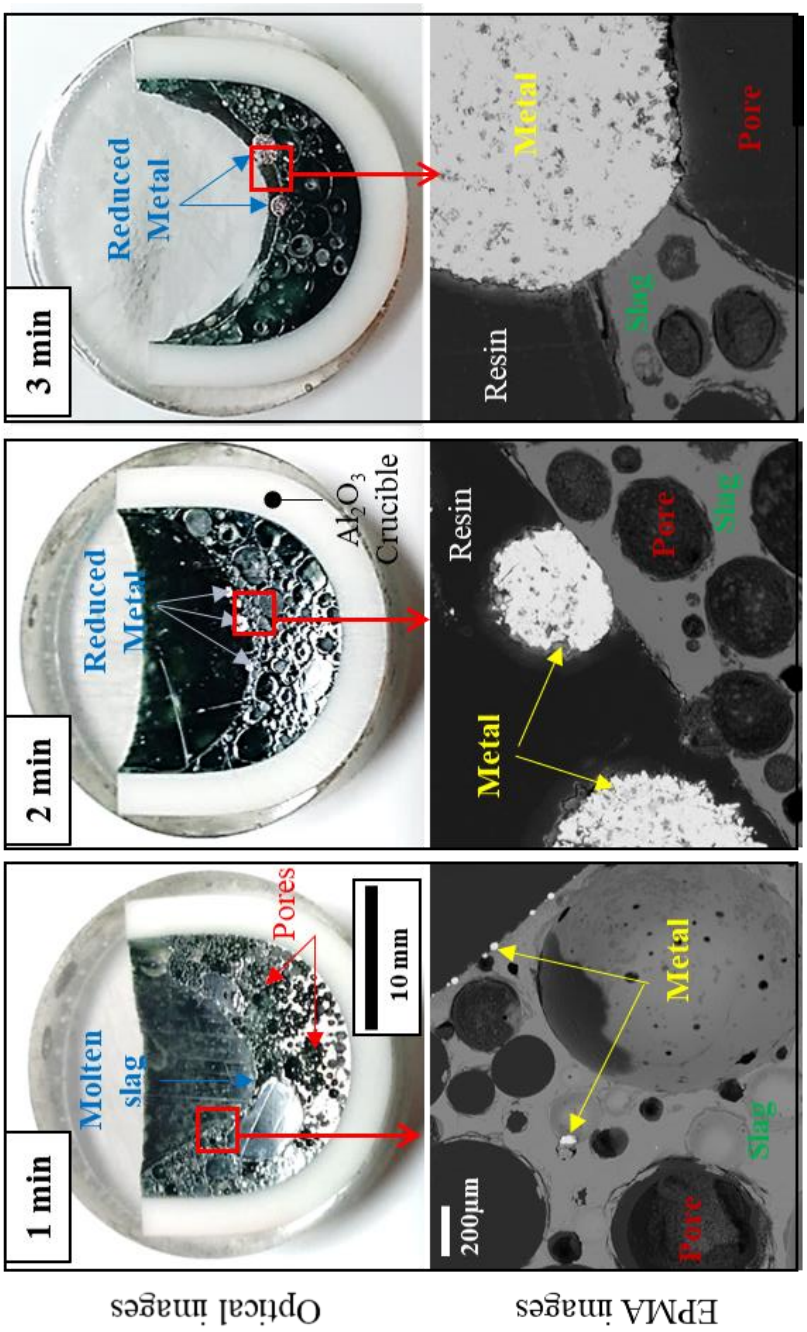

Fig. 4.5 Melting behavior of Slag G (Al_2O_3 = 10 mass %) and formation of metal during short time reduction

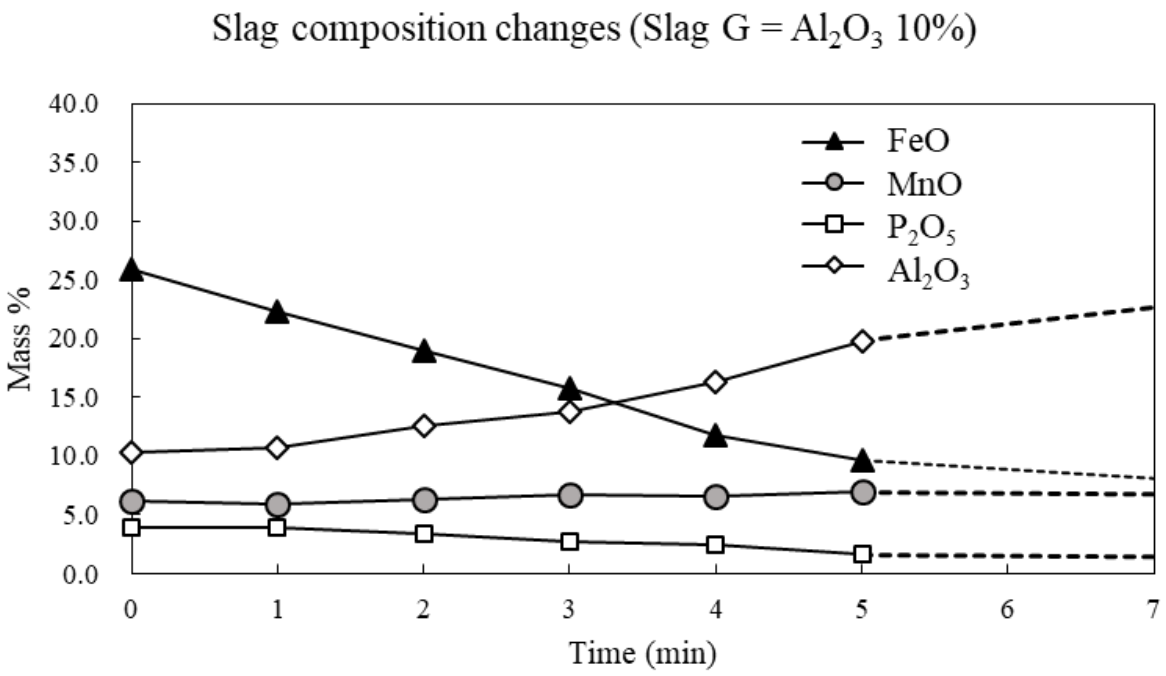

Fig. 4.6 Change in the composition of Slag G (Al_2O_3 = 10 mass %) analyzed by EPMA

The observation of the melting behavior for slag with initial Al_2O_3 content of 20% during reduction is shown in **Fig. 4.7**. With different from Slag G (Al_2O_3 = 10 mass %), the slag was not completely melted even after 3 min, and it took 4 min to be melted completely. At 1 and 2 min, large pores were found which trapped un-melted slag and unreacted graphite powder. Particularly at 2 min, small reduced metal particles were observed near the surface of pores where the molten slag was directly contacted with the graphite powder. Since solid slag particle, graphite powders and metallic particles were mixed together, un-melted slag particles were difficult to analyze. Hence, the mass balance of P and Mn for short time reduction was not obtained. After 4 min, metal particles with larger size were observed on top of the molten slag, and even at crucible bottom after 5 min.

The changes in the composition of the liquid phase in Slag I (Al_2O_3 = 20 mass %) are shown in **Fig. 4.8**. At 1 min, most of the FeO and P_2O_5 were reduced from slag, and the MnO content started to decrease after 1 min. The content of Al_2O_3 gradually increased, but the increment was smaller than that of Slag G (Al_2O_3 = 10 mass %) shown in Fig. 4.6 because of higher initial Al_2O_3 content. Comparing to the melting behavior of slag as shown in Fig. 4.7, when the melting process of slag took more time, both the reduction of Fe and P occurred fast. It is considered as not only due to the increase in the interfacial area between molten slag and graphite powder, but also because of the reduction between solid slag and graphite powder. Moreover, the reduction for Slag J (Al_2O_3 = 25 mass %) for short time was tried, but the slag was completely solid even after 1 min. This supported the reduction of MnO became intense when solid slag reacted with graphite and explained the significant reduced mass of Mn as shown in Fig. 4.4. Details for the effect of slag melting behavior on the reduction of P and Mn will be shown in discussion part.

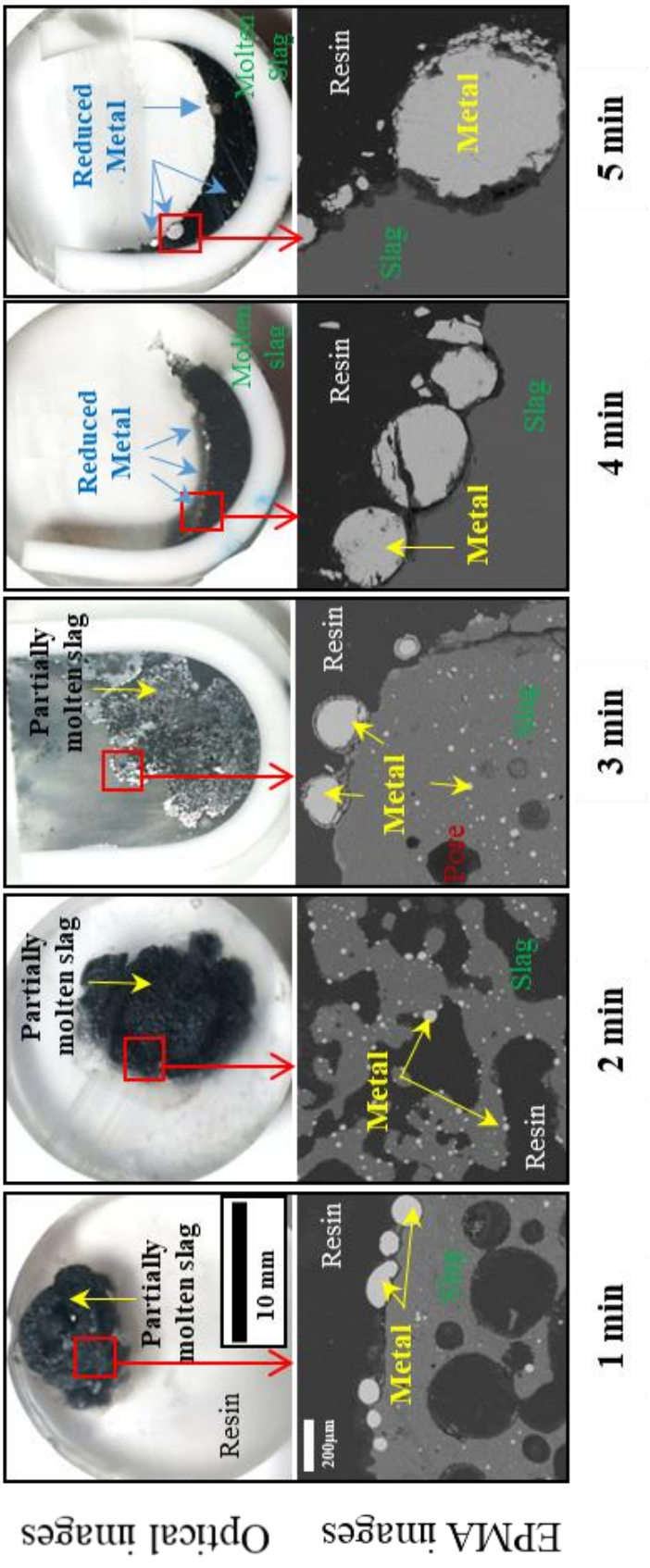

Fig. 4.7 Melting behavior of Slag I (Al_2O_3 = 20 mass %) and formation of metal during short time reduction

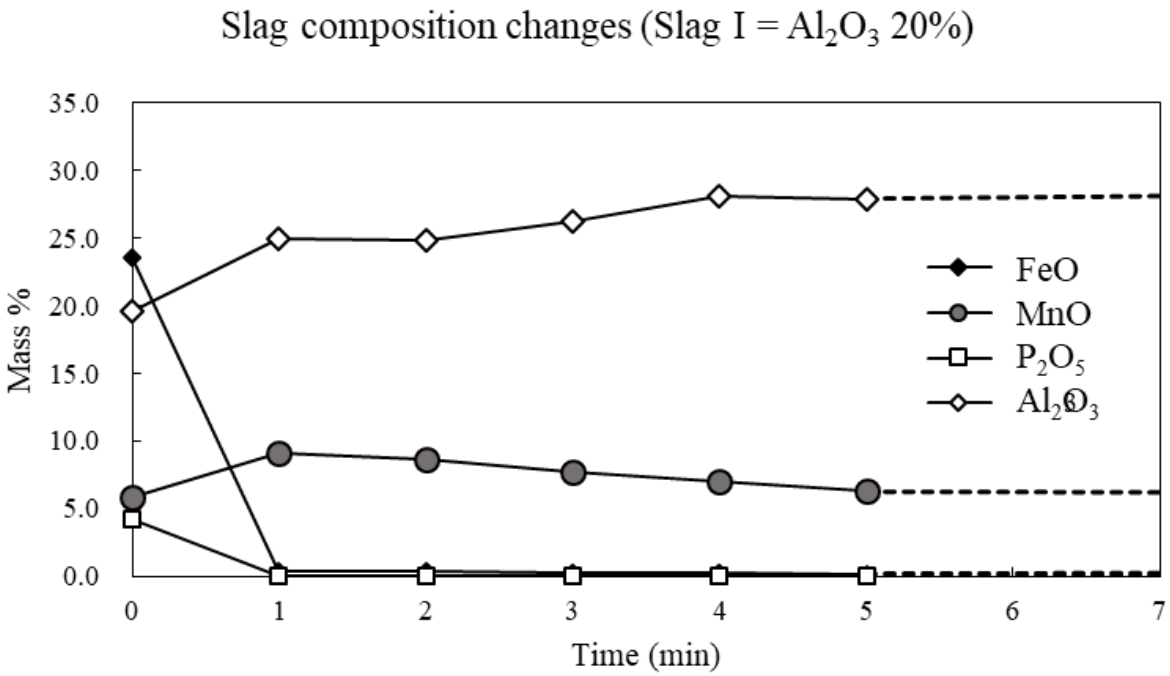

Fig. 4.8 Change in the composition of Slag I (Al_2O_3 = 20 mass %) within short reduction time analyzed by EPMA

4.2.4 Comparison on the reduction behaviors using different crucibles

In previous part, though the initial Al_2O_3 content was controlled, the gradual and continuous dissolution of Al_2O_3 from crucible still occurred. In order to understand the effects of Al_2O_3 crucible dissolution on the reduction behavior, MgO crucible shown in chapter 2 was analyzed as a comparison. **Fig. 4.9** presents the changes in slag and metal composition for the experiments using different crucibles.

Fig 4.9 (a) showed the change in the content of the oxides corresponding to each crucible. In the case of Al_2O_3 crucible, the content of Al_2O_3 in slag increased gradually even after 20 min, and the content exceeded 30 mass %. On the other hand, in the case of MgO crucible, MgO content appeared to reach saturation after 10 min at about 25 mass %. The influence of the basicity on the increases of Al_2O_3 and MgO contents was insignificant. Fig. 4.9 (b) gives the reduction behavior of FeO. The reduction of FeO content became lower when MgO crucibles were used and the slag basicity was increased. Fig. 4.9 (c) represents the reduction behaviors of MnO. Though the changes in the MnO content for all cases were small, the use of MgO crucible lead to larger decrease in MnO content than that of using Al_2O_3 crucible. In Fig. 4.9 (d), when Al_2O_3 crucible was used, the P_2O_5 content decreased with decreasing basicity. When MgO crucible was used, the P_2O_5 content increased with decreasing basicity. This would be caused by the difference of the effects on the P_2O_5 activity, as MgO is basic oxide, but Al_2O_3 is neutral oxide. Comparing to Fig. 4.9 (a), though the increase in the content of either Al_2O_3 or MgO by the dissolution of crucible did not depend on slag basicity, the reduction behavior of P and Mn was affected by both the basicity and the crucible material. The reason was considered as the changes in the activity of MnO and P_2O_5 caused by the difference of basicity and the difference in Al_2O_3 and MgO contents. Details will be shown in the discussion part. Fig. 4.9 (e) and Fig. 4.9 (f) shows the composition of the reduced metal. In all cases, the content of P increased fast within 5 min, and that of Mn increased gradually in accordance with slag composition changes.

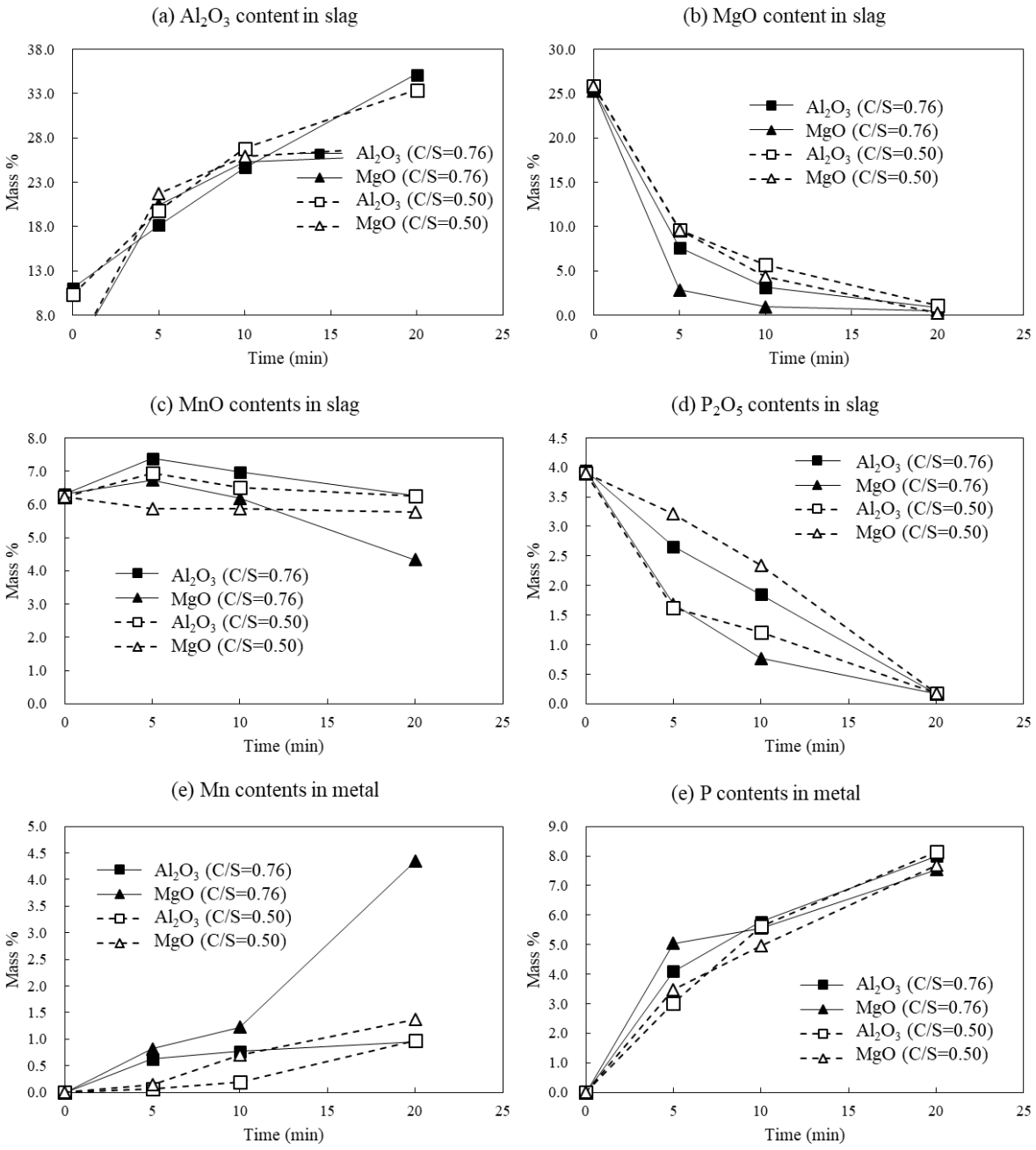

Fig. 4.9 Change in the composition of slags (Slag F and G) and metal with different crucibles

Fig. 4.10 shows the partitions of P and Mn in metal and slags using the experimental results shown in Fig. 4.9. The calculation method was the same as Fig. 4.4. In the partition of Mn, the use of MgO crucible decreased the partition ratio between slag and metal, and the partition ratio was also decreased by increasing slag basicity. In case the partition of P, similar partition ratio between slag and metal was reached at 20 min for all experimental conditions. When MgO crucible was used, the partition ratio of P was slightly higher than that of using Al_2O_3 crucible.

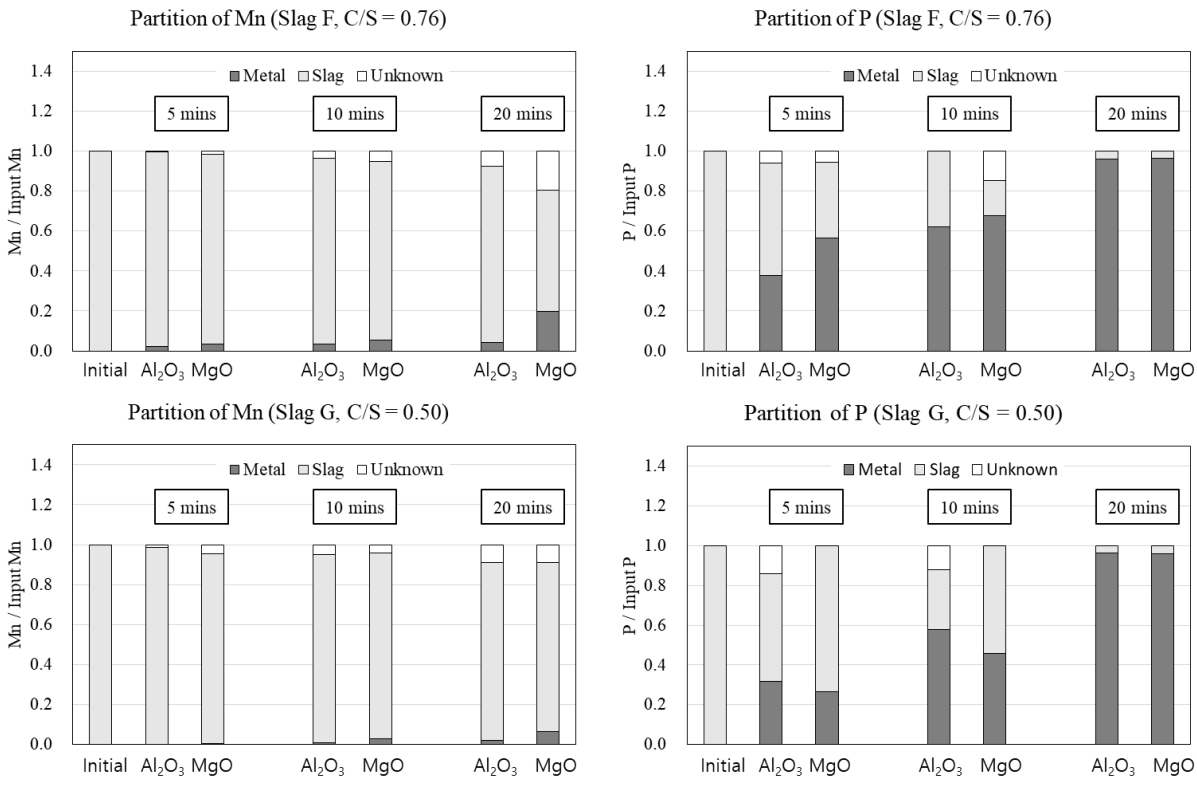

Fig. 4.10 The partitions of P and Mn for the experiments using different crucibles

4.3. Discussion

4.3.1 Influence of the melting behavior of slag on the reduction rate of P and Mn

By varying the initial Al_2O_3 content, different melting behavior of slag was observed, and the reduction rates of P and Mn were changed. Thus, the melting point of slags was considered. **Fig. 4.11** shows the initial slag composition with different Al_2O_3 content plotted on the CaO-SiO_2-Al_2O_3-(25 mass % FeO) phase diagram. As the contents of other components (P_2O_5, MnO, MgO) were low, the melting temperature of slag was considered as increased by increasing initial Al_2O_3 content. Since the slag was heated at the same rate, if the melting point of slag was high, the complete melting of slag requires more time.

To discuss the difference on the melting behavior, the change in the liquid phase ratio in slag as a function of reaction time was estimated. To estimate the liquid ratio, the variation in the slag composition with reaction time was necessary. For this purpose, the change in the mass of a component *N* from 1 min to 10 min was calculated by Eq. (4.6), assuming the linear change with time, and the composition of *N* in slag at *t* was calculated using Eq. (4.7). Here, W^N is the weight of a slag component *N*; *t** means the reaction time at which the slag composition was analyzed. In this calculation, *t** is 10 min and *t* is an arbitrary time between 0 min and 10 min. Temperature of the slag was estimated by Fig.4.1.

$$W_t^N = W_{ini}^N + \frac{W_{ini}^N - W_{t^*}^N}{t^*} \times t, \ (0\ \text{min} < t < 10\ \text{min}) \quad \ldots\ldots\ldots (4.6)$$

$$(N\%)_t = 100 \times \frac{W_t^N}{\sum W_t^i} \quad \ldots\ldots\ldots\ldots\ldots\ldots\ldots (4.7)$$

Fig. 4.12 shows calculated liquid phase ratio with reduction time. The liquid ratio of the slag which contained 10% of Al_2O_3 initially was about 75% at 1 min even though the temperature was 1231 K, and slag was completely melted within less than 2 min. For the slag initially contained 20% of Al_2O_3, the liquid ratio increased gradually with time and reached to 100% at about 5 min. The above calculated results generally agreed with the experimental result shown in Fig. 4.5 and Fig. 4.7. For the slag with the initial Al_2O_3 content of 15%, the melting behavior was slower than that of 10% Al_2O_3 and faster than that of 20% Al_2O_3. For the slag which initially had 25% of Al_2O_3, the melting rate of slag was the slowest and it took almost 9 min until complete melting.

To understand the influence of viscosity on the reduction of P and Mn, the viscosity of the liquid slag formed in short time were calculated by FactSage using the compositions of liquid slag observed in Fig. 4.6 and Fig. 4.8. The calculated viscosity was compared to the reduction rate of P and Mn from slag.

The reduction rate of P and Mn were defined by Eq. (4.8) using the change of composition between the experiment which conducted for t_a min and that for t_a+1 min. This definition on reduction rate was different from chapter 1, because the mass balance could not be obtained for short time reduction due to the existence of solid slag in some cases.

$$\frac{dP_2O_5\%\ (or\ MnO\%)}{dt} = \frac{(P_2O_5\%)_{t_a} - (P_2O_5\%)_{t_a+1}}{(t_a+1) - t_a} \quad \text{..... (4.8)}$$

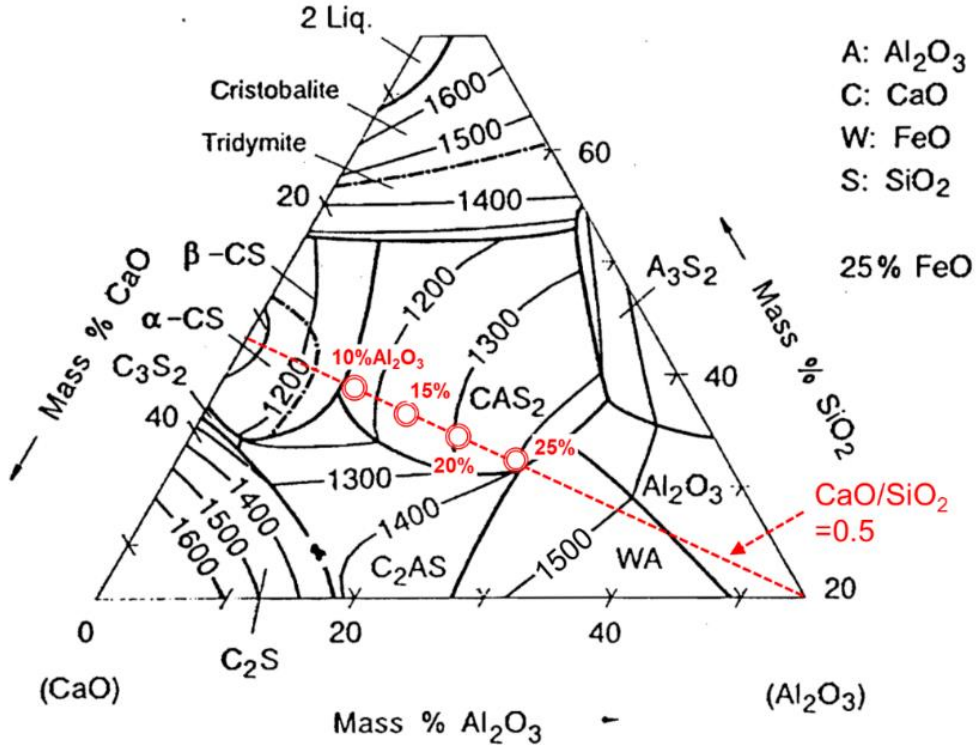

Fig. 4.11 Projection of initial slags on the CaO-SiO_2-Al_2O_3-25%FeO phase diagram [1]

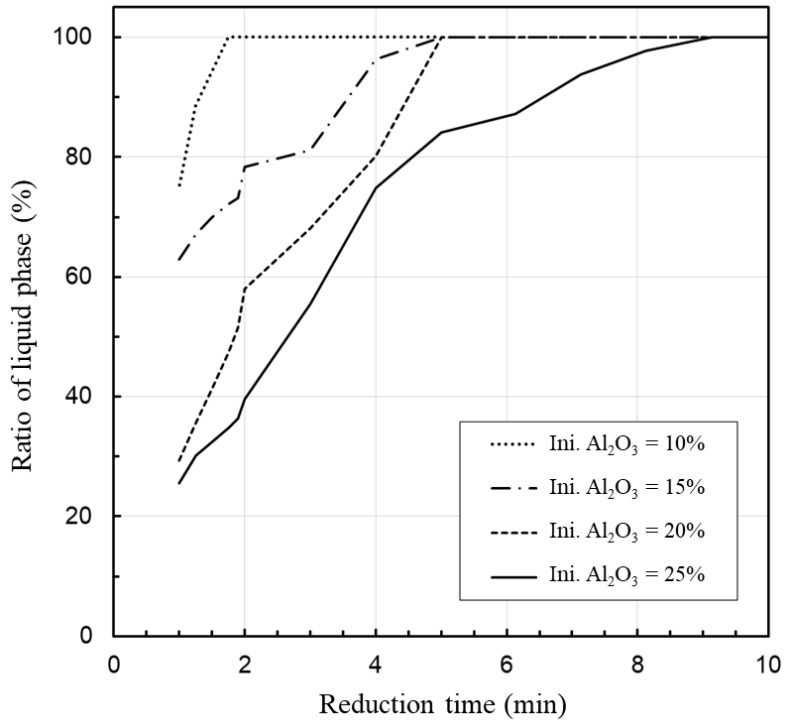

Fig. 4.12 Estimated melting behavior of slag with various initial Al_2O_3 content

Fig. 4.13 presents the relationship between calculated viscosity with reduction rate of P and Mn. As shown in Fig. 4.13 (a), the viscosity of the slag which initially contained 10% of Al_2O_3 was low because the slag has a low melting temperature and thus liquid slag formed easily. Hence, the reduction rate of P was influenced little by viscosity and showed low values. For the slag with an initial Al_2O_3 content of 20%, the viscosity was high, and the reduction rate of P was also high at 1 min. For the slag with an initial Al_2O_3 content of 10%, graphite powder easily floated on the molten slag since the slag has a low viscosity. However, the slag having an initial Al_2O_3 content of 20% trapped graphite powder inside the molten slag due to the high viscosity. As a result, the interfacial area between the liquid slag and the graphite was increased, and it increased the reduction rate of slag. Moreover, the rapid reduction of Fe and P may occur also due to the reduction between solid slag and graphite powder.

Fig. 4.13 (b) shows that the reduction rate of Mn from the slag initially containing 10% of Al_2O_3 was lower than the slag contained 20% of Al_2O_3, which indicated a better selectivity on P reduction for a slag with a lower viscosity. In the slag which contained 20% Al_2O_3, the reduction rate of Mn showed similar values after 2 min. Comparing to the high reduction rate of P at 1 min as shown in Fig. 13 (a), the reduction rate of Mn was smaller, and thus the selective reduction of P could also be found but the selectivity was bad comparing to the slag with low basicity.

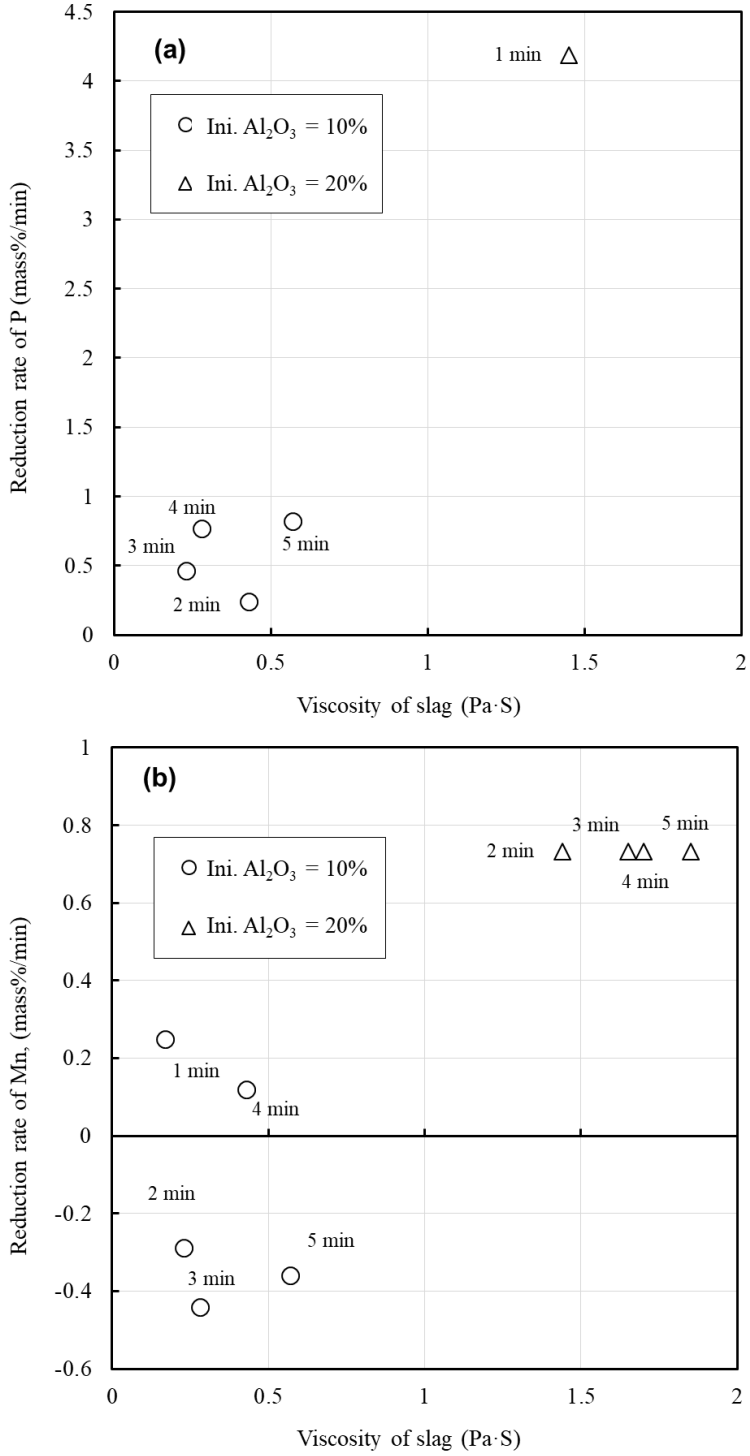

Fig. 4.13 Influence of viscosity on the reduction rate of P (a) and Mn (b)

Noticing that only the liquid slag compositions were used for the above discussion, the reduction behaviors of P and Mn from solid slag by graphite powder were not shown because of the difficulties in analysis as mentioned previously. To understand the reduction behavior of P and Mn from solid slag, the P and Mn contents in metal after the reduction of either solid or liquid slag were estimated using Eq. (4.7). In the estimation, the slag was assumed to be equilibrated with a C saturated Fe-P-Mn-C alloy. To calculate the activity coefficients of P and Mn in alloy, Eq. (4.8) and Eq. (4.9) were used which were determined by last chapter. For the solubility of C in alloy, Eq. (4.10) from last chapter was used. For the activity of MnO and P_2O_5, activities at solid state were assumed as unity, and the values of them in a liquid slag at 1773 K were calculated by FactSage [2] using the initial slag compositions. The Factsage calculation showed that, the activity of P_2O_5 was about the order of 10^{-13}, and that of MnO was the order of 10^{-2}. The calculated relation between the molar ratio of P and Mn were drawn in **Fig. 4.14**, in comparison with the results for the slag with various initial Al_2O_3 content reduced after 10 min which shown in Fig. 4.3.

$$P_2O_5(l) + 5[Mn] = 2[P] + 5MnO(l) \quad \log K = 26950/T + 0.97 \quad \text{..... (4.7)}$$

$$\ln\gamma^{H}_{Mn\ [in\ Fe-P-Mn-C(sat.)]} = -4.72X_P - 0.47X_C \quad \text{..... (4.8)}$$

$$\ln\gamma^{H}_{P\ [in\ Fe-P-Mn-C\ (sat.)]} = -4.72X_{Mn} + 4.26X_P + 6.09X_C \quad \text{..... (4.9)}$$

$$X_{C\ [in\ Fe-Mn-P-C(sat.)]} = 0.19e^{-(6.09X_P - 0.47X_{Mn})} \quad \text{..... (4.10)}$$

As shown in **Fig. 4.14**, four types of relations between X_P and X_{Mn} were considered. The calculation results assuming $a_{P_2O_5}$=1 are almost same in spite of the difference activity of MnO. This indicated that when the reduction of P_2O_5 occurred at solid state, the reduction of P_2O_5 was intense and the reduction of MnO was weak despite of liquid or solid state. When the reduction of P_2O_5 occurred in the liquid state ($a_{P_2O_5}$=10^{-13}), the reduction of MnO became significant when slag was solid.

Comparing to the experimental results, the metal composition reduced from the slag initially contained 10% of Al_2O_3 agreed with the dash line which present both the P and Mn were reduced from liquid phase. In addition, the metal reduced from the slag initially contained 25% of Al_2O_3 agreed with the dot line which assumed that MnO was reduced from solid slag. For the slag initial containing 20% of Al_2O_3, because the slag was partially melted even after 3 min, MnO was reduced from both liquid and solid slag, and thus the metal composition located between the dot and dash lines. For the same reason, the result of slag initially containing 15% of Al_2O_3 also located between the dot and dash lines, but the point was at lower position than that of 20% Al_2O_3 slag, probably due to less solid slag remained during reduction. Therefore, if the melting of slag took time, the reduction of P occurred fast due to solid state reduction and the reduction of liquid slag by trapped graphite particles. After the reduction of P, the reduction of MnO became significant when solid slag remained. To obtain a better selective reduction of P from steelmaking slag, a decreasing in slag melting temperature to allow fast melting is important.

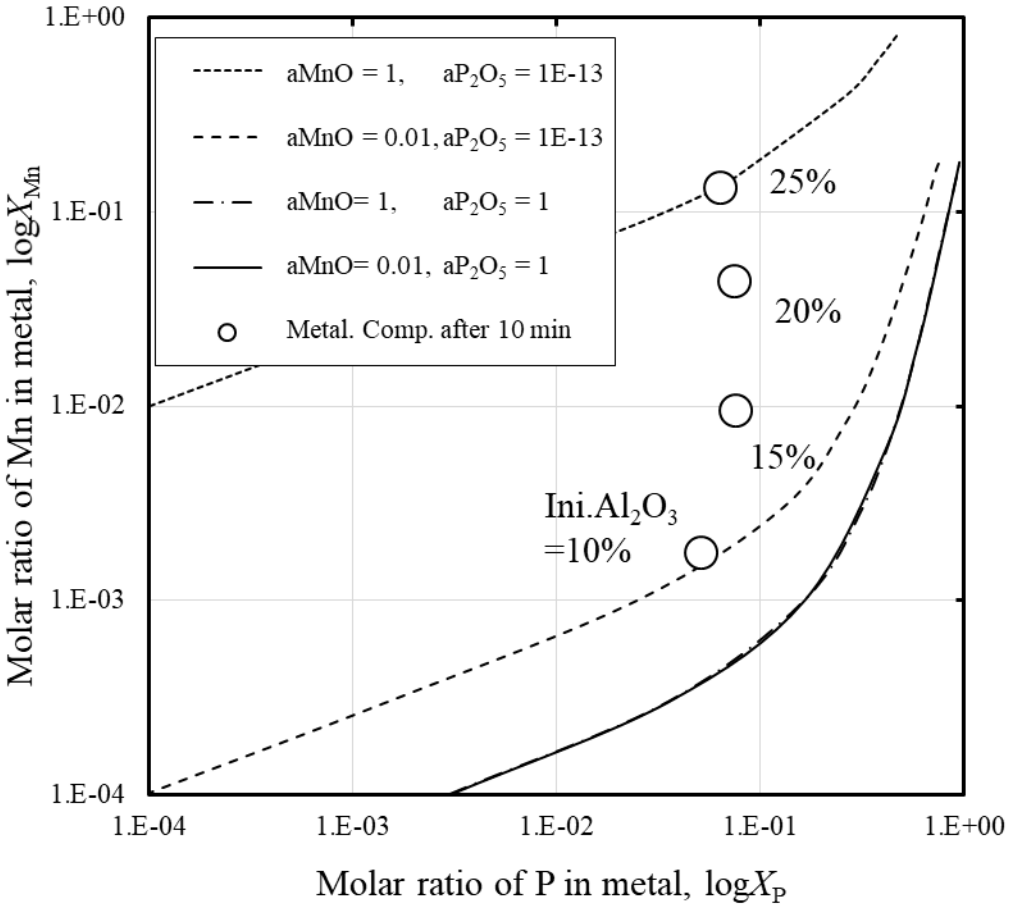

Fig. 4.14 Comparison between the estimated metal phase composition and experimental results

4.3.2 Role of Al_2O_3 and MgO dissolved from crucible on the reduction rate of P and Mn

When different crucibles were used for reduction experiment, the reduction of P and Mn showed different behaviors, and the dissolution behavior of Al_2O_3 and MgO were also different. To understand these differences, the effect of Al_2O_3 and MgO on the melting behavior of slag was considered firstly. **Fig. 4.15** shows the estimated liquid phase ratio during the initial period of the reduction using different crucibles. In this figure, same calculation method for liquid phase ratio to that of Fig. 4.12 was used, and this time the t^* was 5 min. From this estimation, it is clear that the melting rate was fast for each experiment using different crucible, and the difference on the melting behaviors due to slag basicity and crucible material was not large. Considering that the reduction of slag (C/S=0.5, Al_2O_3 crucible) was not influenced much by solid phase as discussed previously, the small differences on the melting behaviors would affect little on the reduction of P and Mn. Therefore, the results were analyzed by the difference of thermodynamic characteristics.

The activity coefficient of P_2O_5 and MnO were calculated using the slag composition shown in Fig. 4.9 by FactSage. The relations between the calculated activity coefficient and the Al_2O_3 or MgO content in slag are shown in **Fig. 4.16**. In Fig. 4.16 (a), the decrement in the P_2O_5 activity coefficient when using MgO crucible were larger than that using Al_2O_3 crucible, except for the results of the slag with a basicity of 0.76 reduced for 5 min using MgO crucible. Because the activity coefficient of P_2O_5 could be decreased by an increase in basic oxide content such as MgO, the decrement of it when using MgO crucible was large. As shown in Fig. 4.16 (b), the MnO activity coefficient in the slag melted using Al_2O_3 crucibles decreased with reduction time, but it increased when MgO crucible was used. In addition, for the slag with basicity of 0.76 melted using MgO crucible, the increase was not significant until MgO content exceeded 20%.

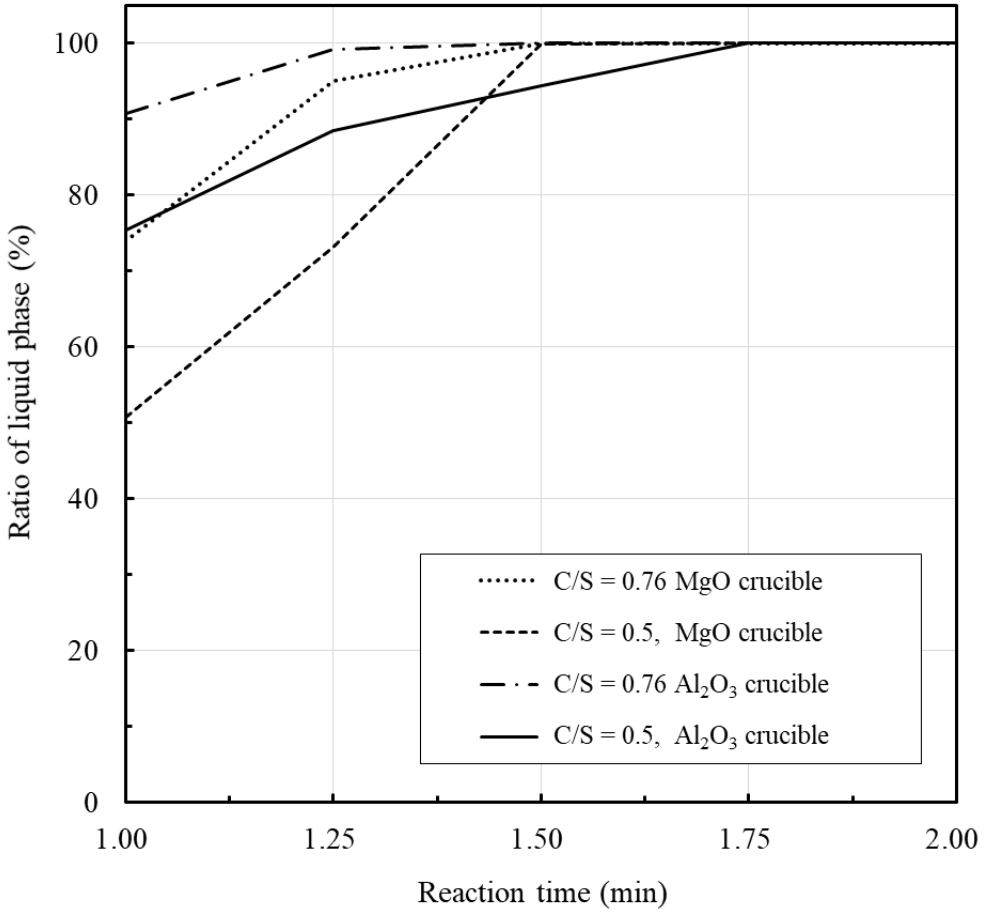

Fig. 4.15 Melting behaviors of slag with different basicity reduced using different crucible material

The comparison between the reduction rate and the activity are shown in **Fig. 4.17**. The reduction rate of either Mn or P was calculated using Eq. (4.11).

$$R_A = (W_{AO_x}^{\text{Initial}} - W_{\text{Slag}} \times (\text{mass }\%AO_x)/\Delta t \quad \ldots\ldots\ldots\ldots (4.11)$$

Here, R_A is the reaction rate of element *A*, g/min; $W_{AO_x}^{\text{Initial}}$ is the initial mass of oxide AO_x, g; W_{Slag} is the mass of slag after a given reaction time; $(\text{mass }\%AO_x)$ is the mass fraction of oxide AO_x in slag at a given reaction time, %; and Δt is the change in the reaction time, min.

As shown in Fig. 4.17 (a) and Fig. 4.17 (b), the reduction rate of both P and Mn decreased with a decrease in their activity. The activity of P_2O_5 in slag decreased by the dissolution of MgO from crucible, the reduction rate of P_2O_5 when using Al_2O_3 crucible was larger than that of using MgO crucible. On the opposite, the reduction rate of MnO when using MgO crucibles was larger than that of using Al_2O_3 crucible, because the dissolution of MgO from crucible increased the activity of MnO in slag. For the results of the slag with a basicity of 0.76, reduced for 5 min using MgO crucible, the reduction rates of P and Mn were similar to the results using Al_2O_3 crucibles, due to the similarity on the activity.

Therefore, the continuous dissolution of Al_2O_3 from crucible barely affected the reduction of P_2O_5 and MnO, but the continuous dissolution of MgO suppressed the reduction of P while enhanced the reduction of Mn. In the perspective of selective reduction of P from steelmaking slag, Al_2O_3 was more beneficial than MgO.

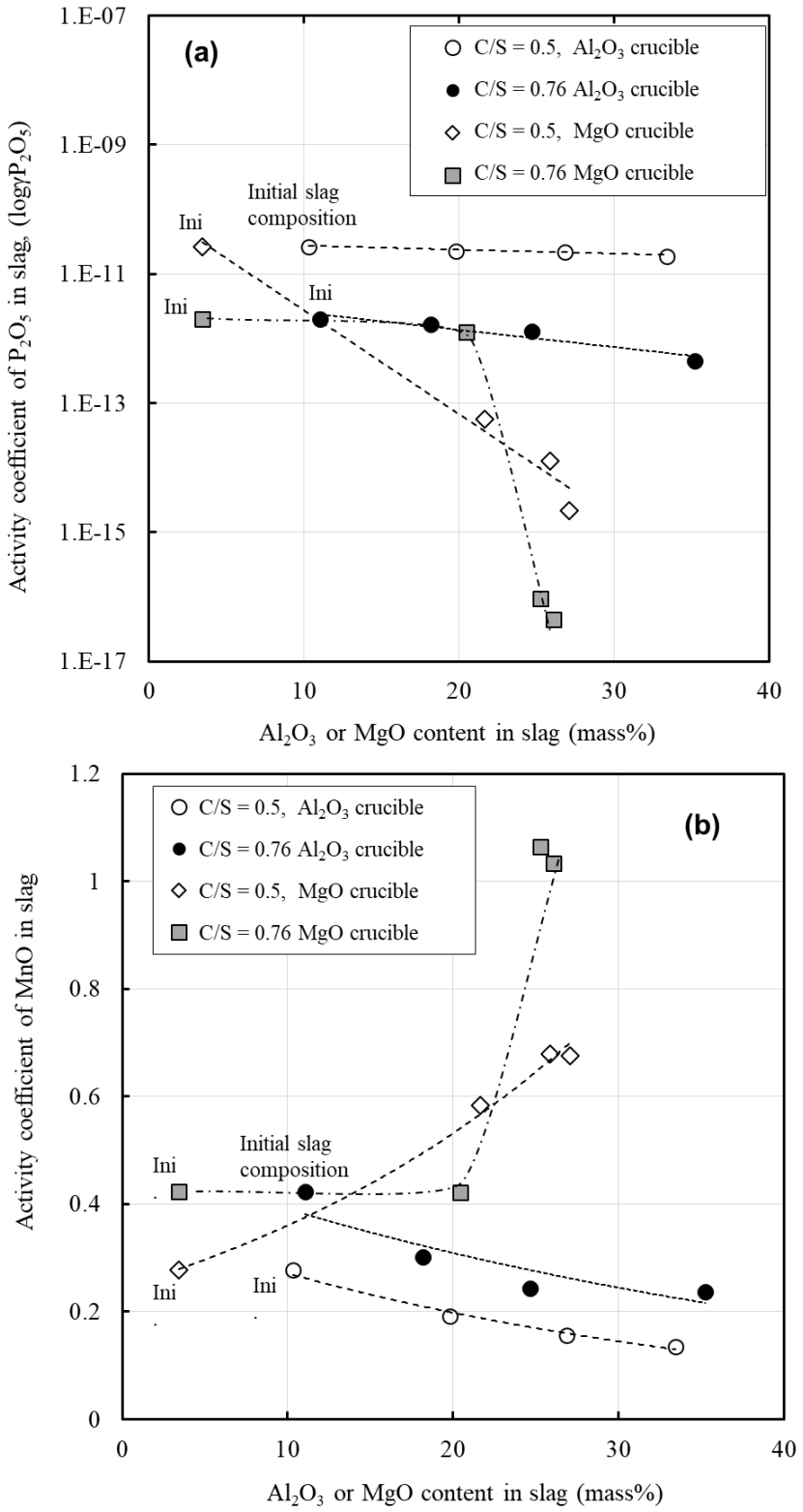

Fig. 4.16 Change in the activity coefficient of (a) P_2O_5 and (b) MnO during reduction

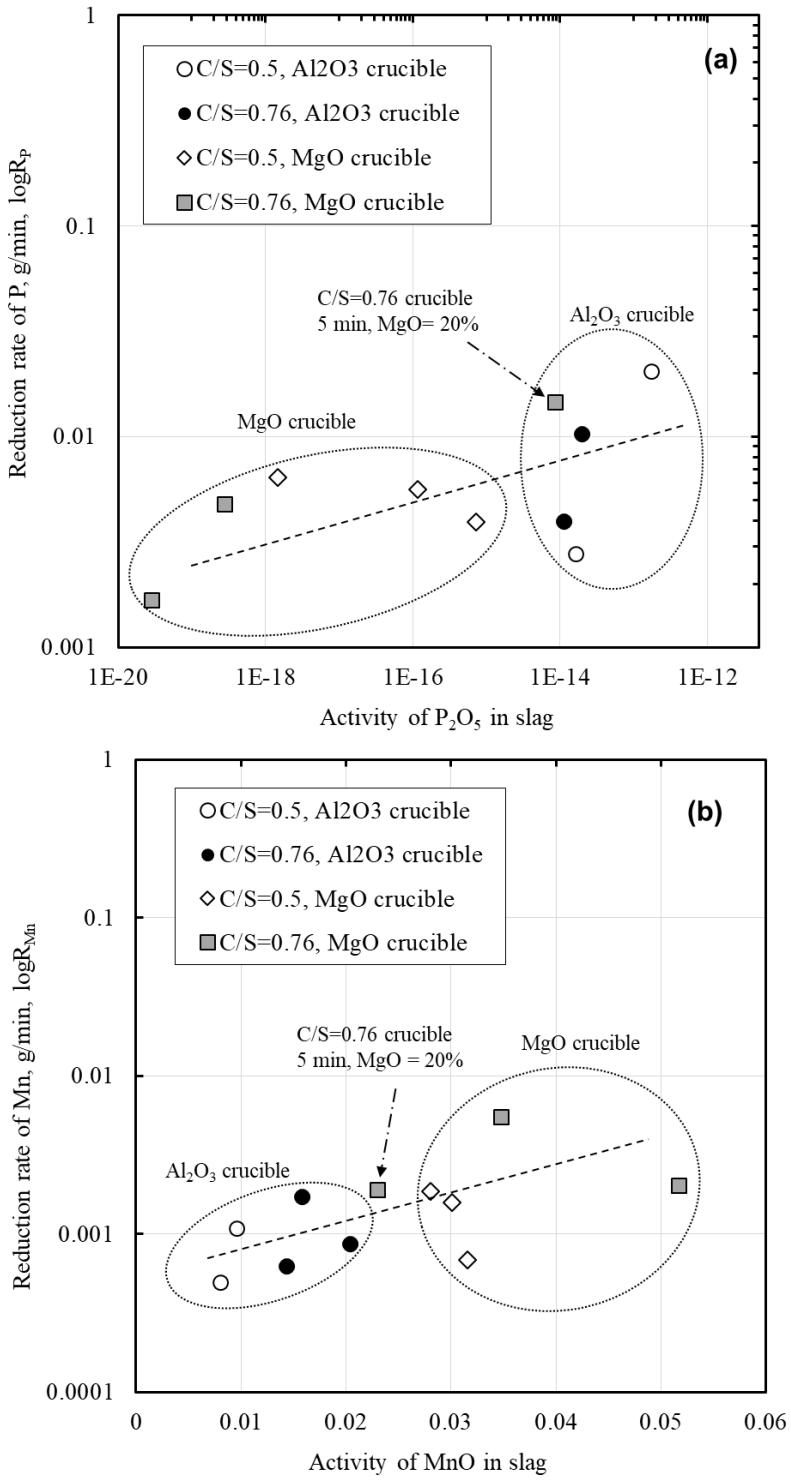

Fig. 4.17 Influence of the activity of MnO and P_2O_5 on their reduction rate

4.4 Summary

In order to understand the role of Al_2O_3 on the selective reduction of P from steelmaking slag, in this chapter, the initial Al_2O_3 contents in slag was varied from 10% to 25% and its effect on the reduction behavior was investigated. In addition, both Al_2O_3 and MgO crucible were used to compare the effect of continuous dissolution of crucibles on the reduction behavior of MnO and P_2O_5. The conclusions were summarized as follows,

1) For the slag with a basicity of 0.5, an increase in the initial Al_2O_3 content increased the melting temperature of slag and changed the melting behavior. When the initial Al_2O_3 content was 10%, slag was mostly melted after 1 min, but it required about 4 min to melt the slag when the initial Al_2O_3 content was 20%. When the slag was melted fast, good selective reduction of P was observed. When the melting of slag took time, the reduction of Mn became intense. Therefore, a slag of low melting temperature which could melt rapidly was beneficial for selective reduction of P from steelmaking slag. Moreover, an evaluation on the role of slag viscosity and the existence of solid slag on reduction of P and Mn were discussed.
2) In Chapter 2, the experiments using different crucibles was shown and the experiments using Al_2O_3 crucibles showed better selectivity on P reduction than that of using MgO crucible. Because the slag melting behavior and viscosity were similar, the above differences on the reduction behaviors of P and Mn were explained by the effect of MgO and Al_2O_3 on the activity coefficient of P_2O_5 and MnO.

4.5 References

6. Atlas, S. (1995). Verlag Stahleisen GmbH, Düsseldorf. *Germany, ISBN*, 3-514.
7. Factsage, Ecole Polytechnique CRCT, Montreal.

Chapter 5 Application of the Selective Reduction to the Production of Low P Ferromanganese Alloy

In previous chapters, separation of P and Mn from steelmaking slag through selective reduction was achieved. By decreasing the slag basicity and increasing the temperature for reduction, Fe and P were reduced into metal while most of the Mn was remained in the slag. The results of the optimum condition showed that the highest removal ratio of P from slag was more than 95%, and the loss of Mn to the metal was less than 5%.

As mentioned in chapter 1, the use of ferromanganese alloy with low content of P became important issue in recent years, because of the increase in the high performance steel products such as high-Mn steel. To produce low P ferromanganese using the conventional reduction process, the use of the Mn-ore with extremely low P content is left to be the only option. However, it is impossible to obtain such a Mn-ore with special grade sustainably.

In this chapter, the selective reduction technique is applied to Mn-ores in order to remove the P in Mn-ore. Two types of Mn-ore (Gabon Mn-ore and South Africa Mn-ore) with different composition were selected as targets. The actual Mn-ores were supplied by JFE Steel Corporation. Using Gabon Mn-ore, the influence of the addition amount of graphite powder, SiO_2, Fe-C(sat.) and the temperature on the reduction behavior were investigated. An optimum condition to remove P was proposed, and this condition was applied to South Africa Mn-ore. In discussion, the differences in the reduction behavior between the brands of Mn-ores were compared, and the possibility on producing ferromanganese with low P after the selective reduction was considered.

Chapter 5

5.1 Selective reduction of P from Gabon Mn-ore

5.1.1 Characteristics of Gabon Mn-ore

Gabon Mn-ore with particle size of smaller than 2 mm was used in this study. The crystalline phases of Gabon Mn-ore identified by XRD is illustrated in **Fig. 5.1**. In natural state of Gabon Mn-ore, Mn and Si existed in both oxide and hydroxide forms, while Al was observed mainly as a hydroxide. Since the hydrated compound evaporates quickly during heating up of reduction experiment which leads to a large volume expansion. Therefore, the hydrated compound in the Mn-ore was removed prior to the reduction experiment by a heat treatment at 1273 K for one hour in air. The changes of crystalline phases of Gabon Mn-ore after dehydration is also illustrated in Fig. 5.1.

After dehydration, approximately 12% of weight loss was observed which was regarded as moisture. After dehydration, the hydroxides were transformed to oxides, forming the $MnSiO_3$, due to the reaction between Mn oxides and SiO2 during the heat treatment. In addition, the valence of Mn in the oxide was changed during heat treatment, but this change was not considered to affect the reduction behavior because the reduction was expected to occur in the molten state.

The chemical composition of the Mn-ore that analyzed by inductively coupled plasma atomic emission spectroscopy (ICP–AES) is listed in **Table 5.1, w**here “T” indicated the total content as the valence states of these oxides did not identified. Comparing to the composition of steelmaking slag used in previous chapters, the content of Fe and P were low, and the Mn content was high. The composition of the Gabon Mn-ore after dehydration is also shown in Table 5.1.

Table 5.1 Chemical composition of Gabon Mn-ore before and after dehydration

	T. Fe	T. Mn	SiO_2	Al_2O_3	T.P	Others (Ca, Mg. Cr, S)
Natural state	3.43	52.31	4.12	6.58	0.14	< 0.5
After dehydration	3.26	65.84	5.21	6.83	0.15	<0.5

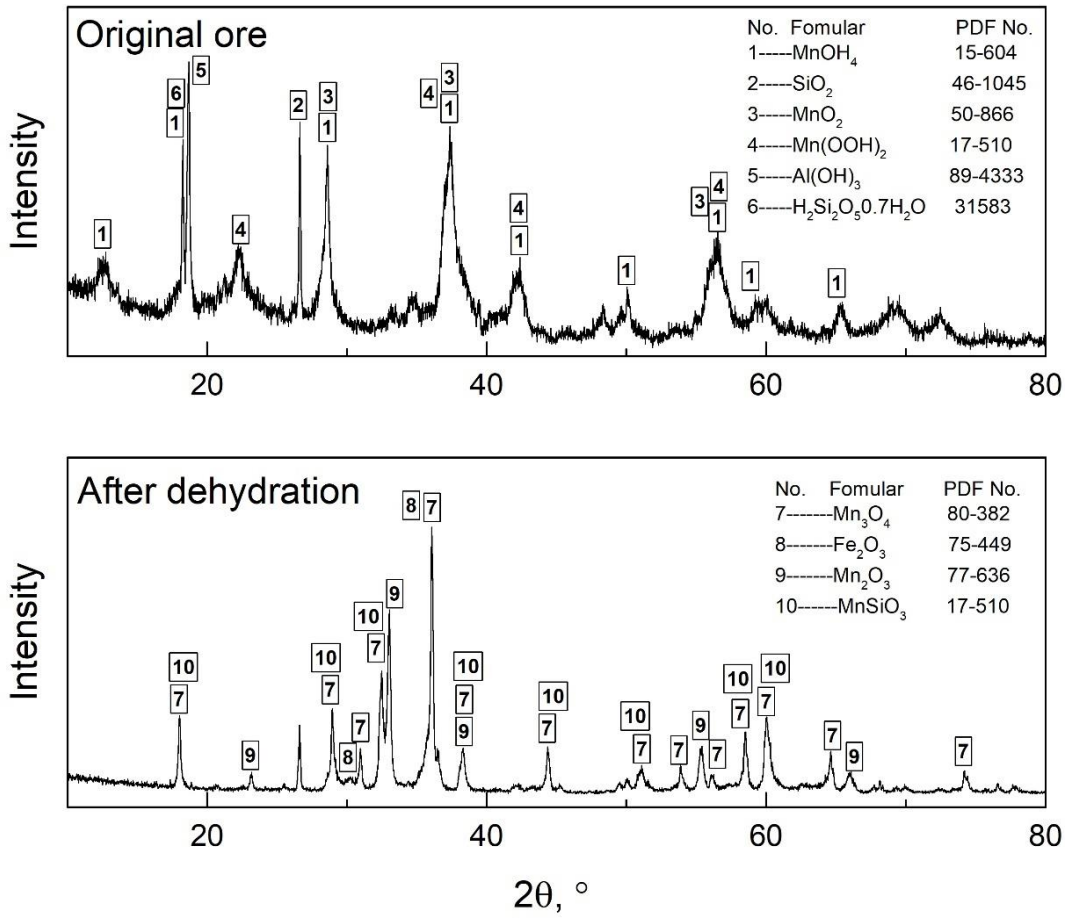

Fig. 5.1 Mineralogical phases in the original Garbon Mn-ore and that after dehydration

(Dehydration condition: Temperature: 1273K, Time: 1 hour, Atmosphere: Air)

5.1.2 Principle for selective reduction of Gabon Mn-ore

Based on the conclusions of the previous chapters, designing of an acidic slag with a low melting point is the key point in order to reduce P into the metal selectively, while suppressing the reduction of Mn. Applying this, SiO_2 was chosen as the slag modifier. Although various Mn-oxides exist with different valence states (MnO_2, Mn_2O_3, Mn_3O_4...), MnO is considered to be stable during the state of smelting reduction. In addition, most of the Fe oxide in the Mn-ore is reduced rapidly; the content of Fe oxide in Mn-ore does not need to be considered. Therefore, the major composition of Mn-ore can be simplified to the ternary system of MnO-SiO_2-Al_2O_3. Calculation for additional amount of SiO_2 was considered in this system.

Fig. 5.2 shows the liquid area of MnO-SiO_2-Al_2O_3 system at each temperature calculated by FactSage[1]. A lower temperature is energetically preferable and protects crucible, but the liquid area decreases with a decrease in temperature. Therefore, the experimental temperature was set as 1673 K, and to investigate the effect of temperature variation, experiments at 1573 K and 1773 K were also conducted. In Fig. 5.2, the average composition of the slag by the addition of SiO_2 to the Mn-ore at 1673 K is shown. The SiO_2 content of the liquid at MnO saturation is 21.3%, and that at SiO_2 saturation is 52%. Converting the mixing ratio of SiO_2 to Mn-ore, the upper and lower limits of SiO_2 addition are 15% and 71%, respectively. Therefore, the mixing ratio of SiO_2 was varied as 30%, 42%, and 54% to investigate the effect of SiO_2 addition on the selective reduction of P from Gabon Mn-ore.

On the other hand, since the content of Fe oxide in Gabon Mn-ore is low as shown in Table 5.1, the amount of metal after reduction is insufficient for accumulating P, and likewise for a better separation between metal and slag. To solve this problem, C-saturated Fe (pig iron) was added. As the P content in the metal is decreased during reduction by the in-mixing of pig iron, the reduction behavior of P is changed. Therefore, the mixing ratio of pig iron to Mn-ore was varied as 10%, 20% and 40%.

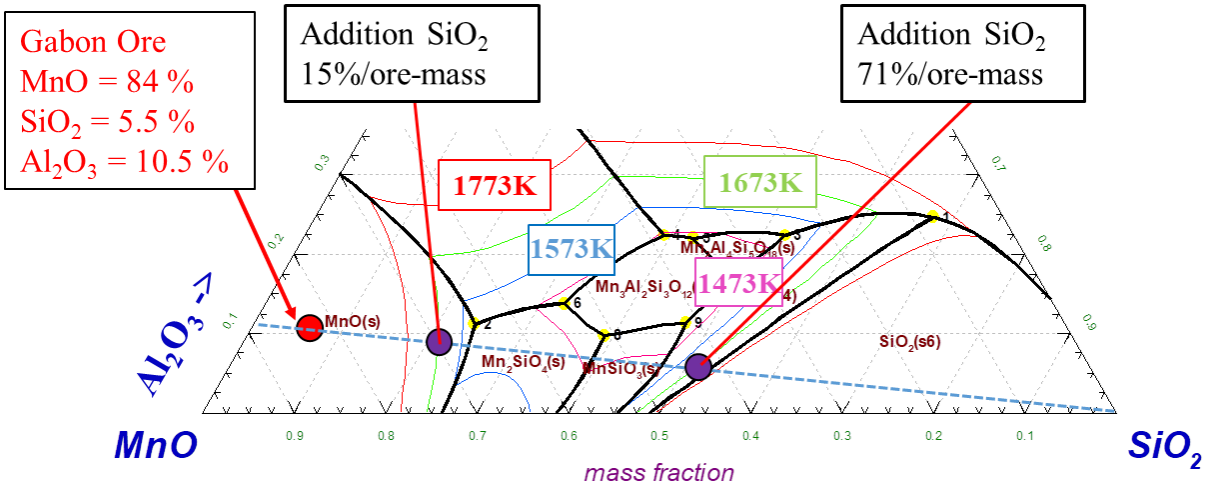

Fig. 5.2 Isothermal liquid line of MnO-SiO_2-Al_2O_3 slag system calculated by Factsage [1]

Table 5.2 List of experiment conditions

Group	Mixing ratio to Mn-ore			Temperature	Reaction time	Note
	Graphite powder	Pig iron	SiO_2			
1	5%	20%	54%	1673K	10 mins, 20 mins	Influence of Graphite powder
	10%					
	20%					
2	10%	10%	54%	1673K		Influence of Pig iron addition
		20%				
		40%				
3	10%	20%	30%	1673K		Influence of SiO_2 addition
			42%			
			54%			
4	10%	20%	54%	1573 K		Influence of Temperature
				1673 K		
				1773 K		

5.1.3 Experimental

5.1.3.1 Sample preparation

Based on previous section, the raw materials for reduction experiments are the Gabon Mn-ore powder after dehydration, SiO_2, pig iron, and graphite powder. To prepare pig iron, lumps of electrolytic iron were melted with graphite powder at 1473 K using a graphite crucible. The mixing ratio of graphite with iron was set at 5 %. The molten metal was poured onto a cold Cu plate for quenching. After quenching, the pig iron was crushed to a flake size smaller than 3 mm and used as a raw material for the experiments. The content of carbon in the pig iron was around 4 % as analyzed by combustion infrared spectrometer (CIP). The mixing ratio of graphite powder was stoichiometrically considered based on following Eqs (5.1) to (5.3).

$$(FeO) + C(s) = [Fe] + CO(g) \quad \text{..... (5.1)}$$

$$(P_2O_5) + 5C(s) = 2[P] + 5CO(g) \quad \text{..... (5.2)}$$

$$(MnO) + C(s) = [Mn] + CO(g) \quad \text{..... (5.3)}$$

According to calculation, the necessary amount of graphite powder to reduce FeO and P_2O_5 in Mn-ore was less than 1 mass % of Mn-ore. In case of including MnO, it required 15 mass % of graphite powder. Therefore, the amount of graphite powder was set from 5% to 20%. The dehydrated Mn-ore, flake size of pig iron, reagent of SiO_2, and graphite powder were mixed with a given ratio before reduction experiment. 5g of Mn-ore was used for each run, and the experimental conditions are summarized in **Table 5.2**.

5.1.3.2 Selective reduction experiment

The experimental method for the reduction of steelmaking slag as described in previous chapters was used in this study. A vertical type of resistance furnace equipped an alumina reaction tube (inner diameter: 42 mm, height: 1000 mm) and a quartz crucible (inner diameter: 20 mm, height: 85 mm) were used for the experiment. Before charging the sample, the furnace was heated to the target temperature (1573 – 1773 K), and its atmosphere was controlled by continuously flowing Ar gas (purity: 99.9999%, flow rate: 500 ml/min). For each reduction experiment, mixtures of Mn-ore, SiO_2, pig iron and graphite were loaded in a quartz crucible and then carefully placed in the hot zone of furnace. **Fig. 5.3** shows heat temperature profile during experiment. The mixtures were heated rapidly and reached the target temperature in about 6 to 8 mins. After a given reaction time, the crucible and sample together were quickly taken out and immediately quenched by water. After quenching, the reduced slag and metal were separated, and their compositions were analyzed by ICP-AES. The carbon content of the metal was analyzed by CIP.

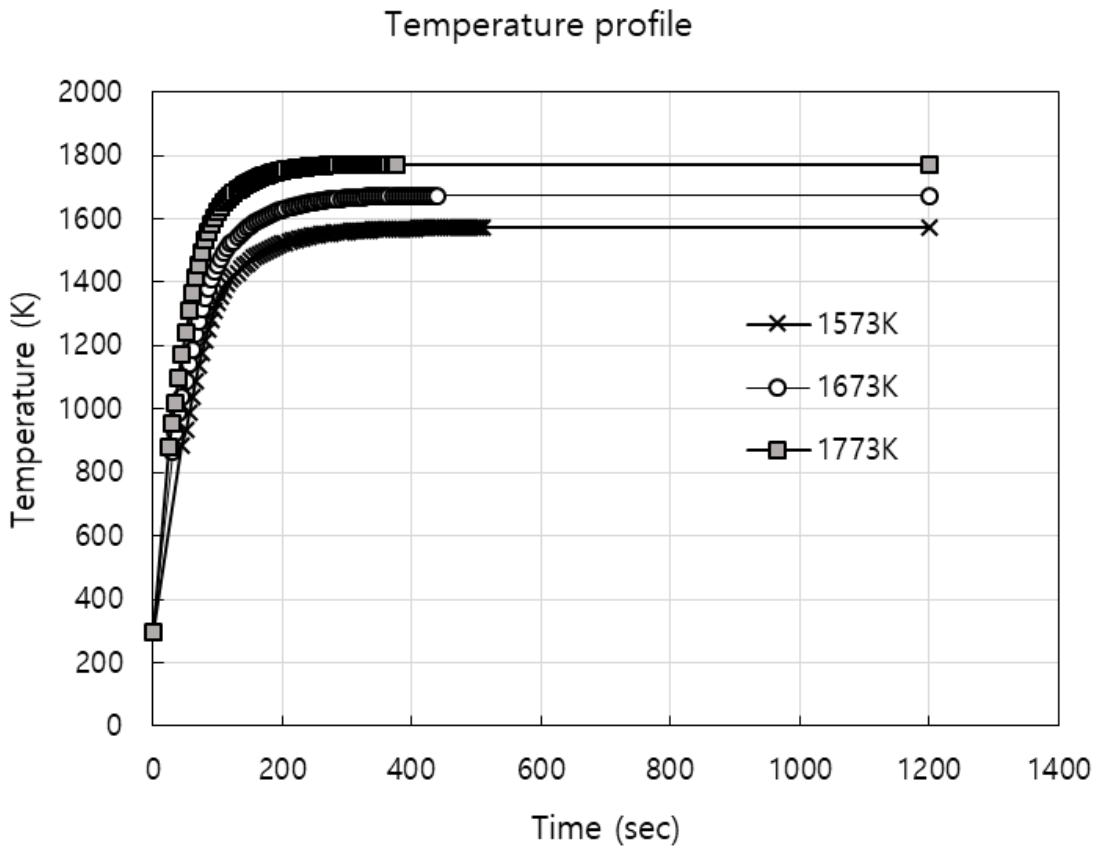

Fig. 5.3 Profile average temperature in sample during heating

5.1.4 Results

Fig. 5.4 shows a typical image of a cross-section of a sample after reduction. A glassy phase of slag with a dark color is present, which represents the molten slag formed from the mixture of the Mn-ore and the SiO_2. Adjacent to that, a light-colored layer is found at the top. This top layer was found by electron-probe microanalysis (EPMA) to consist of a MnO-Al_2O_3-SiO_2 (rich) oxide, formed by to the dissolution of SiO_2 from the quartz crucible. As the content of SiO_2 in slag at top area was high, only the glassy slag with the dark color was used for ICP-AES analysis. At the bottom of the crucible, the solidified hot metal can be easily distinguished and separated from the glassy slag. Some residual graphite powder was observed on the surface of the molten slag, even for the lowest mixing ratio of graphite powder.

Typical composition changes of slag and metal during reduction are presented in **Fig. 5.5**. For the slag composition, most of the Fe in the slag was reduced after 10 mins, and dissolved in the hot metal, and a decrease in the P content of the slag was observed. The content of P in the slag decreased from the initial 0.23% to 0.03% after 10 mins, and further decreased to 0.01% after 20 mins. As a result, the content of P in the metal increased to about 0.6 % after 10 mins and then remained unchanged. In the case of Mn, the content of Mn in the slag barely changed during reduction, but the content of Mn in the metal increased gradually with reaction time. Thus, the selective reduction of P over Mn was achieved for Mn-ore, as a large part of the P was removed from the slag while the content of Mn in the slag remained unchanged. The content of SiO_2 increased only slightly from 10 mins to 20 mins, primarily due to the dissolution of SiO_2 from the crucible. In the metal phase, the Si content was negligibly small. The content of C in the metal decreased continuously with reaction time, despite the excess of graphite powder was used in the experiment. The contribution of the graphite powder and the carbon dissolved in hot metal on the reduction will be discussed later.

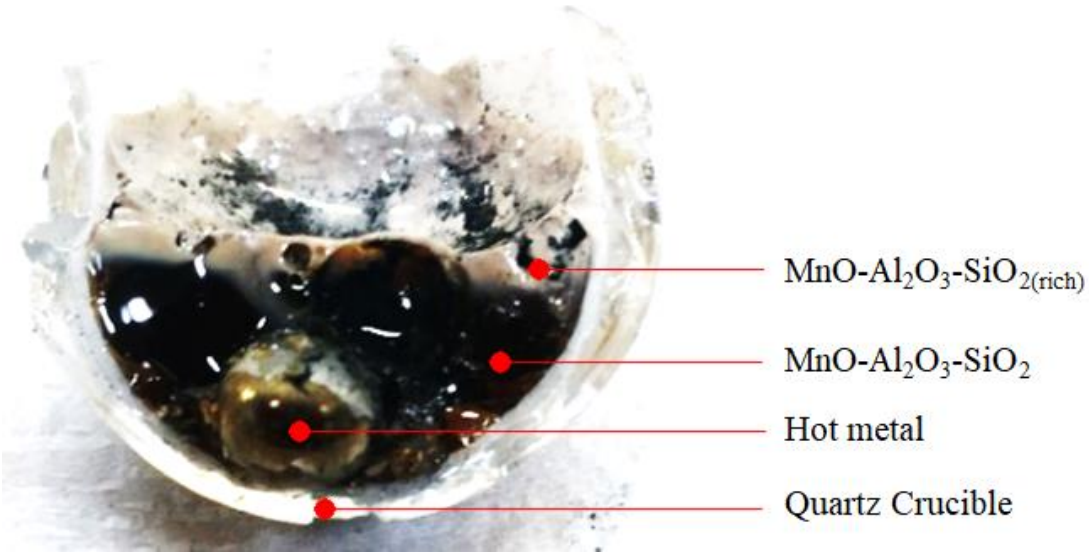

Fig. 5.4 A typical image of sample after 20 mins of reduction

(Mixing ratio: Graphite powder: 5%, SiO_2: 54%, Pig iron: 20% at 1673 K)

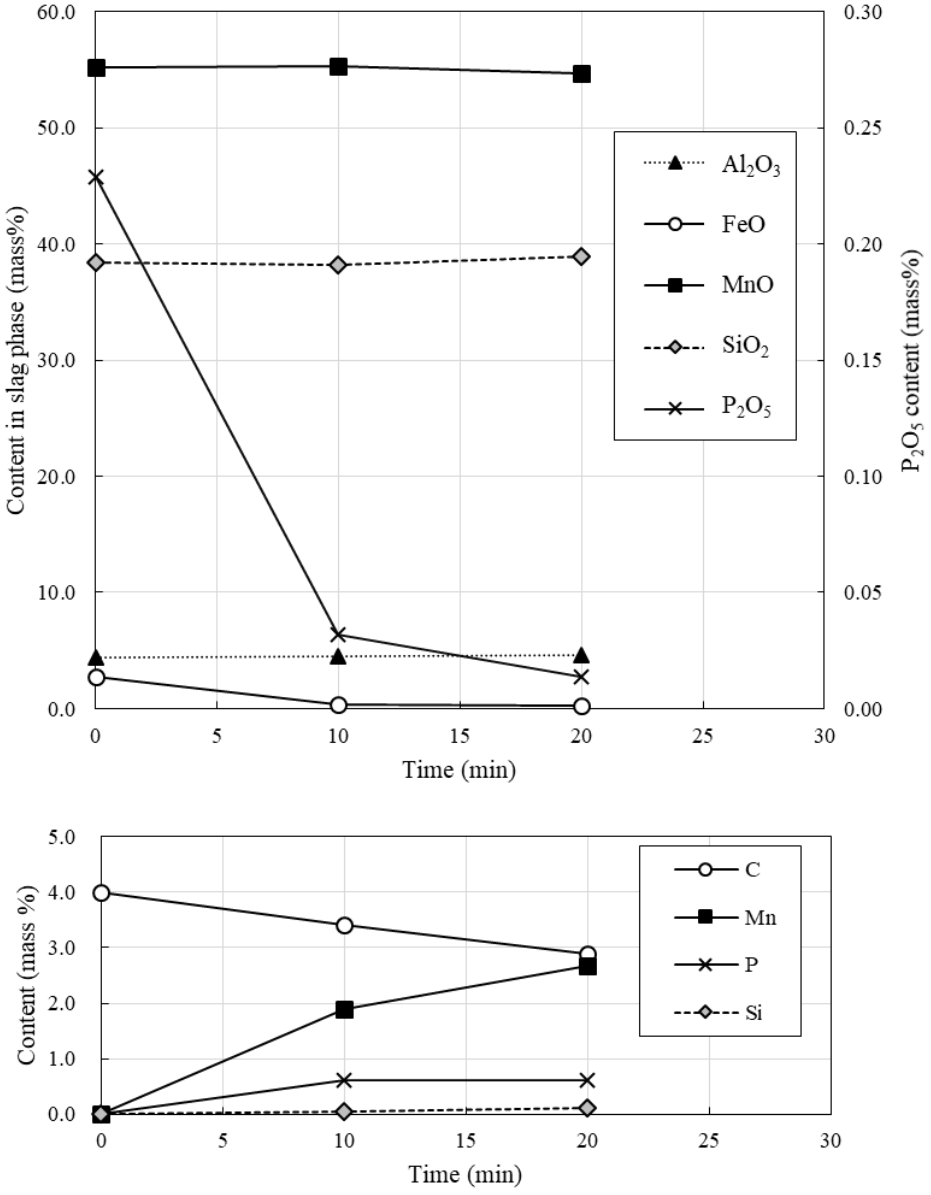

Fig. 5.5 Typical composition changes of slag and metal during reduction

(Mixing ratio: Graphite powder: 10%, SiO_2: 54%, Pig iron: 20% at 1673 K)

5.1.4.1 Influence of mixing ratio of graphite powder on the reduction behavior

The influence of the mixing ratio of graphite powder on the reduction behavior is shown in **Fig. 5.6.** When the mixing ratio was 5%, the reduction of both FeO and P_2O_5 were insufficient. When the mixing ratio was increased to 10% or more, most of FeO and P_2O_5 in the slag were reduced within 10 mins. In the case of the Mn, although an increase in the addition of graphite powder led to an increase in the Mn content in the metal, the content of Mn in the slag was similar for both the mixing ratio of 5% and 10%. An obvious decrease in the content of Mn in the slag was observed by the addition of 20% graphite. The C content of the hot metal decreased in a fashion exhibiting similar trends, and it was not affected by the mixing ratio of graphite powder. There might be two reasons for the decrease in the C content; one was the decrease in C solubility in the metal due to the increase in P content, and the other was the consumption of dissolved C by reduction. Detail explanations will be presented in the discussion part.

In order to compare the partition behavior of P and Mn between slag and metal, the mass balances of P and Mn at given reaction times were calculated. Equation (1) was used to calculate the total mass of slag at a given reaction time using the mass of the Al_2O_3, as the Al_2O_3 was hardly reduced under the experimental conditions studied.

$$W_{Slag} = W_{Al_2O_3}^{Initial} / (mass\ \%\ Al_2O_3)_t \times 100 \quad \ldots\ldots\ldots\ldots\ldots (5.4)$$

where W_{Slag} is the mass of slag, g; $W_{Al_2O_3}^{Initial}$ is the mass of Al_2O_3 contained in the initial slag, g; $(mass\ \%\ Al_2O_3)_t$ is the Al_2O_3 content of slag after reducing for a time t (min). For the total mass of metal, a large lump of metal was easily obtained after reduction. The weight of the metal was directly measured using a mass scale after each experiment.

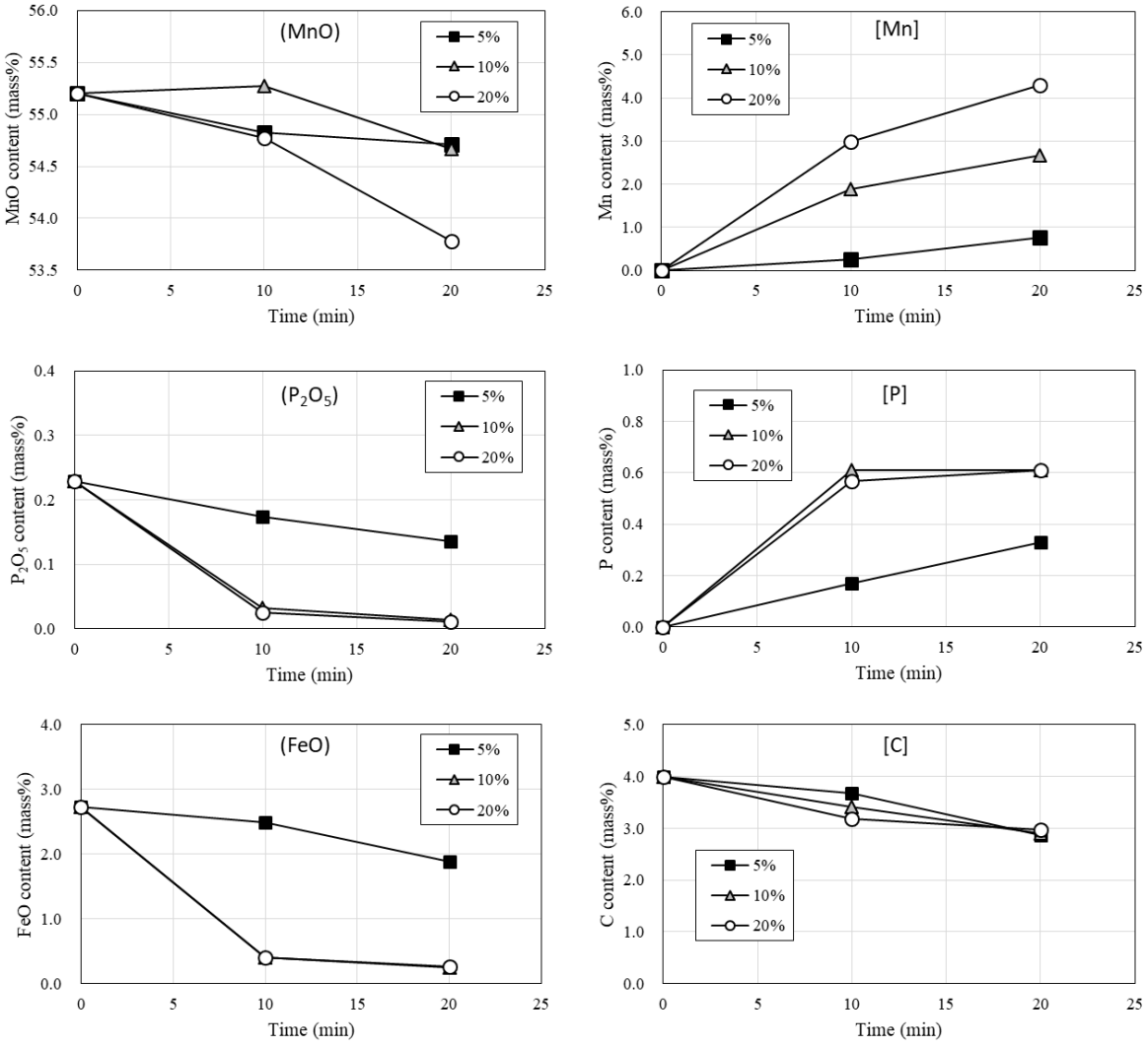

Fig. 5.6 Composition changes of slag and metal by different graphite powder additions

(Mixing ratio: SiO_2: 54%, Pig iron: 20% at 1673 K)

The partitions of P and Mn are shown in **Fig. 5.7**. Because the unknown part of P and Mn after the reduction, vaporization of P and Mn during reduction was considered to be negligible. When 5% of graphite powder was added, the partition ratio of Mn between slag and metal was high, but a large amount of P still remained in the slag. When the mixing ratio of graphite powder increased to 10% or more, although the partition ratio of Mn was slightly decreased, the partition ratio of P metal decreased more significantly. Comparing with the results obtained by the mixing ratios of 10% and 20%, most of the P in the slag was reduced to hot metal after 20 mins in each case, and the partition ratio of Mn was low enough for both conditions. Therefore, to enhance the reduction of P while suppressing the reduction of Mn, the optimum mixing ratio of graphite powder was considered to be 10%.

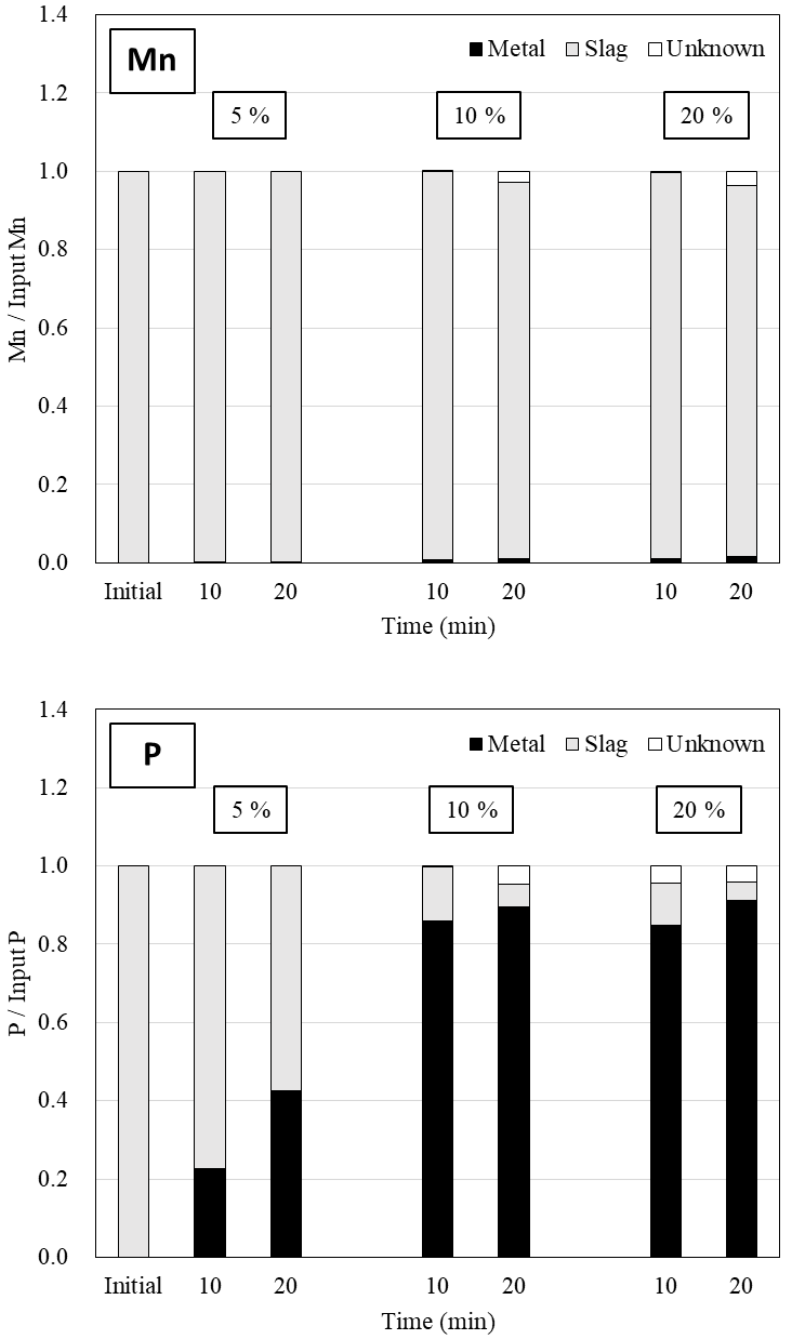

Fig. 5.7 Partitions of P and Mn by different mixing ratio of graphite powder

(Mixing ratio: SiO_2: 54%, Pig iron: 20% at 1673 K)

5.1.4.2 Influence of mixing ratio of pig iron on the reduction behavior

Fig. 5.8 shows the influence of the mixing ratio of pig iron on the reduction behavior. As the mixing ratio of pig iron increased, the content of Mn in slag decreased gradually. The content of P in slag after 20 mins reached to a similar value under all conditions. However, in the case of 10% of mixing, the reduction rate was slower that the other cases. The same trend was observed for the change in content of Fe. These results indicate that the addition of pig iron has an influence on the reduction kinetics. Both P and Mn in metal was high when addition of pig iron was small. It is because the P and Mn were diluted by the increase in the mass of hot metal. The content of C in hot metal decreased with reaction time, but the influence of the mixing ratio of pig iron was negligible.

Fig. 5.9 shows the partitions of P and Mn for the experiments with various mixing ratio of pig iron. When 10% of pig iron was added, although the partition of Mn between slag and metal was enough high, almost 1/3 of the P still remained in slag after 10 mins reduction. When the mixing ratio of pig iron increased to 20%, the partition of P in slag reached enough low and it decreased little even with the further increase in the mixing ratio. In the meantime, the partition of Mn continuously decreased with increasing the mixing ratio of pig iron. Therefore, to achieve a low partition of P and a high partition of Mn between slag and metal, 20% addition of pig iron was considered as an optimum condition.

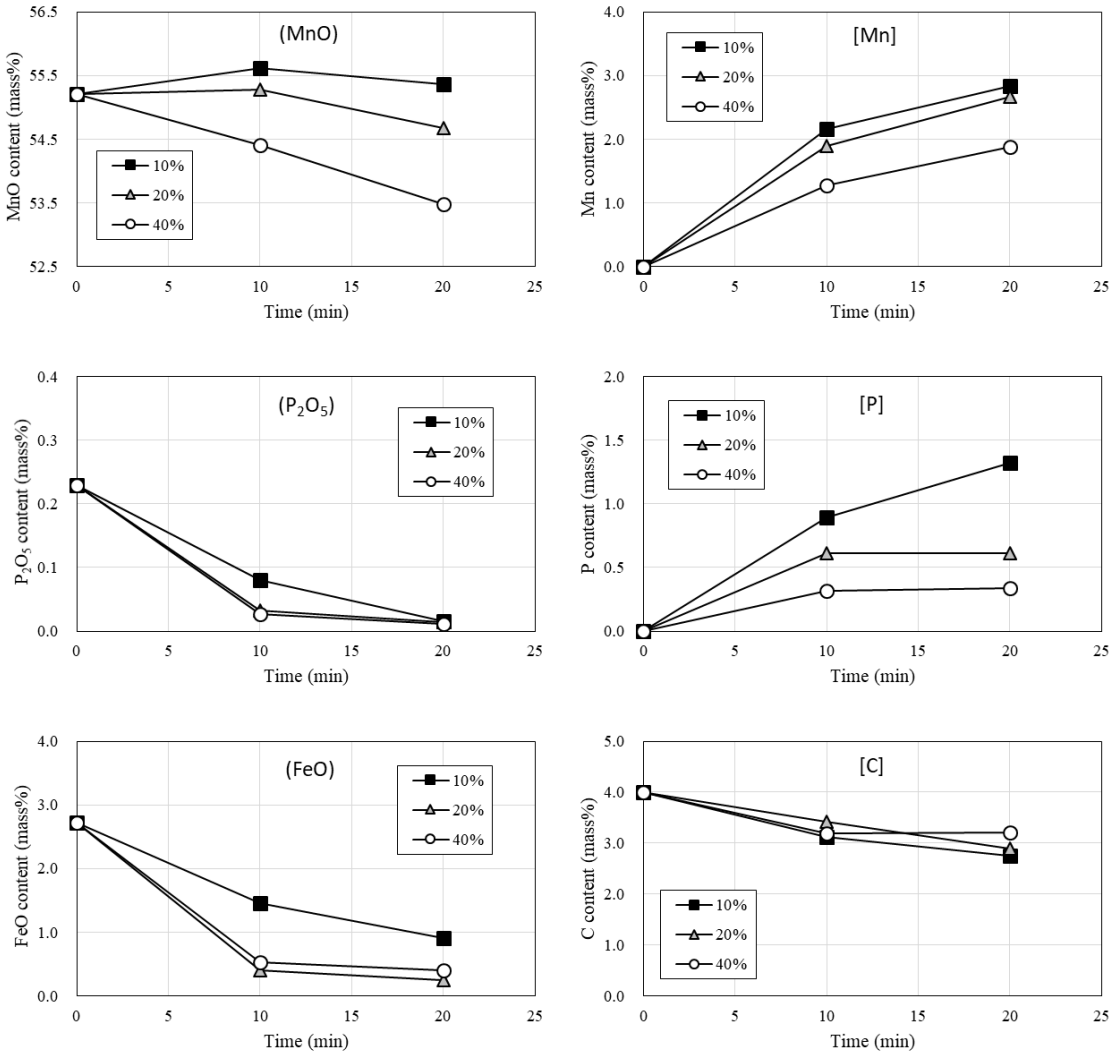

Fig. 5.8 Composition changes of slag and metal by different mixing ratio of pig iron

(Mixing ratio: Graphite powder: 10%, SiO_2: 54% at 1673K)

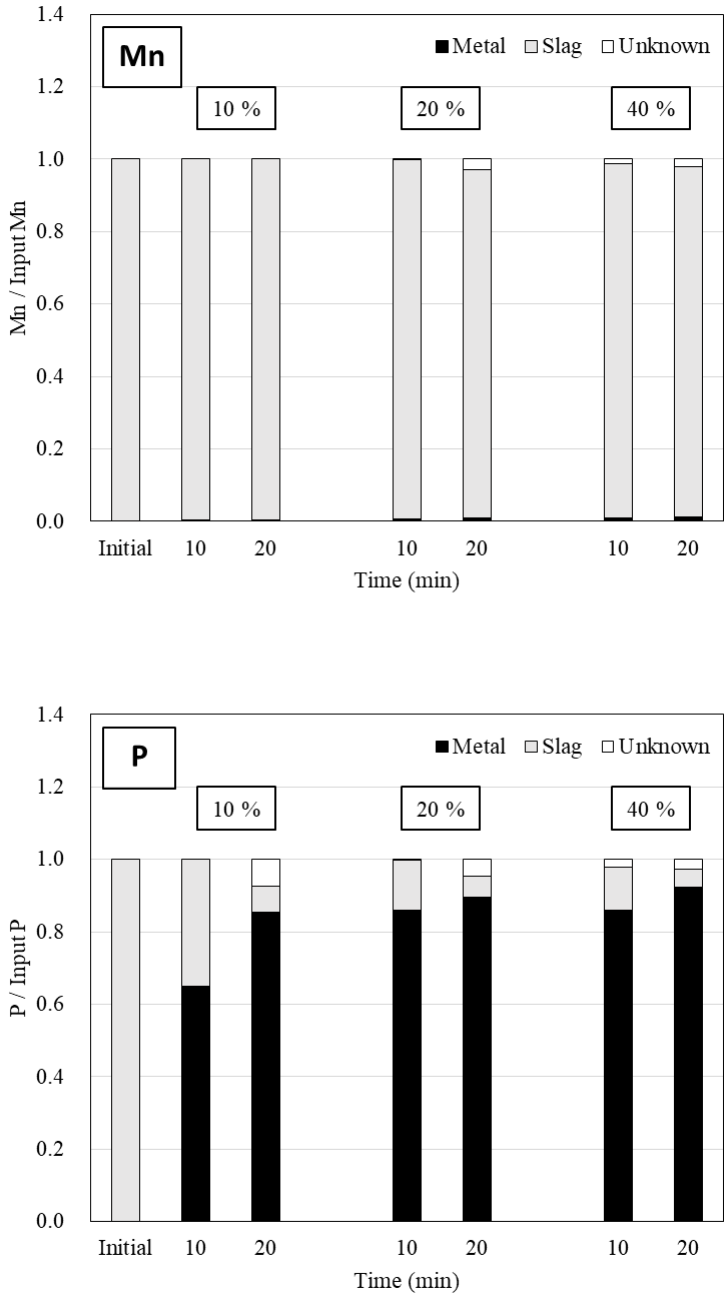

Fig. 5.9 The partitions of P and Mn by different pig iron additions

(Mixing ratio: Graphite powder: 10%, SiO_2: 54% at 1673K)

5.1.4.3 Influence of mixing ratio of SiO_2 on the reduction behavior

Fig. 5.10 shows the influence of mixing ratio of SiO_2 on the reduction behavior. When the mixing ratio of SiO_2 was small, the increase in SiO_2 content became large due to the dissolution of crucible. At 20 mins, the SiO_2 content in slag reached to a similar value for all conditions, indicating that the slag was close to SiO_2 saturation. About the reduction behaviors, although the initial contents of Fe and P in slag were different due to the different mixing ratio of SiO_2, the reduction of Fe and P in slag showed similar trends. In the case of Mn, small mixing ratio of SiO_2 led to enhance reduction in the early stage.

The partitions of P and Mn by different mixing ratio of SiO_2 is shown in **Fig. 5.11.** With an increase in mixing ratio of SiO_2, the partition of Mn increased while the partition of P decreased. This reduction behaviors of P and Mn have also been observed in chapter 2. It was concluded that as the SiO_2 affected the activity coefficients of MnO and P_2O_5 in molten slag, and thus the partitions of P and Mn between slag and metal were changed. Details discussions will be made later. Based on the above results, increase the mixing ratio of SiO_2 is beneficial to separate P and Mn. Therefore, designing SiO_2 content as close to saturation was considered as an optimum condition.

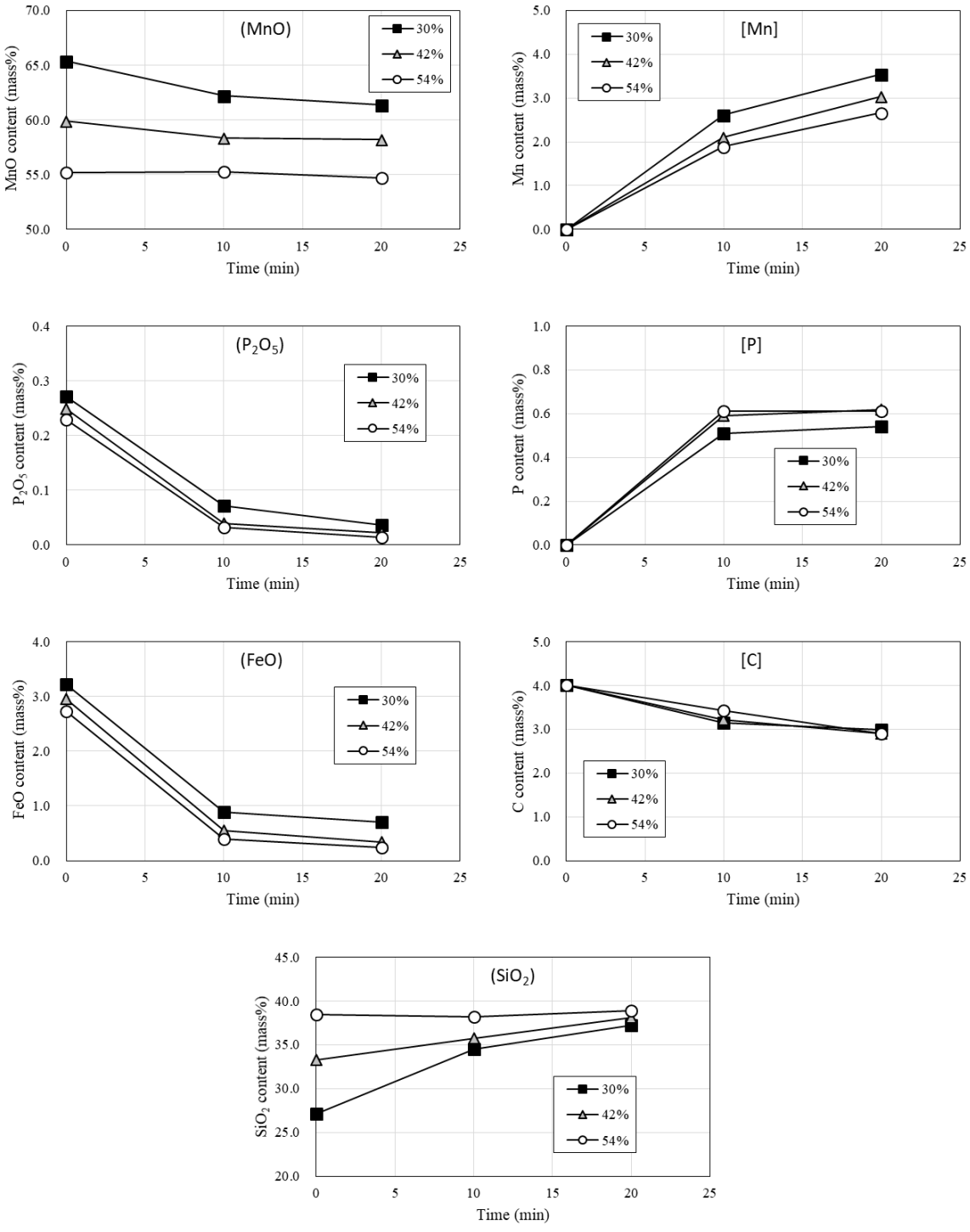

Fig. 5.10 Composition changes of slag and metal by different SiO_2 addition

(Mixing ratio: Graphite powder: 10%, Pig iron: 20% at 1673 K)

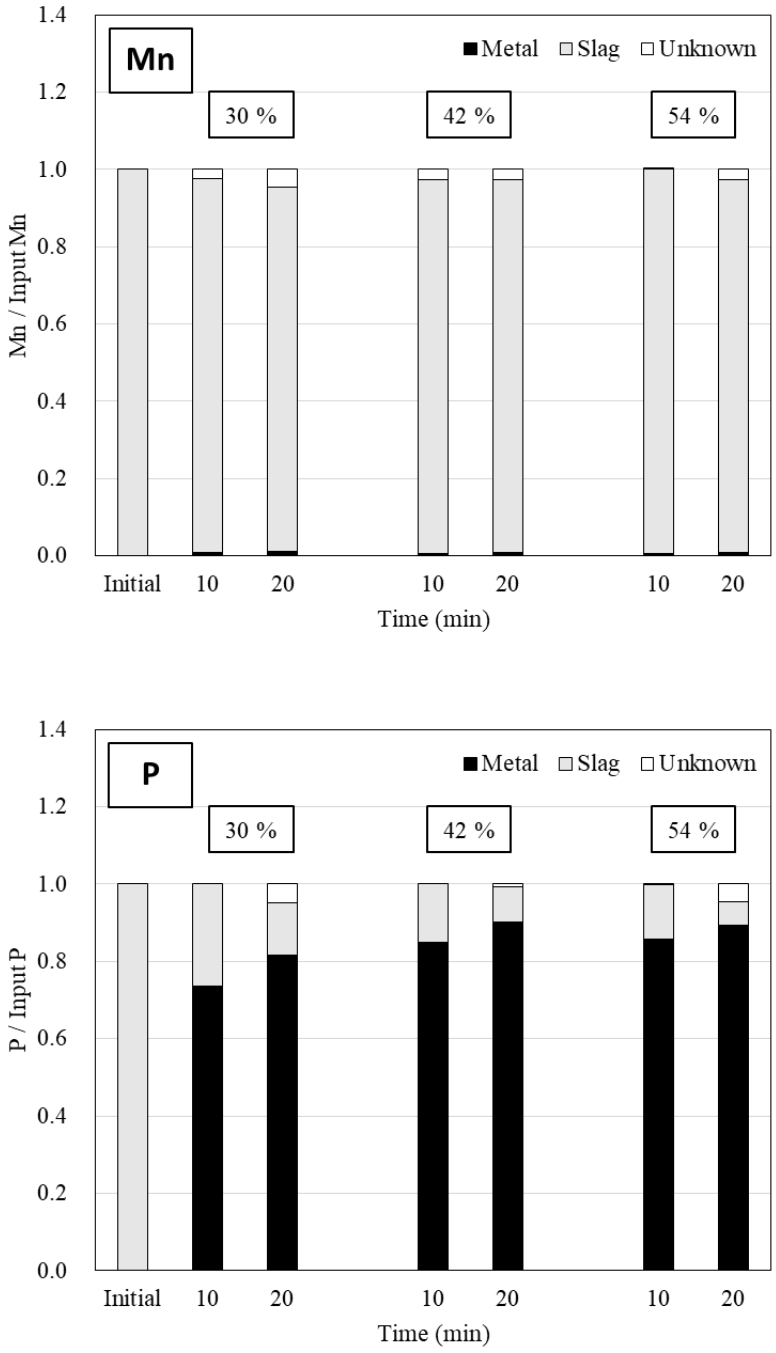

Fig. 5.11 The partitions of P and Mn by different SiO_2 addition

(Mixing ratio: Graphite powder: 10%, Pig iron: 20% at 1673 K)

5.1.4.4 Influence of temperature on the reduction behavior

Fig. 5.12 show the reduction behavior of slag and the changes in metal composition at different temperature. When the temperature was 1573 K and 1673 K, the content of Mn in slag were barely changed even after 20 mins, but the content Mn in slag at 1773 K decreased. In the case of Fe and P, the reduction was insufficient at 1573 K, and similar trends were observed when temperature was higher than 1673 K. For the metal phase, the change in the P and C content were similar, and the Mn content increased with increasing temperature. Therefore, 1673 K was considered as an optimum temperature for selectively reduce P from Mn-ore.

Fig. 5.13 shows the partitions of P and Mn from the reduction results of various temperatures. The partition ratio of Mn decreased slightly when increasing temperature, indicating that the reduction of Mn was enhanced at higher temperature. For P, the partition ratio of P was high at 1573 K, and it decreased by increasing temperature.

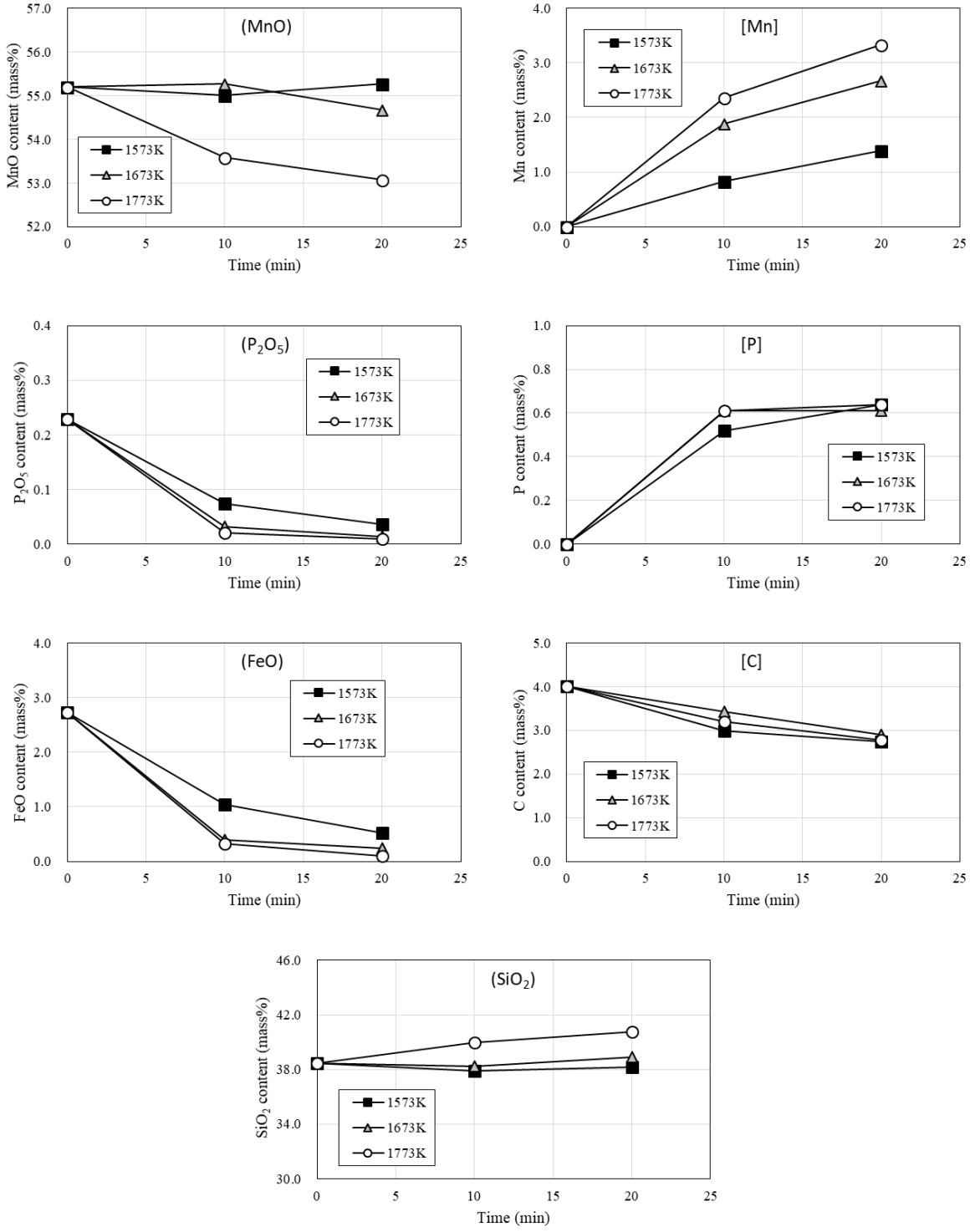

Fig. 5.12 Composition changes of slag and metal by different temperatures

(Mixing ratio: Graphite powder: 10%, SiO_2: 54%, Pig iron: 20%)

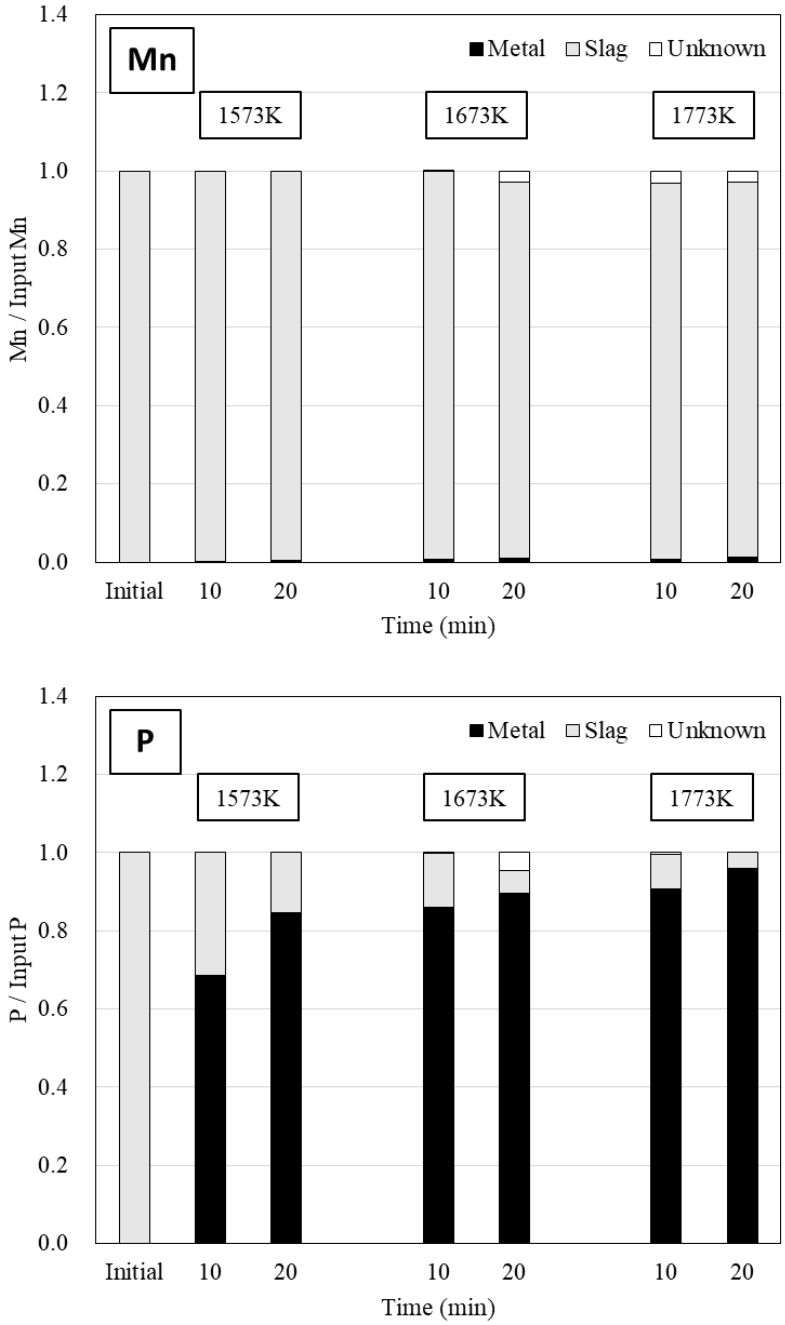

Fig. 5.13 The partitions of P and Mn by different temperature

(Mixing ratio: Graphite powder: 10%, SiO_2: 54%, Pig iron: 20%)

5.1.5 Discussion

5.1.5.1 Contribution of graphite powder and carbon dissolved in hot metal on reduction behavior

As previously showed, the reduction behaviors of P and Mn changed by both the mixing ratio of graphite powder and pig iron. In addition, both results showed that content of C in hot metal gradually deceased with reaction time. In order to find the major reaction site and to understand the decreasing mechanisms of P and Mn in metal, it is necessary to clarify the contribution of graphite powder and dissolved C in hot metal on the reduction.

As the pig iron before used in the experiment of reduction was C saturated, solubility of C in metal and the measured C content in metal was compared. The solubility of C in the reduced metal was calculated by the equation proposed in chapter 3 as shown in Eq. (5.5).

$$X_{C\ [in\ Fe-P-Mn-C(sat)]} = 0.19e^{-(6.09X_P - 0.47X_{Mn})} \text{ (at 1673K)} \quad \ldots\ldots\ldots (5.5)$$

Where, X indicates the mole fraction for each element in metal. Because the molar ratio of Mn in reduced metal under all experimental conditions were in the range of 0.002~0.03, the relation between X_P and C solubility were calculated and compared to the measured C content in metal after reduction, as shown in **Fig. 5.14**.

The comparison showed that, the measured content of C was lower than the C solubility in alloy, and the X_P in metal showed little effect on the C content. When mixture of sample was melted fast, graphite powders floated up to the top surface of molten slag due to low density, and the graphite powder had little chance to contact with hot metal. Therefore, as the carburization of hot metal by graphite powder was difficult, the decreased content of C in hot metal was considered to be consumed by reduction reaction.

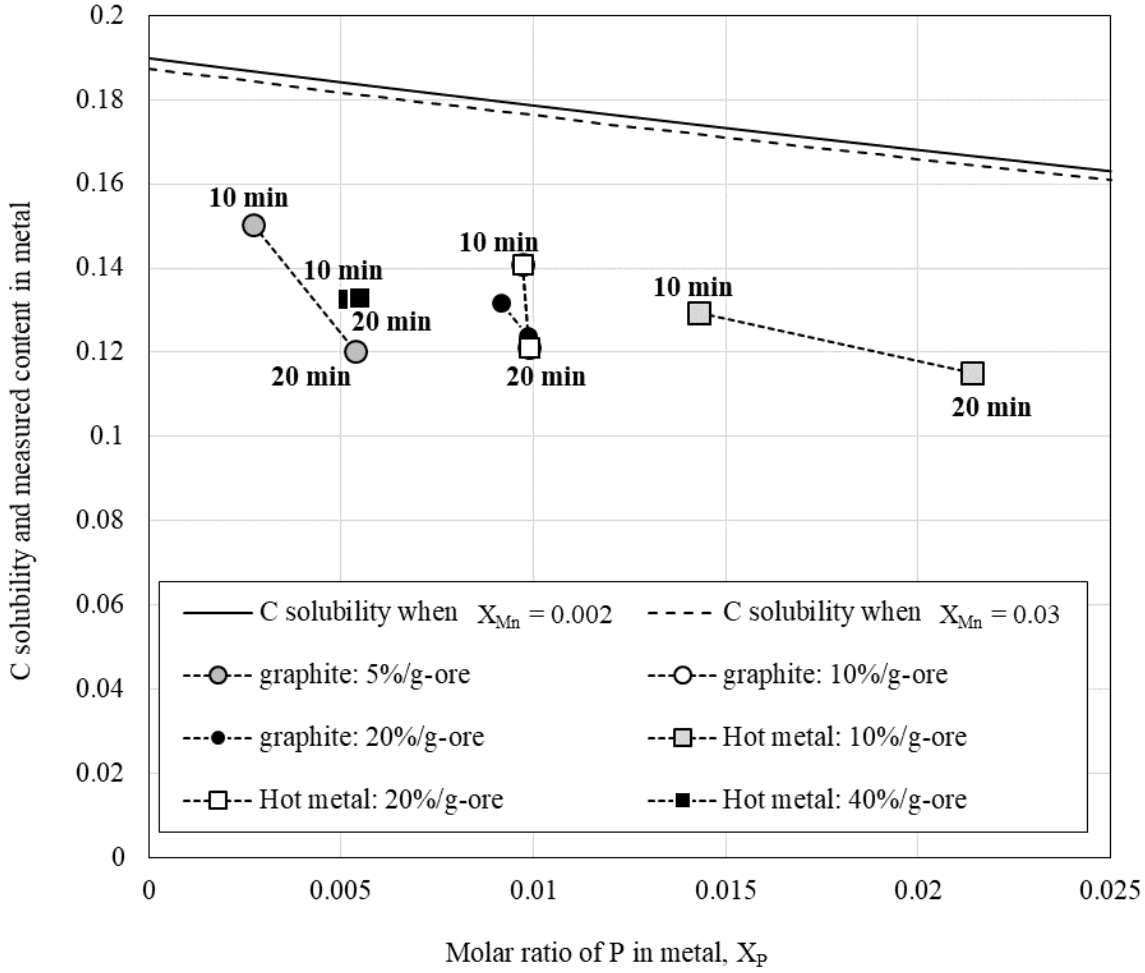

Fig. 5.14 Difference between carbon content measured in hot metal after reduction and the calculated C solubility in Fe-P-Mn-C alloy

Based on the above comparison, the reduction occurred majorly at two sites. One is the interface between hot metal and molten slag, another one is the contacting area between graphite powder and molten slag. For clarify this, the C balance before and after reduction was calculated. In the calculation, the mass of C for reducing FeO, MnO, and P_2O_5 was estimated by the stoichiometric relation of the reactions (5.1) to (5.3), and the changes in the mass of FeO and P_2O_5 in slag was used. The mass of C in hot metal was calculated using the C content and measured weight of metal.

The calculated C balance before and after reduction is shown in **Fig. 5.15**. The amount of graphite powder was not considered, because its amount is much large and some of it remained unreacted after experiment. The mass of C required to reduce FeO in slag was larger than that of MnO and P_2O_5, because the T.Fe content in slag was much higher than P and the reduced amount of Mn was small. Comparing to the necessary mass of C to reduce FeO, MnO and P_2O_5, the decrease in the mass of C in hot metal was not enough. Therefore, the graphite powder floating on the slag surface was dominantly used as reductant than dissolved C in hot metal.

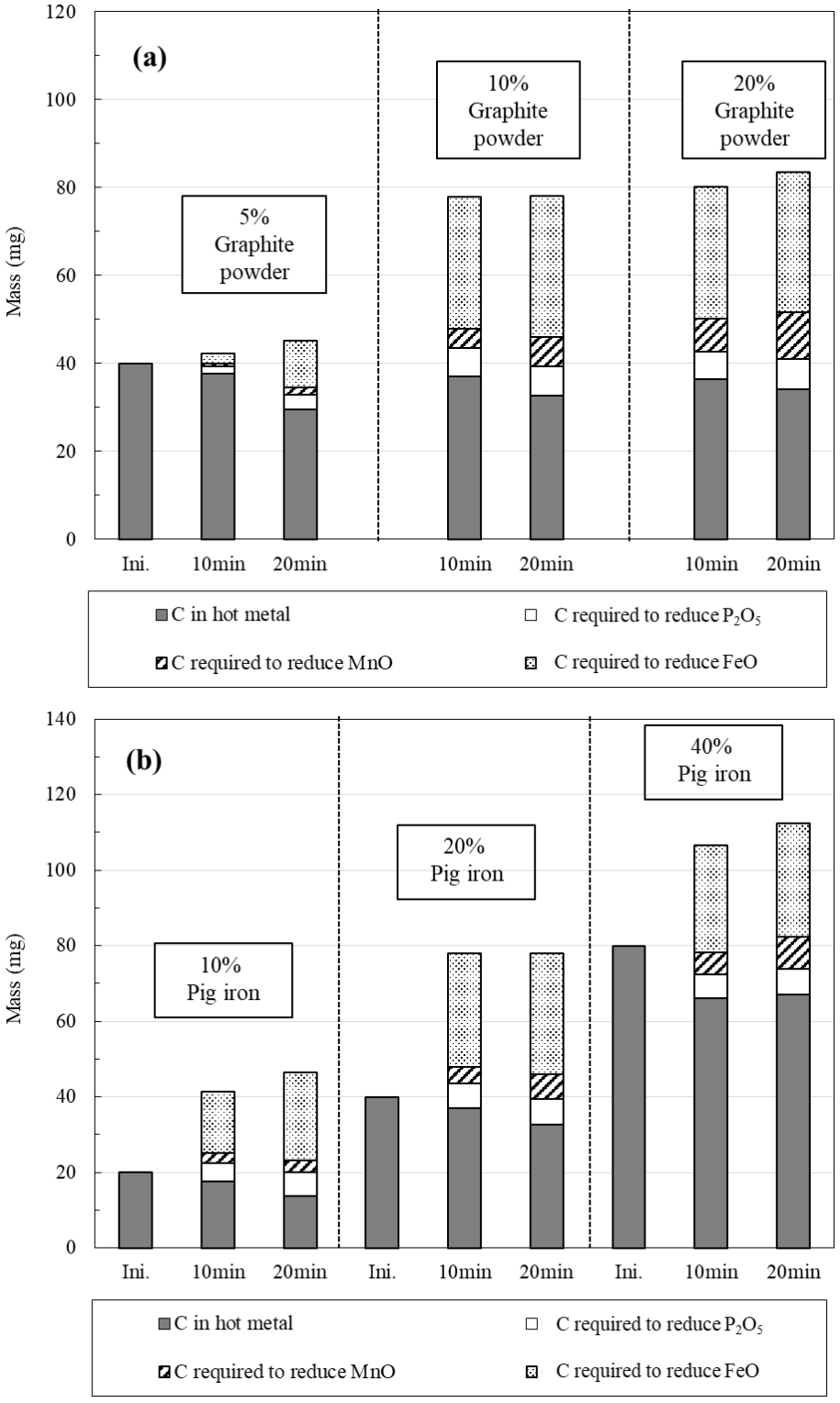

Fig. 5.15 The calculated C balance before and after

5.1.5.2 Influence of SiO_2 on the reduction behavior of P and Mn

To understand the influence of SiO_2 addition on the reduction behavior of P and Mn, the change in the activity coefficient of both MnO and P_2O_5 were considered. **Fig. 5.16** presents the influence of SiO_2 addition on activity coefficient of P and Mn in slag. In this figure, the activity coefficient of MnO and P_2O_5 during experiment were calculated by Factsage based on the results shown in Fig. 5.10.

With an increase in SiO_2 addition, the activity coefficient of MnO decreased while that of P_2O_5 increased. These changes in the activity coefficients preferred the selective reduction of P from slag. **Fig. 5.17** shows the effect of the activity coefficient on the distribution of P and Mn between slag and metal after 10 mins of reduction. The distribution ratio (L) for P and Mn between slag and metal phase was calculated by Eq. (5.6).

$$L_P = (\%P) / [\%P],\ L_{Mn} = (\%Mn) / [\%Mn] \text{…….. (5.6)}$$

Where, (%A) and [%A] represent the content of element A in the slag and metal, respectively.

From the results show in Fig. 5.17, although the slag and metal were not in equilibrium, the distribution of P and Mn between slag and metal decreased with increasing activity coefficients. Therefore, the SiO_2 addition is beneficial to the selective reduction of P over Mn.

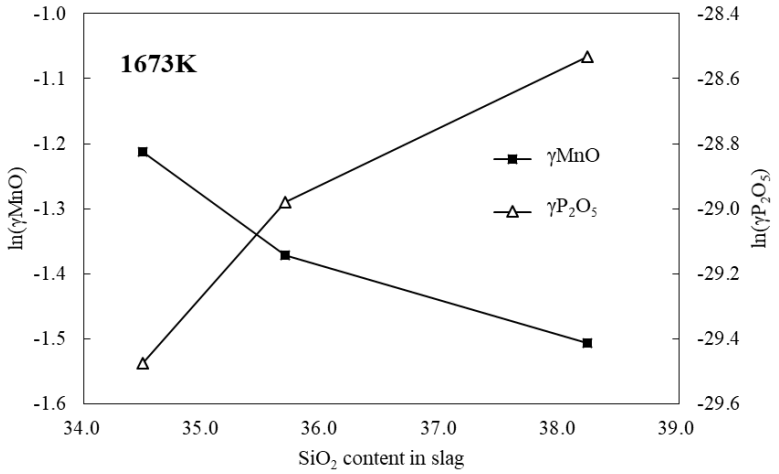

Fig. 5.16 Influence of initial SiO_2 content on the activity coefficients of MnO and P_2O_5

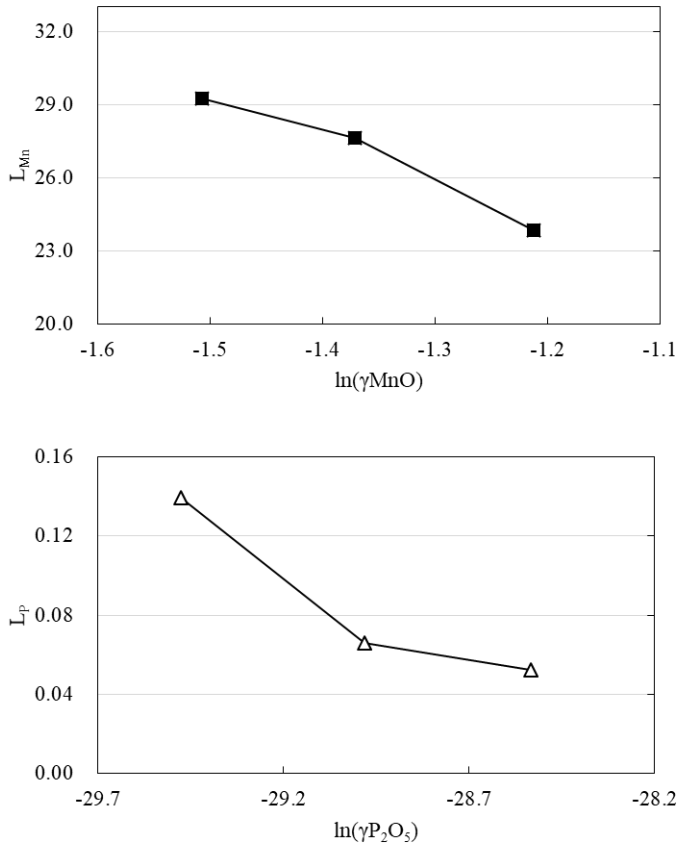

Fig. 5.17 Influence activity coefficient on distribution ratios of P and Mn

5.1.5.3 Estimation on the rate controlling step of reduction

As the reduction reaction mainly took place when the slag was in molten state, considering the conclusions of chapter 1, the mass transfer in the slag was considered as the rate control step of reduction. As content of P in slag was too small, the decreasing rate of Mn in the slag was considered. The rate constant of Mn (k_{Mn}, 1/min) was determined by **Eq. (5.7)**, here, $(\%Mn)_a$ and $(\%Mn)_b$ indicate Mn content in slag after the reaction time of t_a and t_b, respectively.

$$d(\%Mn)/dt = [\ln(\%Mn)_a - \ln(\%Mn)_b\ ]/(t_a - t_b) = k_{Mn}\ (\%Mn) \quad \text{…….(5.7)}$$

The rate constants of Mn (k_{Mn}) for each temperature were obtained by using the result after 10 mins, and the temperature dependence of k_{Mn} was discussed. The result is summarized in the form of Arrhenius equation as shown in **Fig. 5.17**, and **Eq. (5.8)** was obtained.

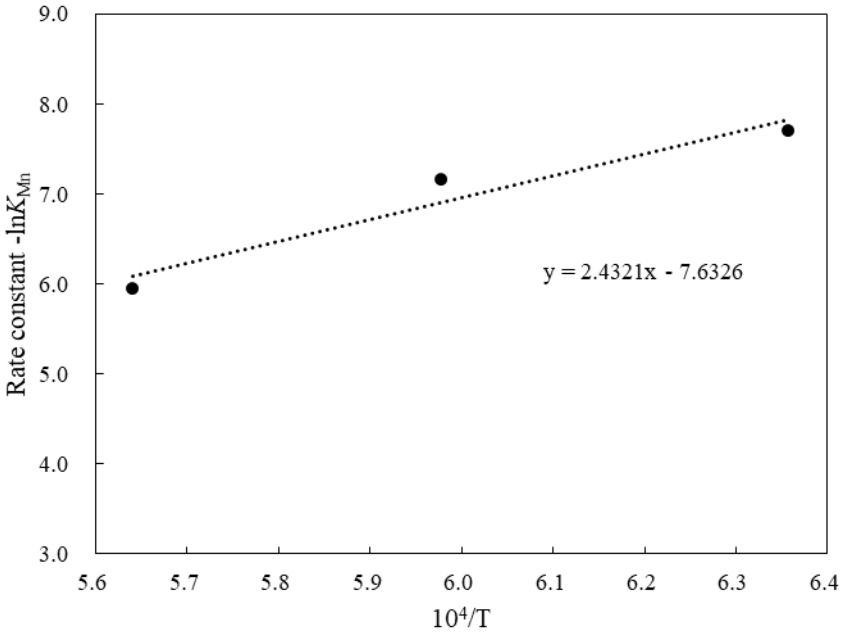

Fig. 5.18 Temperature dependence of the rate constant calculated by equation (5.7)

$$\ln k_{\mathrm{Mn}} = 2.4321/\mathrm{T} - 7.58 \text{…….. (5.8)}$$

As a result of using this Eq. (5.8), the activation energy was calculated as about 202 kJ / mol. The activation energy of Mn diffusion in molten slag is about 194.5 kJ / mol [2]. The rate-controlling step can be regarded as the diffusion of MnO in the film layer of slag.

5.2 Selective reduction of P from South Africa Mn-ore

5.2.1 Characters of SA Mn-ore and slag designing

Based on the optimum conditions for the reduction of the Gabon Mn-ore, another Mn-ore (from South Africa, SA Mn-ore) was used for selective reduction. The chemical composition of SA Mn-ore analyzed by ICP-AES is listed in **Table 5.3**.

Table 5.3 Chemical composition of SA Mn-ore analyzed by ICP (mass %)

	T.Fe	T.Mn	SiO_2	CaO	MgO	P	Others (Al_2O_3 Cr, S)
Natural state	7.42	33.86	7.32	11.60	2.90	0.04	<0.05
After dehydration	8.43	37.98	8.10	12.94	3.39	0.05	<0.05

Comparing to the Gabon Mn-ore, instead of Al_2O_3, the content of CaO was high in the SA Mn-ore. In addition, both the content of T.Mn and T.P were lower than Gabon Mn-ore. To remove the hydrations before reduction, similar to the method for the Gabon ore, SA Mn-ore powder (< 2mm) was heated at 1273 K for 12 h in air. The composition of SA Mn-ore after dehydration was also shown

in Table 5.3. The mineralogical phases in the SA Mn-ore identified by XRD before and after dehydration are shown in **Fig. 5.19**. In the natural state of SA Mn-ore, the major phases of Mn showed differences to that of the Gabon Mn-ore. The phase of Mn in SA Mn-ore was not only the oxide and hydroxide, but also a compound phase consisting of Ca, Mg, Mn, Fe oxides was found. After dehydration, some Mn oxides changed to solid compounds containing either SiO_2 or CaO.

Different from Gabon Mn-ore, to consider the mixing ratio of SiO_2, for SA Mn-ore, CaO-MnO-SiO_2 system should be used. The phase diagram of CaO-MnO-SiO_2 system is shown in **Fig. 5.20.** To make SiO_2 saturated slag, mixing ratio of SiO_2 was set to be 50% (about 38. 7% in the slag system). The mixing ratios of graphite powder and pig iron were set as 10% and 20%, respectively, and the temperature was selected as 1673 K. The same experimental procedure and analysis was conducted for SA Mn-ore.

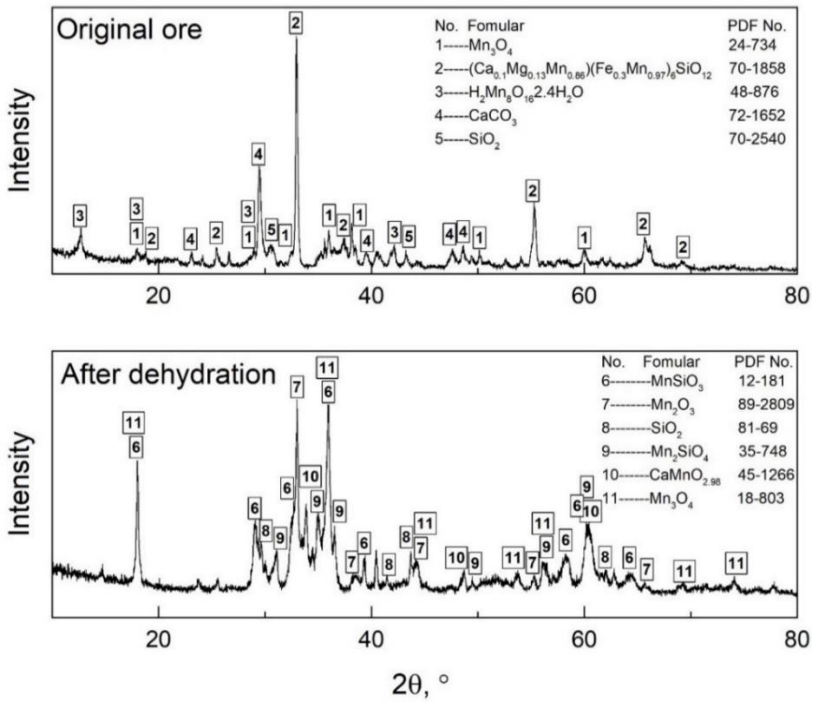

Fig. 5.19 The mineralogical phases in SA Mn-ore before and after dehydration

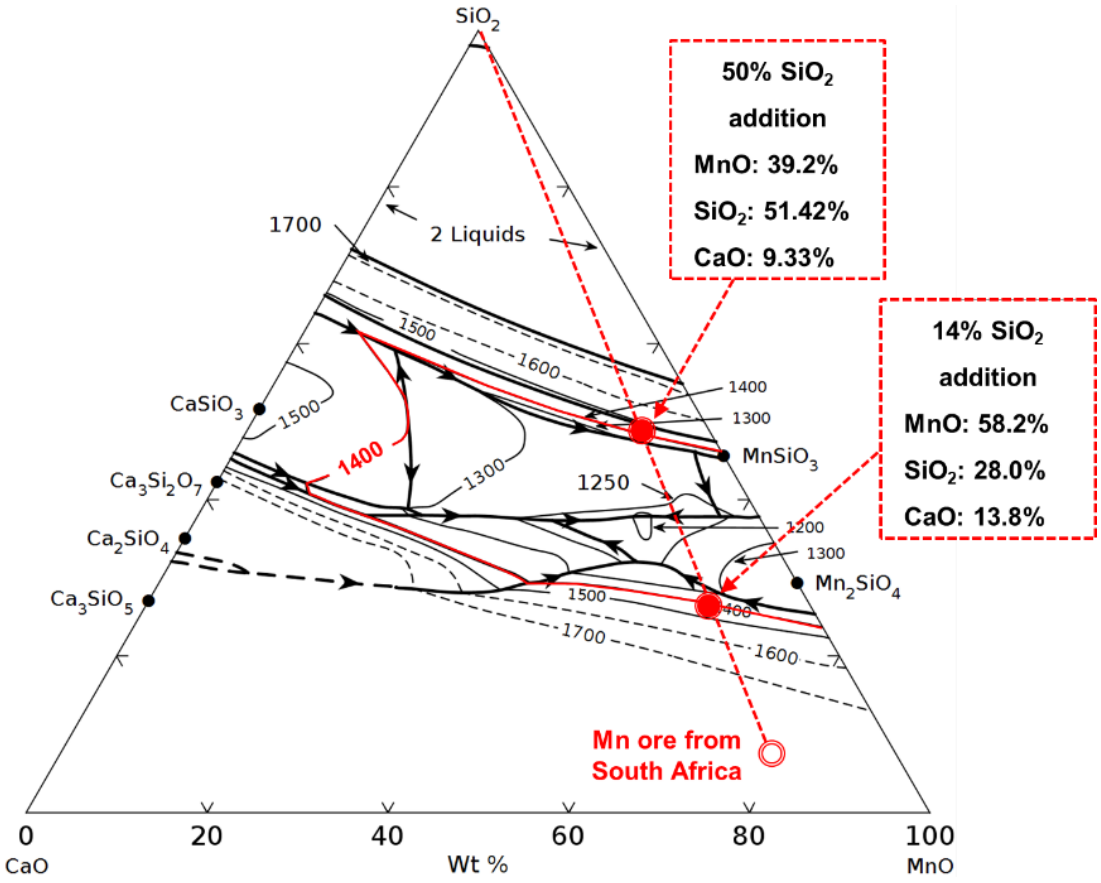

Fig. 5.20 Phase diagram of MnO-SiO_2-CaO system [3]

5.2.2 Results

The reduction behavior of SA Mn-ore with the metal composition are shown in **Fig. 5.21**. For the slag composition, similar trend to the Gabon Mn-ore was observed. The content of Fe and P in slag decreased quickly, and that of Mn, CaO, and MgO contents were close to or slightly higher than their initial values. In the metal phase, both the P and Mn content increased fast within 10 mins, and by the elongation of reduction time, they further increased slightly.

Using the results shown in Fig. 5.21, the partitions for P and Mn during the reduction of SA Mn-ore was calculated, and the results are shown in **Fig. 5.22**. The mass of the slag after the reduction is calculated from the Eq. (5.4) replacing the Al_2O_3 to CaO content. The result showed that large part of the P was reduced to metal and most of the Mn was remained in the slag. Therefore the selective reduction of P over Mn was also achieved for the SA Mn-ore.

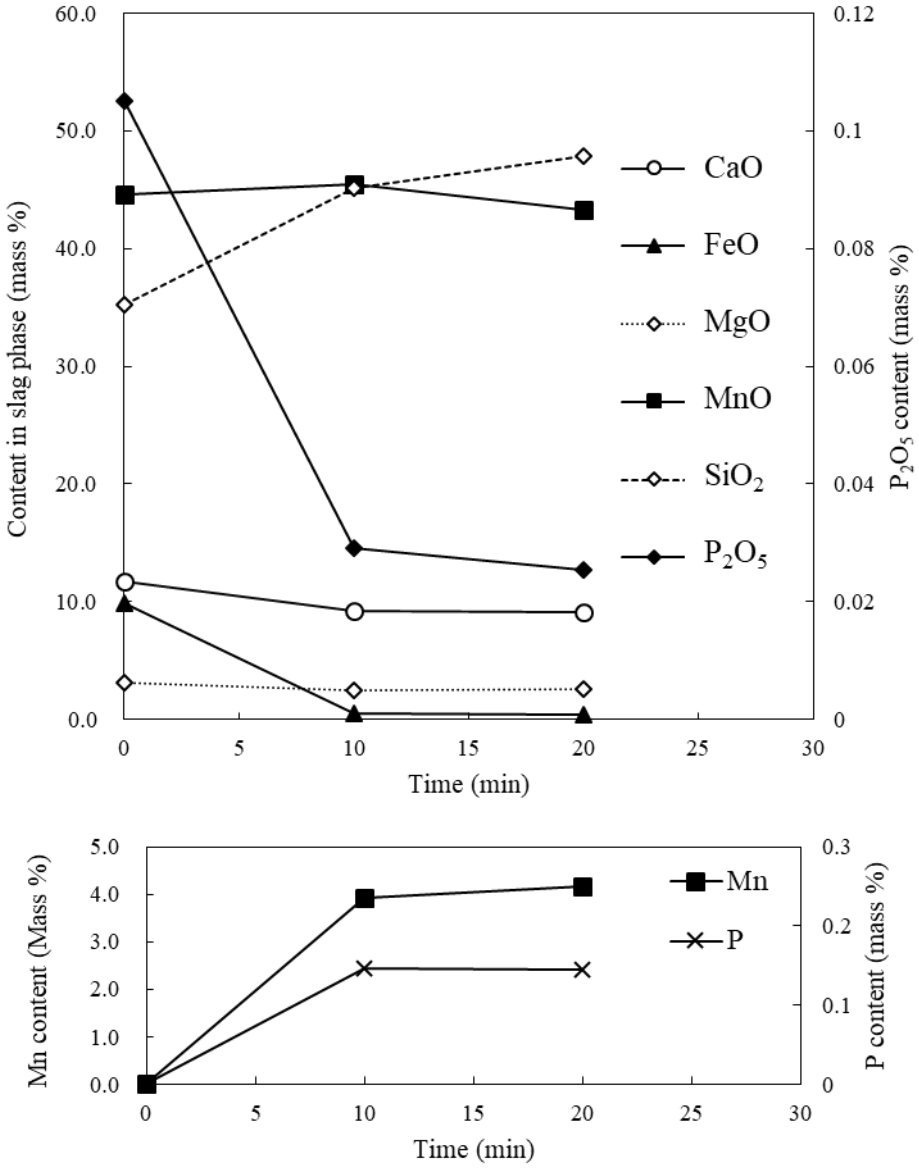

Fig. 5.21 Reduction behavior of SA Mn-ore and the change in the metal composition

(Mixing ratio: Graphite powder: 10%, SiO_2: 50%, Pig iron: 20% at 1673 K)

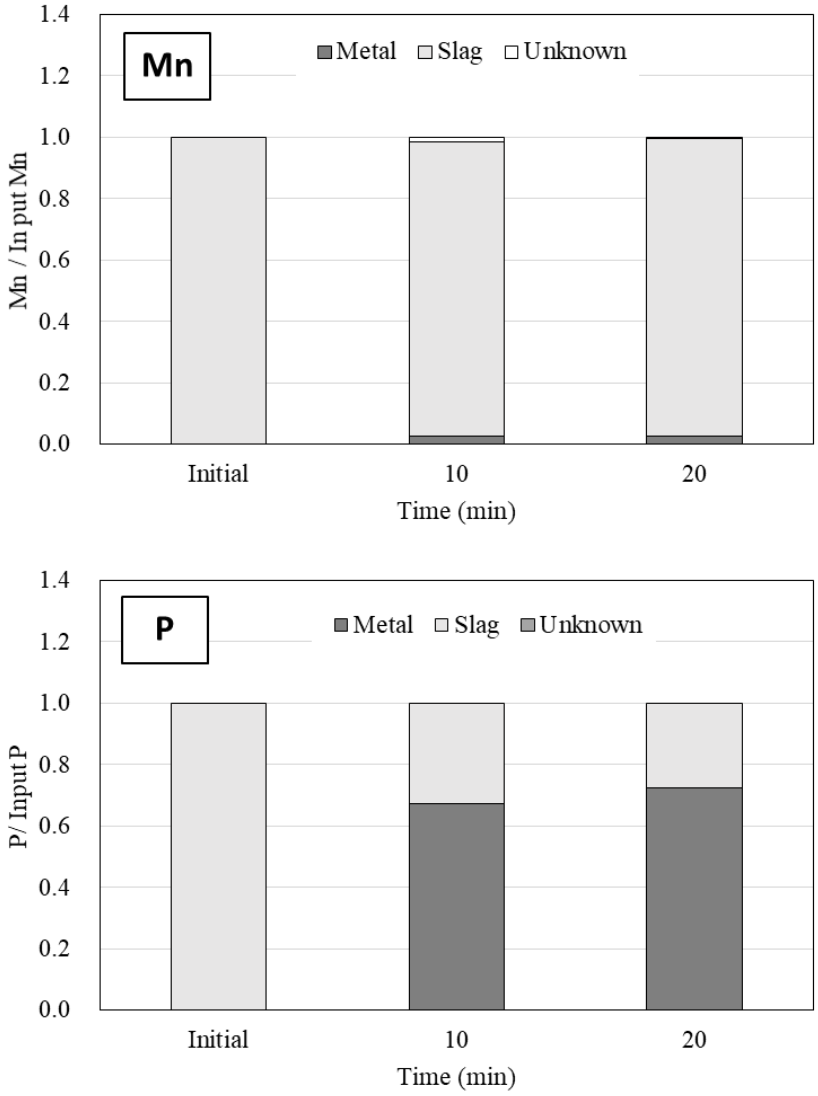

Fig. 5.22 The partitions of P and Mn during the reduction of SA Mn-ore

(Mixing ratio: Graphite powder: 10%, SiO_2: 50%, Pig iron: 20% at 1673 K)

5.3 Comparison on the reduction behavior of Gabon and SA Mn-ores

Although the selective reduction of P was achieved for both Gabon and SA Mn-ores, the slag systems were different, and the partition behaviors of P and Mn are also slightly different. To clarify the change in the slag system on the reduction behavior, and reduction behavior of Gabon and SA Mn-ore were compared.

Fig. 5.23 shows the distribution ratios of P and Mn for Gabon Mn-ore and SA Mn-ore for each reduction time. In both case, the mixing ratios of graphite and pig iron and the temperature are the same and the slag was saturated by SiO_2. The distribution ratio of Mn by Gabon Mn-ore was higher than that of SA Mn-ore, and the distribution ratio of P by Gabon Mn-ore was lower than that of SA Mn-ore. It indicated that the selectivity of P over Mn was better for Gabon Mn-ore than that of SA Mn-ore. The reason was considered as existence of the basic oxides such as CaO and MgO. In case of Gabon Mn-ore, the contents of CaO and MgO are very low, but their contents were relatively high in SA Mn-ore. The existence of basic oxide in slag system may affect the activity coefficient of MnO and P_2O_5 and it may influences the reduction behavior of P and Mn.

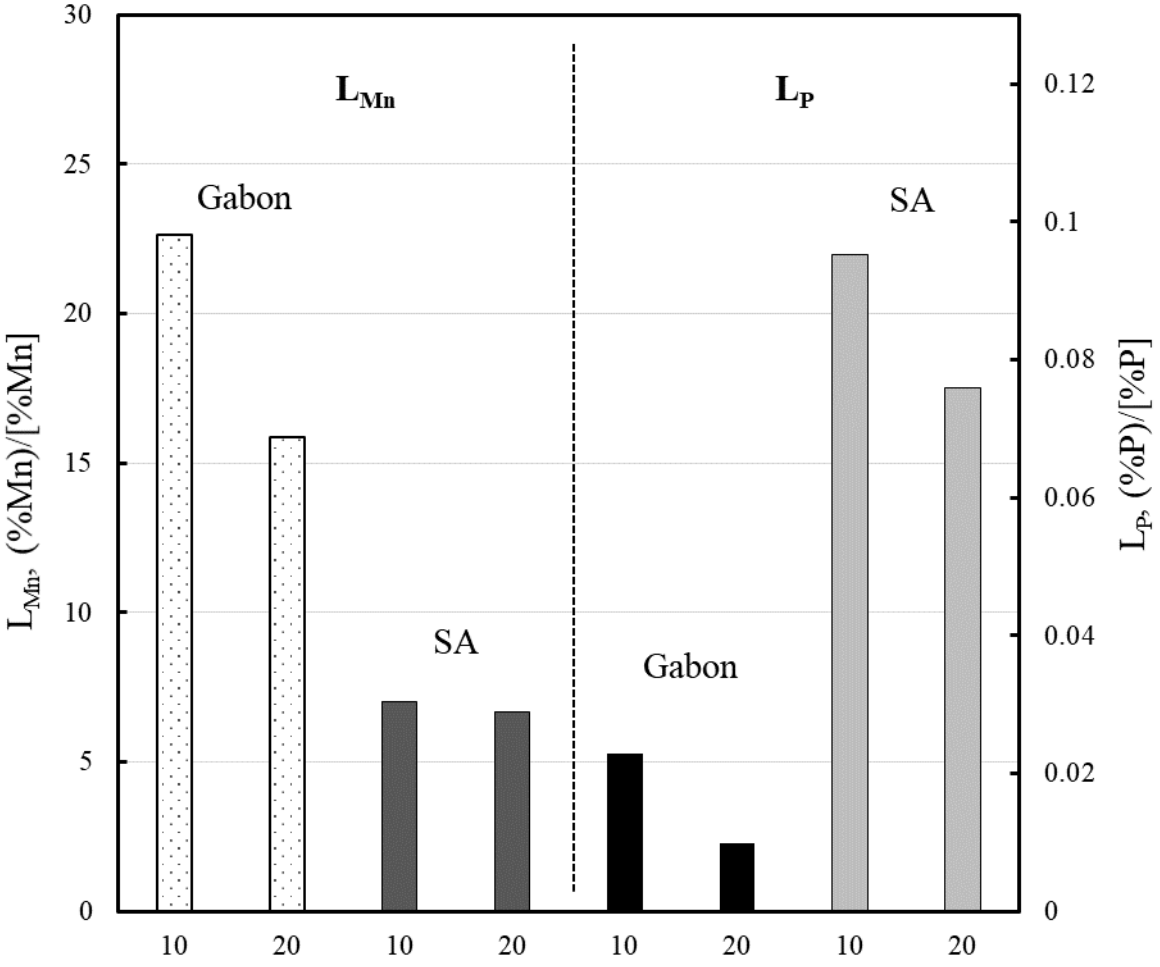

Fig. 5.23 Comparison on the distribution of P and Mn using Gabon and SA Mn-ore

(Mixing ratios: <Gabon Mn-ore: Graphite powder: 10%, Pig iron: 20%, SiO_2: 54% at 1673K>

<SA Mn-ore: Graphite powder: 10%, Pig iron: 20%, SiO_2: 50% at 1673 K>)

The effect of the activity coefficient of MnO and P_2O_5 were compared to the reduction rate of P and Mn, as shown in Fig. 5.15. The reduction rate ($\mathrm{d}\frac{W_{Mn(or\,P)}}{t}$, g/min) was calculated using Eq. (5.9), using the change in the mass of Mn or P from reaction time t_2 to t_1.

$$\mathrm{d}\frac{W_{Mn(or\,P)}}{t} = \frac{W_{Mn(pr\,P)}^{t_2} - W_{Mn(pr\,P)}^{t_1}}{t_2 - t_1} \quad \text{..... (5.9)}$$

The activity coefficients were calculated by either FactSage or Regular solution model [4] using the measured slag composition. **Fig. 5.24** shows the relation between activity coefficient and reduction rates of P and Mn.

As shown in Fig. 5.24 (a), though the activity coefficient of P_2O_5 calculated by two methods revealed small differences, the reduction rate of P_2O_5 decreased when the activity coefficient of P_2O_5 was decreased. This trend was similar to the reduction of steelmaking slag as expressed in previous chapters. However, in the case of MnO, the reduction rate of Mn decreased when the activity coefficient of MnO increased, and such decrease was found for the activity coefficient calculated by both models. In addition, the activity coefficient of MnO in the case of Gabon Mn ore was larger than that of SA ore, probably due to the higher content of MnO in the ore. Even though, the Gabon ore stilled showed a smaller reduction rate of Mn. This indicated that the difference on the reduction behavior of Mn from two Mn-ores could not be explained through the change in the activity coefficient, and other reasons needed to be considered.

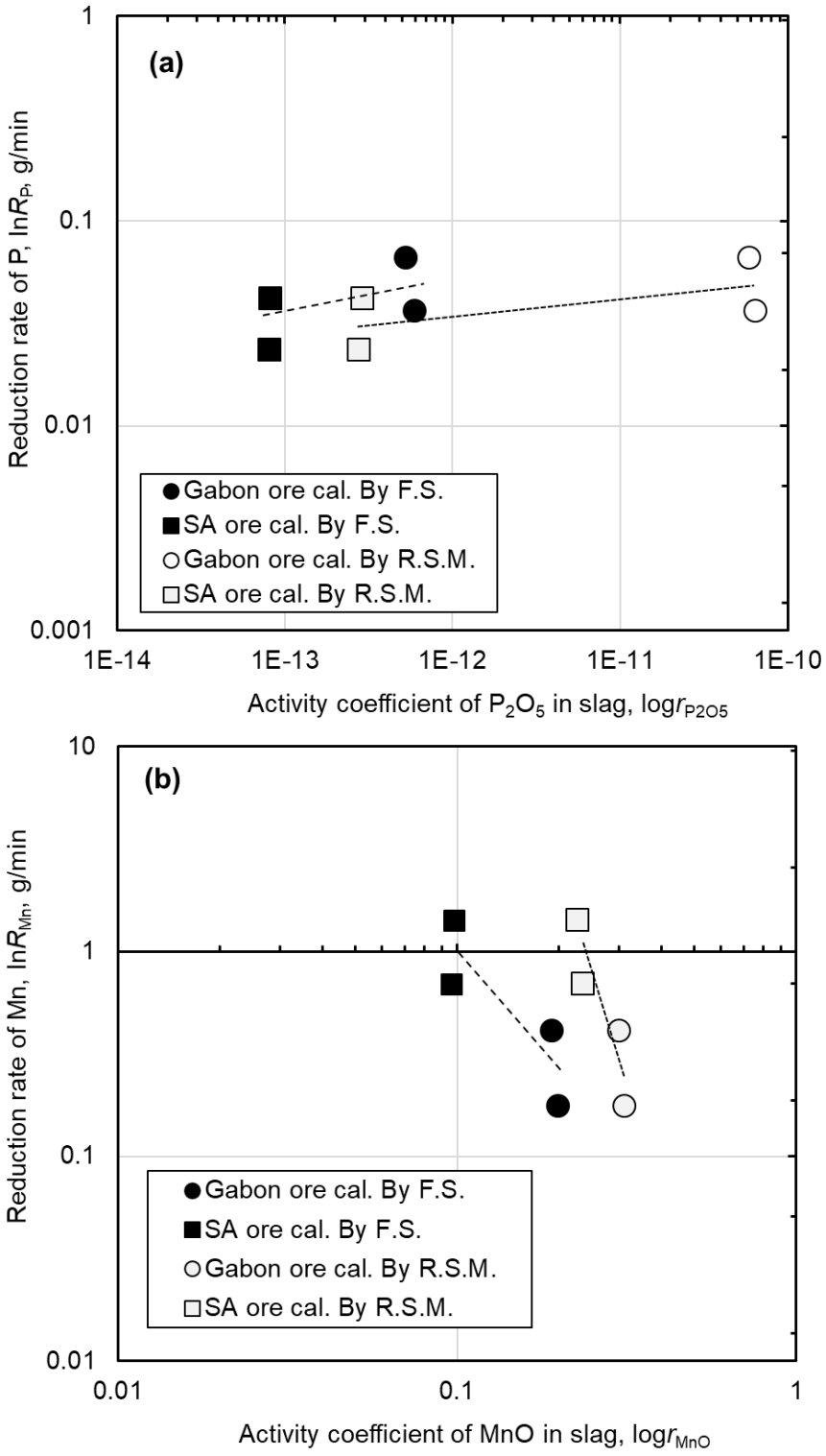

Fig. 5.24 Effect of activity coefficient of (a) P_2O_5 and (b) MnO on their reduction rates from slag

In last chapter, since different melting behavior of slag changed the reduction behaviors of P and Mn, it is worthy to compare the difference of melting behavior between two Mn-ores. The P and Mn contents in metal after the reduction of either solid or liquid slag were estimated using Eq. (5.10) [5,6].

$$P_2O_5(l) + 5[Mn] = 2[P] + 5MnO(l) \quad \log K = 26950/T + 0.97 \text{..... (5.10)}$$

In the estimation, the slag was assumed to be equilibrated with a C saturated Fe-P-Mn-C alloy. For the activity coefficients of P and Mn in alloy, Eq. (5.11) and Eq. (5.12) were used which were determined in Chapter 3.

$$\ln\gamma^{H}_{\text{Mn [in Fe-P-Mn-C(sat.)]}} = -4.72X_{\text{P}} - 0.47X_{\text{C}} \text{..... (5.11)}$$

$$\ln\gamma^{\text{H}}_{\text{P [in Fe-P-Mn-C (sat.)]}} = -4.72X_{\text{Mn}} + 4.26X_{\text{P}} + 6.09X_{\text{C}} \text{..... (5.12)}$$

For the solubility of C in alloy, Eq. (5.2) was used. The activity of MnO and P_2O_5 at solid state was assumed as unity, and the values of them in a liquid slag at 1673 K were calculated by FactSage using the initial slag compositions. The calculated relation between the molar ratio of P and Mn were drawn in Fig. 5.24, in comparison with the results for the slag made from both Gabon and SA Mn-ore. The Factsage calculation showed that, the activity of P_2O_5 was about the order of 10^{-16}, and that of MnO was order of 10^{-1}.

As shown in **Fig. 5.25**, the line of a_{MnO}=1 locates at an upper position to that of a_{MnO}=0.1. This indicated that, when the reduction of P_2O_5 occurred in the liquid state ($a_{P_2O_5}=10^{-16}$), the reduction of MnO became significant when solid MnO existed in slag. Comparing to the experimental results, the result of Gabon ore located close to the assumed equilibrium relation calculated by the activities of MnO and P_2O_5 in liquid slag. Therefore, it was considered the reduction of MnO and P_2O_5 occured mainly in the liquid slag for Gabon Mn-ore. For the SA Mn-ore, the results located between the dash and solid lines, and this revealed that part of the Mn from SA Mn-ore could be reduced in solid slag.

Different from the previous Chapter, which used reagent of MnO, the actual Mn ore was used as raw material. In the dehydrated SA Mn ore, Mn_2O_3 and MnO_2 were found by XRD shown in Fig.5.19. As these oxide is unstable at high temperature under the reduction atmosphere, pure MnO would be formed in the solid slag during the heating.

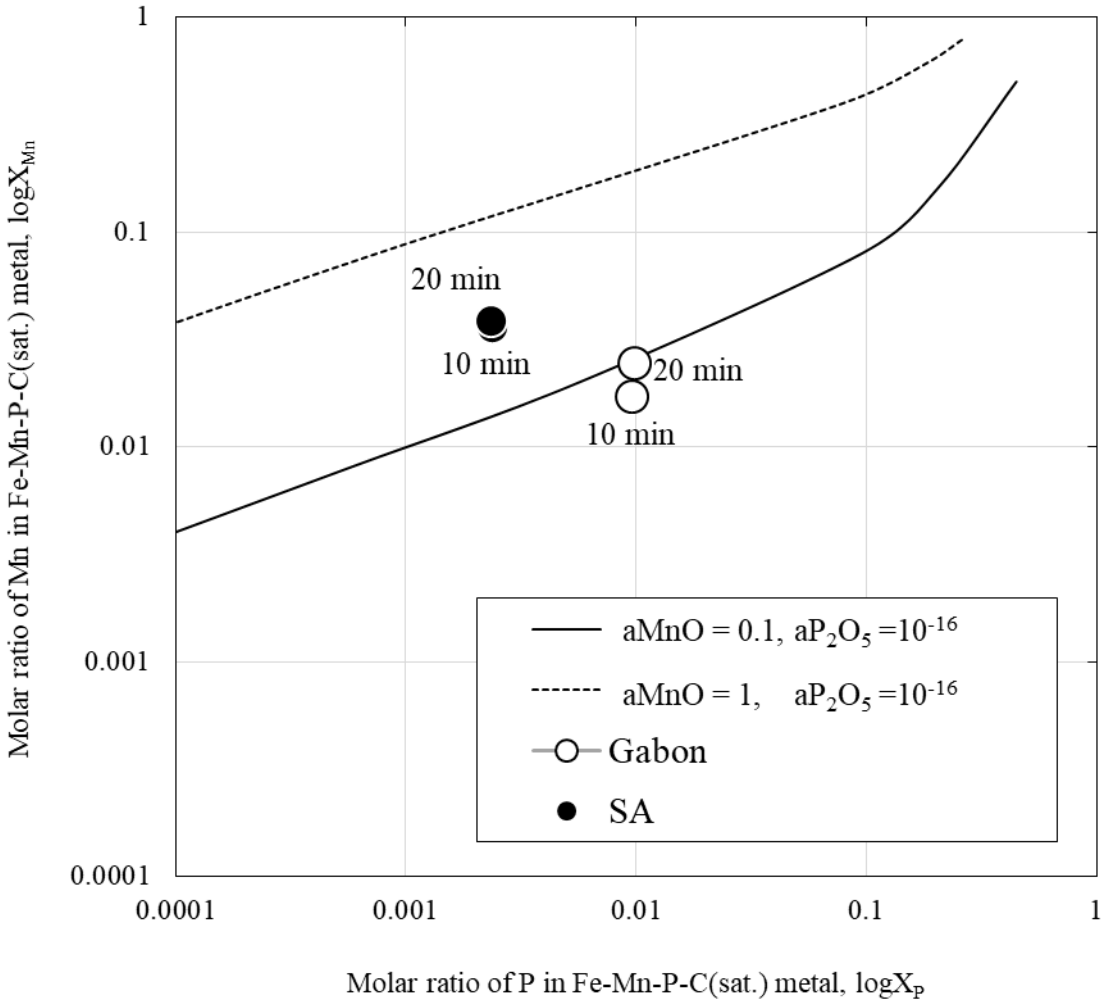

Fig. 5.25 Comparison between the assumed equilibrium composition of metal and the experimental results

The changes in the ratios of liquid slag and solid phase at the initial heating stage of reduction were estimated by FactSage using the experimental results. For this estimation, as the short time experiment were not conducted, same assumption used in previous chapter 4 was applied. The average reaction rate of each component in slag within 10 mins were assumed by Eqs. (5.13) and (5.14).

$$W_t^N = W_{ini}^N + \frac{W_{ini}^N - W_{t^*}^N}{t^*} \times t, \ (0 \text{ min} < t < 10 \text{ mins}) \quad \ldots\ldots\ldots (5.13)$$

$$(N\%)_t = 100 \times \frac{W_t^N}{\sum W_t^i} \quad \ldots\ldots\ldots\ldots\ldots\ldots\ldots (5.14)$$

W^N is the weight of a slag component N; t^* means the reaction time at which the slag composition was analyzed. In this calculation, t^* is 10 mins and t is an arbitrary time between 0 min and 10 mins. The calculated slag composition was then inputted to Factsage and estimate the liquid and solid phase ratio. Temperature profile shown in Fig. 5.3 was used.

The calculated results are shown in **Fig. 5.26**. According to the calculation, both Gabon and SA Mn-ore became complete liquid phase after 2 mins. But the increase in the liquid phase ratio showed difference between two Mn-ores within in the initial 2 mins. For Gabon Mn-ore, the liquid phase ratio gradually increased with time, and about 26% of the slag was liquid phase after 1 min when temperature reached about 1233 K. In case of SA Mn-ore, the slag was completely solid until 1.8 mins, from where the liquid phase started to form. The solid phase was mainly $MnSiO_3$ and Mn_2SiO_4 according to the calculation, which agreed with the XRD results as shown in Fig. 5.18, and also agreed with the reaction product between solid ore and SiO_2 as shown in both the phase MnO-SiO_2-Al_2O_3 and MnO-SiO_2-CaO phase diagrams. Based on the above results, the difference of the liquid phase ratio in the initial 2 mins of reduction can be considered as the reason for the larger reduction of Mn from SA Mn-ore than that of Gabon Mn-ore. During this period, some of Mn was reduced from the solid compound which contained high content of Mn.

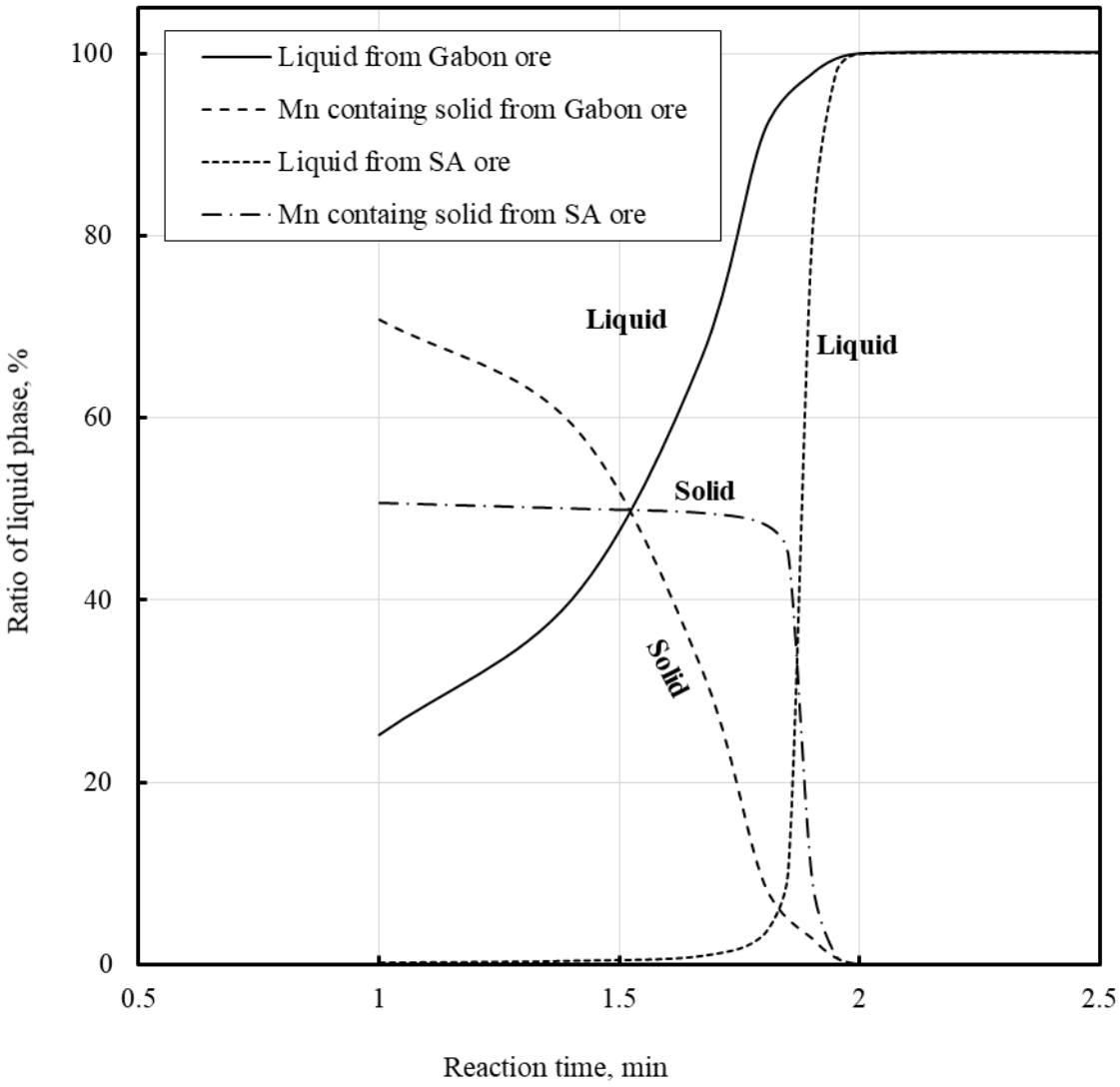

Fig. 5.26 Estimated phase ratios of liquid and solid during the initial period of reduction

5.4 Possibility on the production of low P ferromanganese alloy

As the purpose of the selective reduction of P from Mn-ore was to produce ferromanganese alloy with low phosphorus content. The possibility on producing this high grade of ferromanganese from the slag after the removal of P by the following reduction was evaluated by calculation. In this calculation, the production of high carbon ferromanganese alloy was considered, and thus the target content of Mn in the product alloy was assumed to be 80.0 mass %, and carbon content was 7.0 mass %. Because the ferromanganese alloy was generally produced by smelting reduction process, the yields ratios of Fe, P and Mn by smelting reduction were assumed as 98%[7], 60% [7] and 90% [8] using references data respectively. The slag composition after 20 mins of reduction for Gabon Mn-ore with optimum conditions, and that of SA Mn-ore after 20 mins reduction were used in the calculation. As a comparison, the reduction of the original ore without the selective reduction treatment was also calculated. **Table 5.4** gives the calculated composition of ferromanganese alloy.

Table 5.4 Expected P content in ferromanganese alloy by different raw materials (mass %)

Raw material	Gabon Mn-ore (raw)	SA Mn-ore (raw)	Reduced slag (From Gabon Mn-ore)	Reduced slag (from SA Mn-ore)
T.Mn	52.0	33.86	42.0	27.74
T.P	0.14	0.04	0.006	0.011
T.Fe	3.4	7.42	0.5	0.5
		Ferromanganese alloy (Expected)		
Mn	80.0	68.40	80.0	80.0
Fe	Bal.	Bal.	Bal.	Bal.
C	7.0	7.0	7.0	7.0
P	0.323	0.121	0.017	0.048

When the original Gabon Mn-ore was used directly, the content of P in the ferromanganese alloy reached to 0.32%, and in the case of SA Mn-ore, the P content in final alloy was 0.16%. In particular, the Mn content in ferromanganese alloy by SA Mn-ore did not reach 80 mass % due to low ratio of Mn/Fe. On the other hand, by using P removed slag obtained by selective reduction, in both case, the P content in the alloy is less than 0.05%. Based on this result, the selective reduction of P from Mn-ore was considered as a valid option to produce high grade ferromanganese alloy with low P content.

Noticing that some metal droplets might be trapped within the molten slag after reduction, if these metal droplets contained high content of P, the P content in the ferromanganese alloy may show higher values than the ones shown in Table 5.4. However, as shown in **Fig. 5.27**, the sum of the P mass in the metal and reduced slag balanced well with the inputted mass of P, and the deviation was small. Therefore, there is less chance that the uncollected metal droplets trapped in slag would carry large mass of P to influence the P content of the ferromanganese after secondary reduction.

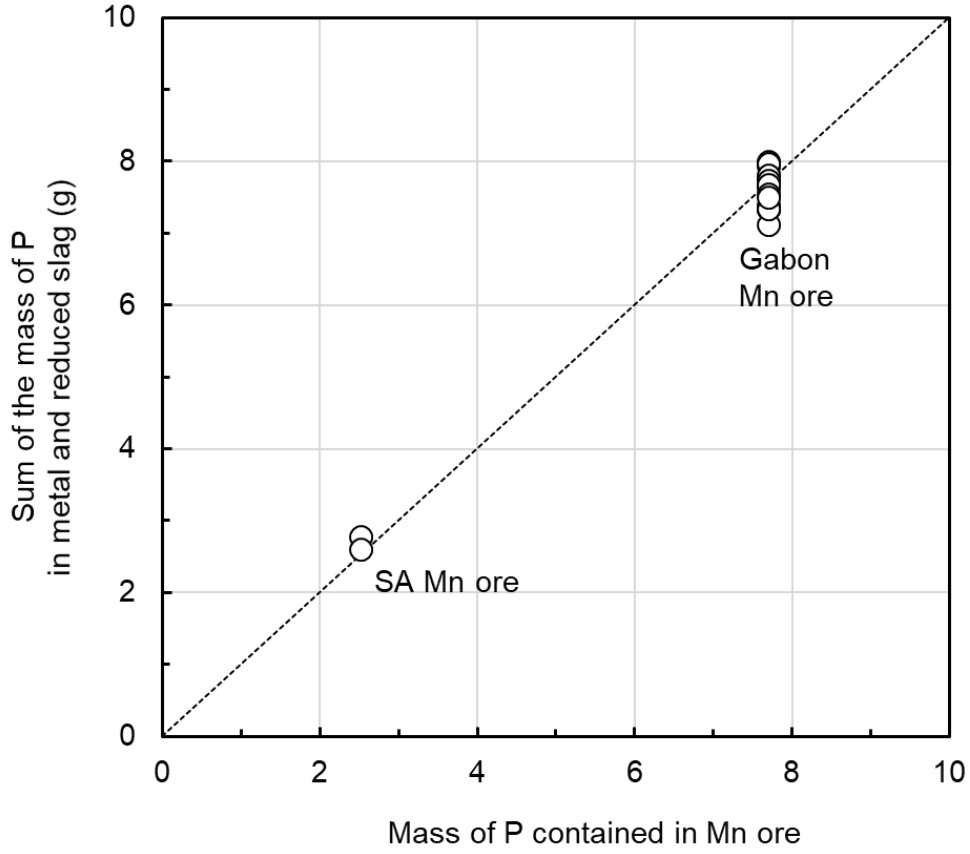

Fig. 5.27 Comparison on the mass of P before and after reduction

5.5 Summary

The selective reduction technique of P was applied to two types of Mn-ore in this chapter. The purpose was to decrease the P content from the original ore, and thus to provide a measure to produce ferromanganese with low content of P from normal grade of Mn-ore. Through the reduction experiments, some conclusions have been drawn as follows;

(1) By adding SiO_2 as slag modifier to make acidic slag with low melting temperature, and by adding graphite powder and pig iron as reductant and receiver, the selective reduction of P without the reduction of Mn was achieved for both Mn-ores.

(2) Using the Gabon Mn-ore, the influence of the mixing ratio of graphite powder, pig iron, and SiO_2 on the reduction behaviors were studied. The results showed that both the graphite powder and pig iron contributed to the reduction, and the reduction of P and Mn were enhanced with higher addition of graphite powder and pig iron. To suppress the reduction of Mn from slag while to obtain a high removal ratio of P from slag, the optimum mixing ratio of graphite and pig iron were 10% and 20%, respectively. In addition, some discussions were made to understand the contributions of graphite power and the dissolved C in Pig iron on the reduction.

(3) An increase in SiO_2 addition suppressed the reduction of Mn and enhanced the reduction of P. Because the slag needed to be a liquid state, the optimum mixing ratio of SiO_2 at 1673 K was 54% for Gabon Mn-ore. The effects of SiO_2 on the reduction behavior of P and Mn were discussed through the changes of activity coefficient and distribution ratio.

(4) When the reduction was conducted at 1573 K, the results of Gabon Mn-ore showed that the reduction of both Fe and P from slag was insufficient, and a high temperature at 1773 K increased the loss of Mn from slag to metal. Therefore, the optimum temperature for reduction was determined as 1673 K.

(5) Applying optimum condition obtained for Gabon Mn-ore to SA Mn-ore, the selective reduction of P was achieved. Comparing reduction rate of Mn between two ores, SA Mn-ore was faster than that of Gabon Mn-ore. Even though, the calculated activity coefficients of P_2O_5 and MnO in Gabon ore were larger than SA Mn-ore, fast melting behavior of Gabon Mn-ore suppressed reduction of Mn.

(6) When the slag obtained after the selective reduction of both Mn-ores was used in the smelting reduction process to produce ferromanganese alloy, significant decrease in the P content of ferromanganese was estimated through a mass balance calculation. Therefore, the selective reduction of P from Mn-ore was considered as a valid option to produce high grade ferromanganese alloy with low P content.

5.6 Reference

8. Factsage, Ecole Polytechnique CRCT, Montreal.
9. Dolan, M. D., & Johnston, R. F. (2004). Multicomponent diffusion in molten slags. *Metallurgical and Materials Transactions B*, *35*(4), 675-684.
10. Atlas, S. (1995). Verlag Stahleisen GmbH, Düsseldorf. *Germany*, *ISBN*, 3-514.
11. Ban-Ya, S. (1993). Mathematical expression of slag-metal reactions in steelmaking process by quadratic formalism based on the regular solution model. *ISIJ international*, *33*(1), 2-11.
12. Turkdogan, E. T., & Pearson, J. (1953). Activities of constituents of iron and steelmaking slags. *Journal of the Iron and Steel Institute*, *12*, 398-402.
13. The Japan Society for the Promotion of Science, the 19th Committee on Steelmaking: *Steelmaking Data Sourcebook (Revised Edition)*, 1988, Gordon and Breach Science Publications, New York.
14. Eissa, M., Ghali, S., Ahmed, A., & El-Faramawy, H. (2012). Optimum condition for smelting high carbon ferromanganese. *Ironmaking & Steelmaking*, *39*(6), 419-430.
15. Groshkova, A. L., Polulyakh, L. A., Travyanov, A. Y., Dashevskii, V. Y., & Yusfin, Y. S. (2007). Phosphorus distribution between phases in smelting high-carbon ferromanganese in the blast furnace. *Steel in Translation*, *37*(11), 904-907.

Chapter 6 Conclusions

In order to separate P and Mn from steelmaking slag by selective reduction, this thesis investigated influence of slag basicity, temperature, graphite mixing ratio and crucible on the reduction behavior of steelmaking slag. The interaction coefficients of P and Mn in carbon saturated iron were measured and the reduction behavior was thermodynamically discussed. In addition, the reduction mechanism of steelmaking slag was observed and discussed kinetically. Finally, the developed condition was applied to Mn-ores to produce low P ferromanganese alloy. The conclusions of this study are as follows:

6.1 The optimum condition for the selective reduction of steelmaking slag

Firstly, decreasing the slag basicity from 1.49 to 0.50, suppressed the reduction rate of Mn while enhancing that of P. When slag basicity was lower than 0.76 at 1773K, the selective reduction of P was achieved.

Secondly, the effect of temperature on the reduction rates of Mn and P was investigated. The reduction of P at 1573K was slow but the reduction of Mn at 1773K was relatively large. . Therefore, the appropriate temperature which shows high reduction rate of P supressing the reduction of Mn is necessary. From the relation between the rate constant for P_2O_5 reduction in the slag and temperature, the activation energy was evaluated. The obtained value was close to the activation energy required for the diffusion of P in the slag.

Thirdly, the reduction behavior of FeO, MnO and P_2O_5 were influenced by the mixing ratio of graphite powder. The reduction reaction was considered to mainly occur at the interface between slag

and graphite powder.

Finally, with a change in the crucible type, the reduction rate and distribution ratio of Mn changed, while those of P did not change much.

6.2 Thermodynamic analysis

To accurately describe the activity of P and Mn in a Fe-P-Mn-C(sat.) alloy, the activity coefficients for P and Mn in this type of an alloy system were measured by equilibrating Fe-P-Mn-C(sat.) alloy with Ag by using a graphite crucible at 1673 K.

Firstly, when $0 < X_{\mathrm{Mn}} < 0.06$ and P $0 < X_{\mathrm{P}} < 0.25$, a liner relationship was obtained between the activity coefficient of Mn and the molar fraction of P. Thus, the interaction parameter between P and Mn in a Fe-P-Mn-C(sat.) alloy is determined as follows:

$$\varepsilon_{\mathrm{Mn}}^{\mathrm{P}} = -4.72 \pm 0.27 \ \text{(1673K)}.$$

Subsequently, the activity coefficient of Mn is obtained as follows:

$$\ln\gamma_{\mathrm{Mn\ [in\ Fe-P-Mn-C\ (sat.)]}} = -4.72X_{\mathrm{P}} - 0.47X_{\mathrm{C}} - 0.87 \text{ (1673 K)}.$$

Secondary, a linear relation between the activity coefficient of C and the molar fraction of P was observed under the current experimental conditions. Therefore, the interaction parameter between C and P is obtained as follows:

$$\varepsilon_{\mathrm{C}}^{\mathrm{P}} = 6.09 \pm 0.15, (X_{\mathrm{Mn}} < 0.06, X_{\mathrm{P}} < 0.25, 1673 \text{ K})$$

Additionally, the C solubility of Fe-P-Mn-C(sat.) alloy is obtained as follows:

$$X_{C\ [in\ Fe-Mn-P-C(sat.)]} = 0.19\mathrm{e}^{-(6.09X_{\mathrm{P}}-0.47X_{\mathrm{Mn}})}$$

Thirdly, the following equations were indicated as accurate in terms of describing the activity coefficient of P in the Fe-P-Mn-C(sat.) alloy when X_{P} was lower than 0.2.

$$\ln\gamma^{\mathrm{H}}_{\mathrm{P\ [in\ Fe-P-Mn-C(sat.)]}} - \ln\gamma^{\mathrm{H}}_{\mathrm{P\ [in\ Fe-P-C]}} = \varepsilon^{\mathrm{Mn}}_{\mathrm{P}} X_{\mathrm{Mn}} = -4.72X_{\mathrm{Mn}}$$

$$\ln\gamma^{\mathrm{H}}_{\mathrm{P\ [in\ Fe-P-Mn-C\ (sat.)]}} = -4.72X_{\mathrm{Mn}} + 4.26X_{\mathrm{P}} + 6.09X_{\mathrm{C}}$$

Finally, a comparison to the results for the selective reduction of steelmaking slag in a previous chapter indicated that the activity coefficients of P and Mn obtained in the study are applicable.

6.3 Mechanism of selecting reduction based on the melting behavior

In order to understand the role of Al_2O_3 on the selective reduction of P from steelmaking slag, the initial Al_2O_3 contents in slag was varied from 10% to 25% and its effect on the reduction behavior was investigated. In addition, the result using MgO crucible was analyzed to compare the effect of continuous dissolution of crucibles on the reduction behavior of MnO and P_2O_5.

Firstly, for the slag with a basicity of 0.5, an increase in the initial Al_2O_3 content increased the melting temperature of slag and changed the melting behavior. When the initial Al_2O_3 content was 10%, slag was mostly melted after 1 min, but it required about 4 mins to melt the slag when the initial Al_2O_3 content was 20%. When the slag was melted fast, good selective reduction of P was observed. When the melting of slag took time, the reduction of Mn became intense. Therefore, a slag of low melting temperature which could melt rapidly was beneficial for selective reduction of P from

steelmaking slag. Moreover, an evaluation on the role of slag viscosity and the existence of solid slag on reduction of P and Mn were discussed.

Secondly, the experiments using Al_2O_3 crucibles was analyzed which showed better selectivity on P reduction than that of using MgO crucible shown in Chapter 2. Because the slag melting behavior and viscosity were similar, the above differences on the reduction behaviors of P and Mn were explained by the effect of MgO and Al_2O_3 on the activity coefficient of P_2O_5 and MnO.

6.4 Selective reduction of P and Mn from Mn-ore

The selective reduction technique of P was applied to two types of Mn-ore. The purpose was to decrease the P content from the original ore, and thus to provide a measure to produce ferromanganese with low content of P from normal grade of Mn-ore.

Firstly, by adding SiO_2 as slag modifier to achieve an acidic slag with low melting temperature, and by adding graphite powder and pig iron as reductant and receiver, the selective reduction of P without the reduction of Mn was achieved.

Using the Gabon Mn-ore, the influence of the mixing ratio of graphite powder, pig iron, and SiO_2 on the reduction behaviors were studied. The results showed that both the graphite powder and pig iron contributed to the reduction, and the reduction of P and Mn were enhanced with higher addition of graphite powder and pig iron. To suppress the reduction of Mn from slag while to obtain a high removal ratio of P from slag, the optimum mixing ratio of graphite and pig iron were 10% and 20%, respectively. In addition, some discussions were made to understand the contributions of graphite power and the dissolved C in Pig iron on the reduction.

Secondary, an increase in SiO_2 addition suppressed the reduction of Mn and enhanced the reduction of P. Because the slag needed to be a liquid state, the optimum mixing ratio of SiO_2 at 1673 K was 54% for Gabon Mn-ore. The effects of SiO_2 on the reduction behavior of P and Mn were discussed through the changes of activity coefficient and distribution ratio.

When the reduction was conducted at 1573 K, the results of Gabon Mn-ore showed that the reduction of both Fe and P from slag was insufficient, and a high temperature at 1773 K increased the loss of Mn from slag to metal. Therefore, the optimum temperature for reduction was determined as 1673 K.

Thirdly, applying optimum condition obtained by Gabon Mn-ore experiment to South Africa Mn-ore, the selective reduction of P was achieved. Comparing reduction rate of Mn between two ores, South Africa Mn-ore was faster than that of Gabon Mn-ore. Even though, the calculated activity coefficients of P_2O_5 and MnO in Gabon ore were larger than South Africa Mn-ore, fast melting behavior of Gabon Mn-ore suppressed reduction of Mn.

Finally, assuming the slag obtained after the selective reduction of both Mn-ores was used in the smelting reduction process to produce ferromanganese alloy, significant decrease in the P content of ferromanganese was confirmed through a mass balance calculation. Therefore, the selective reduction of P from Mn-ore was considered as a valid option to produce high grade ferromanganese alloy with low P content.

List of achievements

Peer Reviewed paper and Proceeding:

1. D. Shin, X. Gao, S. Ueda and S. Kitamura, Proceeding 5th International Slag Valorization Symposium, K. U. Leuven, Belgium, 2017, 161−164.
2. D. Shin, X. Gao, S. Ueda and S. Kitamura, Proceedings of the 9th International Symposium on High Temperature Metallurgical Processing, TMS Annual Meeting & Exhibition, TMS, USA, 2018, 305−311.
3. D. Shin, X. Gao, S. Ueda and S. Kitamura "Separation of Phosphorus and Manganese from Steelmaking Slag by Selective Reduction", Metallurgical and Materials Transactions B (Submitted)
4. D. Shin, X. Gao, S. Ueda and S. Kitamura "Measurement on the activity coefficients of P and Mn in carbon saturated Fe-P-Mn-C alloy", Metallurgical and Materials Transactions B (Under review)
5. D. Shin, X. Gao, S. Ueda and S. Kitamura "Selective reduction of phosphorus from manganese ore to produce ferromanganese alloy with low phosphorus content", Journal of Sustainable Metallurgy (In submitting)

Engineering Report:

1. 申東俊、高旭，植田滋，北村信也，選択還元による製鋼スラグからのPとMnの分離回収，日本学術振興会 製鋼第19委員会，反応プロセス研究会第77回 (札幌, 2018.10)

List of Achievements

International Conference:

1. D. Shin, X. Gao, S. Ueda and S. Kitamura, Selective Recovery of Phosphorus and Manganese from Steelmaking Slag by Carbothermic Reduction, 5th International Slag Valorization Symposium, (Leuven, Belgium, 2017.4)
2. D. Shin, X. Gao, S. Ueda and S. Kitamura, Selective Recovery of P and Mn from Steelmaking Slag by Carbothermic Reduction, TMS (Phoenix, USA, 2018.3)

Domestic Conference (in Japan)

1. D. Shin, X. Gao, S. Ueda and S. Kitamura, Separation of Phosphorus and Manganese in Dephosphorization Slag by Carbothermic Reduction, 日本鉄鋼協会第173会春季講演大会, (東京, 2017.3)
2. D. Shin, X. Gao, S. Ueda and S. Kitamura, Measurement of Activity Coefficients of Mn and P in Carbon saturated Fe-Mn-P-C Alloy, 日本鉄鋼協会第175会春季講演大会, (東京, 2018.3)
3. D. Shin, X. Gao, S. Ueda and S. Kitamura, Influence of Melting Behavior on the Selective Reduction of Phosphorus from Steelmaking Slag, 日本鉄鋼協会第176会春季講演大会, (仙台, 2018.9)

Awards & Scholarship

1. 多元物質科学研究奨励賞 受賞 仙台, 日本 2016年12月
2. 公益財団法人旭硝子奨学会, 日本 (2017年 4月~2018年 9月)

Acknowledgement

First of all, I would like to give my deepest appreciation to my supervisor, Professor Shinya Kitamura who gave me the opportunity to study and do research in Kitamura laboratory. As supervisor, he priceless tried to guide me for paving a way to be wise and considerate carefully. Opportunity to enter and experience in his laboratory is turning point for me to change my stereotype and prospective in future. Thanks deeply for his patient and enthusiastic encouragement.

Secondary, I would like to thank Professor Hiroshi Nogami, Professor Hiroyuki Shibata to become the committee in my oral dissertations. Through discussions, I could review my research results thoroughly from various points of view and hence, my thesis has been greatly improved.

I would like to express my thanks to Associate Prof. Shigeru Ueda, Assistant Prof. Sun-joong Kim (Chosun University) and assistant Prof. Xu Gao. Their involvement and vigorous suggestions were considerably helpful in my entire Ph.D. period. Also, their considerate opinions and sharp advices during progress report made me to think more carefully. They are very experienced professors. Meeting them in Kitamura laboratory is a great blessing in my research life. Thanks very much.

Extended gratitude is also addressed to the rest of staffs and members in Kitamura laboratory; Jiang Liu, Junpei Suzuki, Masaaki Kageyama, Ryosuke Sasaki, Motomi Yagi, Hiroki Yoshida, Du Chaoming, Shouhei Koizumi, Takayuki Iwama, Kengo Sugiyama, Masanori Tanno, Shinsuke Oku, Zuoqiao Zhu, Akihiro Hatayama, Isshi Hosoi, Chunyang Liu,

Lichun Zheng, Ryo Yamashina, Satoshi Nakagawa, Yosuke Baba, Hayato Tachibana, Kohei Moriya, Yosuke Okamura and Megumi Obara for direct or indirect helps during my research and daily life. I would like to thanks Takumi Akiyama, Takashi Kamaya, Masaya Hino, and Yuki Dohi for helping me analyze experimental samples.

I would like to thanks to Prof. Jeong-Mo Yoon and Il-Song Park in Chonbuk National University. They helped me to pave a way for future as supervisor and think harder by myself. I could carry out my graduate student period from master to doctoral course by their patient and wise guidance. Their leadership for students will be of great compass for my entire life in the future.

My deep thanks will continue for Korean students studying in Tohoku University. Thanks to Assistant Prof. Soo-Hyun Joo. PhD. Gun-Ho Park, PhD. Yong-Jun Seo, PhD. Kyung-Ho Kim, PhD. Seung-Geun Yu, PhD. Hyun-Jin Hong, Mr. Jin-Yeop Yoo, PhD. Dong-Soo Kang, Mr. Tack Lee, Mr. Hae-Cheol Lee, Mr. Seong-Ho Lee, Ms Su-Jin Choi, and Mr. Won-Young Park. I could adjust and enjoyed life and studying in Japan for all my colleagues.

Finally, I want to express further my appreciation to my family. I deeply thanks to my father (Gyu-Sik Shin) mother (Si-Young Lee), sister (Hyun-Jung Shin) her husband (Kang-Woo Choi), father in law (Eui-Hyun Kim) mother in law (Min-young Cho), and the other members of family. Their endless encouragement for me during my doctoral course was a great strength to focus on studying. And my treasure my wife. I have no valuable words to express my gratitude for my wife Yu-Kyoung Kim. She always dedicated and sacrificed a lot of part for my studying. I never forget her devotional support and trust. Thanks very much.